

**MODEL PREDICTIVE CONTROL FOR
WIND ENERGY CONVERSION SYSTEM BASED
PERMANENT MAGNET SYNCHRONOUS GENERATOR**

**A Thesis submitted
in partial fulfillment of the requirements
for the degree of**

**MASTER OF TECHNOLOGY
in
POWER SYSTEMS & CONTROL**

**by
PRAVIN GARG
Enrollment No - 11704500643**

**Under the Supervision of
Prof. V K Maurya, Head of Department
Prof. Rakesh Sharma
(Electrical Engineering Department)**



**to the
School of Engineering
BABU BANARASI DAS UNIVERSITY
LUCKNOW
May, 2019**

CANDIDATE'S DECLARATION

I, **Pravin Garg** hereby declare that the work contained in this thesis entitled '**Model Predictive Control for Wind Energy Conversion System based Permanent magnet Synchronous Generator**', in partial fulfillment for the award of degree of **Master of Technology** in '**Power System and Control**' from **Babu Banarasi Das University, Lucknow** is a record of my own investigations under the guidance of **Prof. V K Maurya, HOD**, and **Prof. Rakesh Sharma** of **Electrical Engineering Babu Banarasi Das University, Lucknow**.

I have not submitted the matter presented in this dissertation anywhere for the award of any other degree.

(Pravin Garg)
May 2019

CERTIFICATE

It is certified that the work contained in this thesis entitled '**Model Predictive Control for Wind Energy Conversion System based Permanent magnet Synchronous Generator**', by **PRAVIN GARG** (Enrollment No - **11704500643**), for the award of **Master of Technology in 'Power System and Control'** from **Babu Banarasi Das University, Lucknow** has been carried out under our guidance/ supervision and that this work has not been submitted elsewhere for a degree.

(Signature of Guide)
(Prof Rakesh Sharma)
BBD University, Lucknow.
May 2019

(Signature of Guide)
(Prof V K Maurya, Head of the Deptt)
Elect. Engg., BBD University, Lucknow.
May 2019

ABSTRACT

Problem of global warming has pushed smaller size power generation and its utilization in distributed generation system connected with distribution grid system. The distributed generation can be located close to load consumers and it has some merits, likewise: Increasing the available power, Improving the overall system reliability, lower costs, and reduced emissions. The wind energy is one of the distributed resources and made to work in tandem with the regular supply. In case of faults in the system, wind power is used to act as backup for the original supply. Also in case of extra power demand in peak time periods, it has been used to complement the power sources there by maintaining the power quality and frequency in the system.

Due to wind energy generation linked with availability of wind speed, connecting wind turbine generator to distribution grid system leads stability problem. Therefore, it is very important to analyze a suitable control design for wind generators connected to the grid with enhanced stability. In WECS, using PMSG is a better option as it used with full rating Back to Back Power Converter, as offers high controllability and allows maximum power extraction. The VSWT-PMSG is, in general, connected to the utility power system through the voltage source power converters. The converter permits very flexible control of active and reactive power flowing to the grid system and totally decouples the PMSG from the grid; hence grid disturbances have no direct impact on the generator.

The converter operates at high switching frequencies between 2-15 kHz, resulting high order harmonics which can disturb devices on the grid and generate power losses. In order to reduce harmonic currents injected to the grid, LCL filter is an attractive solution because of its many potential advantages such as higher harmonic attenuation and smaller inductances compared with L filter. However, resonance at high frequency caused by the filter can lead stability problem. Determination of controller parameters should be considered in design application. To avoid the resonance problem, a passive damping resistance should be adopted in the LCL filter although this method can reduce the filter effectiveness and increase losses. Selection of a damping resistance value should also be taken into account in the controller design of VSC as well as the filter effectiveness and its losses.

The implementation of advanced control schemes increases the VS-WECS performance. Among various advanced control schemes, model predictive control (MPC) is the most common. It can be predicted by using the system model to predict the behavior of the controlled variables. A cost function is used as a criterion to select the voltage vector that minimizes the error between the controlled variable and its reference. MPC has several advantages such as, it can be used with a variety of systems and contrarians, nonlinearities can be easily included, and multi-variable case can be considered. Moreover, it depends on its own predictions for the next step.

The WT mechanical output power changes with the wind speed. Therefore MPPT algorithm is used to maintain maximum mechanical power at all wind speed conditions. PMSG is tied to the utility grid at the point of common coupling (PCC) via a 3 ϕ back-to-back (BTB) converter. Two MPC based control schemes are developed for machine and network side converters. A shunt capacitor is used as a dc-link between the two converters. The MPC is applied in the MSC to extract maximum power. MPC is also used in the GSC to add only active power into the grid. A tip speed ratio (TSR/ λ) algorithm is used to maintain the mechanical power to its optimal value.

The grid-side controller is used to keep the DC-link voltage constant and to make the grid side run at unity power factor, so that no reactive power is flowing between the generator and the grid. The power converter controls the active and reactive power flow and the DC voltage of the DC-link capacitor between the PMSG and the grid by feeding the pulse width modules (PWM) to the converter. The system dynamics are tested/ assessed with the help of the simulation program using MATLAB and its inbuilt components provided in SIMULINK library.

ACKNOWLEDGEMENT

First and foremost, I am truly indebted and wish to express my gratitude to **Prof Rakesh Sharma, BBD University, Lucknow** for his inspiration, excellent guidance, continuing encouragement and unwavering confidence and support during every stage of this endeavor without which, it would not have been possible for me to complete this undertaking successfully.

I, also thank him for his insightful comments and suggestions which continually helped me to improve my understanding of subject.

I am very much obliged to the **Prof. V K Maurya, Head of the Department of Electrical Engineering, School of Engineering, BBD University, Lucknow** for providing all possible facilities towards this work. My Heartfelt thanks to all other faculty members in the department for their support and guidance.

I also express my deep gratitude to entire Staff of Electrical Engineering Deptt, School of Engineering, BBD University Lucknow, for their loving advice and support.

I would also like to express my heartfelt gratitude to my friends **Ishteyaq Ahmad** and **Rohan Srivastava**, who always inspired me and particularly helped me in my work. Lastly, I pay my whole hearted gratitude to my parents and family for their constant encouragement and support.

Above all, I thank Almighty who bestowed his blessings upon us.

Pravin Garg
Lucknow,
May 2019

TABLE OF CONTENTS

Chapter No	Content	Page No
	Candidates' Declaration	ii
	Certificate	iii
	Abstract	iv
	Acknowledgement	vi
	Contents	vii
	List of Tables	xi
	List of Figure	xii
	List of Symbols	xiv
	Abbreviations	xv
Chapter 1	INTRODUCTION	1
	1.1 Provocation	1
	1.2 Wind Energy Scenario Across World	2
	1.2.1 Key Highlights	3
	1.3 Wind energy in India	6
	1.4 Literature Survey	7
	1.5 Objective	11
	1.6 Scope of Work	12
	1.6.1 Problem Statement	12
	1.6.2 Constraints	12
	1.6.3 Methodology	13
	1.7 Thesis outline	13
Chapter 2	THEORY OF WIND ENERGY SYSTEM	14
	2.1 Overview of wind energy	14
	2.1.1 Stand-Alone and Grid-Connected Applications	14
	2.1.2 On-Land and Offshore Applications	15
	2.2 Wind Turbine technology	15
	2.2.1 Horizontal- and Vertical-Axis Wind Turbines	15
	2.2.2 Fixed- and Variable-Speed Turbines	16
	2.2.3 Stall and Pitch Aerodynamic Power Controls	16
	2.3 Wind energy conversion system configuration	17
	2.3.1 Fixed Speed WECS w/o power convertor interface	18
	2.3.2 variable Speed systems with reduced capacity convertors	18
	2.4 Grid codes	18
	2.5 Wind turbine components	19
	2.5.1 Turbine Blade	20
	2.5.2 Pitch Mechanism	22
	2.5.3 Gear box	23
	2.5.4 Rotor Mechanical Brake	23

Chapter No	Content	Page No
	2.5.5 Generator	23
	2.5.6 Yaw Drive	24
	2.5.7 Tower and Foundation	25
	2.5.8 Wind sensor	25
	2.6 Wind Energy Conversion System Configuration	26
	2.6.1 Type 1 : Fixed Speed(± 1 %) WECS Configuration	27
	2.6.2 Type 2 : Semi variable Speed(± 10 %) WECS Configuration	28
	2.6.3 Type 3 : Semi variable Speed(± 30 %) WECS Configuration	29
	2.6.4 Type 4 : Full variable Speed($\pm 0-100$ %) WECS Configuration	30
	2.6.5 Type 4 : Full variable Speed($\pm 0-100$ %) WECS Configuration with WRSG	31
	2.7 Mathematical Expression of wind power and wind turbine power	32
	2.8 Power Characteristics of a wind turbine	33
	2.9 Maximum power point tracking Control (MPPT)	35
	2.10 MPPT with optimal tip speed ratio	35
Chapter 3	Permanent Magnet Synchronous Generator	37
	3.1 PMSG	37
	3.1.1 Surface Mounted PMSG	37
	3.1.2 Inset PMSG	38
	3.2 Mathematical Modelling of PMSG	39
Chapter 4	Study of PMSG Stand alone operations	42
	4.1 Stand alone Operation of PMSG	42
	4.2 SIMULINK Results and Conclusion	46
	4.2.1 Block Diagram	46
	4.2.2 Simulink Model	46
	4.2.3 Results	48
	4.3 Conclusion	49
Chapter 4	Model Predictive Control and modelling of 2L- Back to Back Convertors	50
	5.1 Control of WECSs	50
	5.1.1 Supervisory Control (Level VI)	52
	5.1.2 Wind Farm Centralised Control (Level V)	52
	5.1.3 WT Centralised Control (Level IV)	52
	5.1.4 Grid Integration and MPPT Control (Level III)	53
	5.1.5 Convertors, Generator and Grid Control (Level I and II)	54
	5.1.5.1 Power Convertor Control (Level I)	55

Chapter No	Content	Page No
	5.1.5.2 Wind Generator and Grid Control (Level II)	55
	5.2 Finite Control Set - MOPC	57
	5.2.1 Main Features of FSC –MPC	57
	5.2.2 Challenges of FSC – MPC	60
	5.3 Model Predictive Control of WECSs	61
	5.4 Comparison of Classical and Model Predictive Control	62
Chapter 6	Review of Controller Design for PMSG Based WESC with LCL Filter	63
	6.1 Abstract	63
	6.2 Introduction	63
	6.3 VSWT-PMSG modelling Systems	64
	6.3.1 Wind Turbine Model	65
	6.3.2 Dynamic Model of PMSG	66
	6.3.3 Mathematical model of LCL Filter	68
	6.4 VSWT-PMSG Controller Modelling systems	69
	6.4.1 Machine side Controller (MSC)	69
	6.4.2 Grid side Controller (GSC)	70
	6.4.3 LCL Filter Parameters	72
	6.5 Simulation and system study	72
	6.6 Conclusion	74
	6.7 Appendix	75
Chapter 7	Review of Predictive Control Strategy for WECS based on PMSG	76
	7.1 Abstract	76
	7.2 Introduction	76
	7.3 WESC	78
	7.3.1 Wind Turbine Model	78
	7.3.2 PMSG Model	80
	7.4 MPPT Technique	81
	7.5 Control of Machine and grid side Controller (MSC & GSC)	81
	7.6 Model Predictive Control	81
	7.7 MPC of Convertors	82
	7.8 MPC based control of MSC	83
	7.9 MPC based control of GSC	86
	7.10 Simulation Results and discussion	89
	7.10.1 Algorithm	89
	7.10.2 Optimization Program	90
	7.10.3 M File	91
	7.11 Conclusion/ Simulation results	95
	7.12 Scope of future Work	99

Chapter No	Content	Page No
	Reference	87
	Appendices	95
	Plagiarism Report	100
	List of Publications	101
	Certificate of Final Thesis Submission	102
	Curriculum Vitae	103

LIST OF TABLES

Table No.	Description	Page No.
1.1	Top ten countries Installed WTs in 2018	5
1.2	Generation based Incentive	6
4.1	2.45 MW, 4000V, 53.33Hz non salient pole PMSG parameters	42
5.1	Comparison between classical and predictive control schemes	62
6.1	PMSG System Parameters (Along with LCL Filter)	72
6.2	PI Controller Gains	75
7.1	SGSC/ MSC switching states and corresponding output voltage vector $V_{sdq(j=0to7)}^j$	85
7.2	GSC switching states and corresponding output voltage vector $V_{convdq(j=0to7)}^j$	88
7.3	Simulation Parameters of PMSG System Parameters (Along with LCL Filter)	94

LIST OF FIGURES

Table No.	Description	Page No.
1-1	Global cumulative installed wind power Capacity (Up to 2018)	3
1-2	Global annual installed wind power Capacity (Up to 2018)	4
1-3	Worldwide regional WTs installation capacity in 2018	4
1-4	Top ten countries installed capacities in 2018	5
1-5	State wise installed cumulative wind power capacity in 2018	7
2-1	Components of wind turbine	20
2-2	Yaw drive of wind turbine	24
2-3	Foundations for off shore wind turbines	25
2-4	Type 1: Fixed Speed ($\pm 1\%$) WECS with SCIG	27
2-5	Type 2: Semi-variable speed ($\pm 10\%$) WECS with WRIG	28
2-6	Type 3: Semi variable speed ($\pm 30\%$) WECS configuration with DFIG	29
2-7	Type 4: Full variable speed (0-100%) WECS Configuration	30
2-8	Type 5: Full variable speed (0-100%) WECS configuration with WRSG	31
2-9	Curve between the C_p and Lambda (λ , tip speed ratio) at various Pitch angles	33
2-10	Turbine power characteristic of 3MW wind turbine	34
2-11	MPPT with optimal tip speed ratio	36
3-1	Surface-mounted non salient PMSG (sixteen-pole configuration)	38
3-2	Inset PMSG with salient poles (four-pole configuration)	38
3-3	General dq-axis model of SG in the rotor field Synchronous reference frame	39
3-4	Matlab Block diagram for dynamic simulation of synchronous generators	41
4-1	Block Diagram PMSG in standalone mode Simulation	43
4-2	Simulink Model PMSG in standalone mode Simulation	45
4-3 to 9	Results PMSG in standalone mode Simulation	46-48
5-1	Block diagram of the overall control scheme for variable-speed WECS	51
5-2	Features MPC	57
5-3	Predictive current control of 2L-VSR-based PMSG WECS	61
6-1	Model and control system of PMSG based variable speed wind turbine	65
6-2	$C_p - \lambda$ characteristic for different pitch angle	66
6-3	Turbine power characteristic ($\beta = 0^0$)	66
6-4	Single phase LC filter equivalent circuit	68
6-5	Block diagram of LC filter in the d-q rotating reference frame	69
6-6	Stator side controller system	70
	Grid side controller system	71
6-8	Model system	73
6-9	Power Output	73

LIST OF FIGURES

Table No.	Description	Page No.
6-10	THD Calculation	74
7-1	PMSG Wind Energy Conversion System Configuration	78
7-2	Power Coefficient(C_p) vs. Tip Speed Ratio (TSR/λ)	79
7-3	Generated Mechanical Power vs. Rotor Speed at different Wind Speed	79
7-4	Basic Principles of MPC	82
7-5	MPC based control for the MSC/ SGSC	89
7-6	MPC based control for the GSC	87
7-7	Algorithm MPC	89
7-8	PMSG Speed wr	96
7-9	PMSG Power Generation 'P' & 'Q'	96
7-10	PMSG Convertor Voltages	97
7-11	PMSG Convertor Currents	97
7-12	PMSG Grid Voltages	98
7-13	PMSG Grid Currents	98
7-14	Comparative Simulation Results	99
A.2.1	SPWM with carrier and three phase modulating signal and switching states	111
A.3.1	Principle of Hysteresis band current control	113
A.3.2(a)	Matlab model of HB controller	114
A.3.2 (b)	Matlab response of HB controller	114

LIST OF SYMBOLS

$V_{ab}, V_{bc}, V_{ca},$	-	Three Phase Stator Voltages
i_{sa}, i_{sb}, i_{sc}	-	Three Phase Stator Current
i_{ra}, i_{rb}, i_{rc}	-	Three Phase Rotor Current
i_{ga}, i_{gb}, i_{gc}	-	Three Phase Grid Current
i_{la}, i_{lb}, i_{lc}	-	Three Phase Load Current
$i_{gsca}, i_{gs cb}, i_{gsc},$	-	Three Phase Grid Side Converter Currents
i_{dr}	-	Direct Axis Rotor Current
i_{qr}	-	Quadrature Axis Rotor Current
i_{ld}	-	Direct Axis Load Current
Ψ_{qs}, Ψ_{ds}	-	Stator q and d axis fluxes
P_{opt}	-	Optimal power
P_{ref}, P_{loss}	-	Reference active power & system power loss
P_g	-	Active Power fed to Grid
Q_g	-	Reactive Power fed to Grid
P_s	-	Stator Active Power
Q_s	-	Stator Reactive Power
P_l	-	Load Active Power
Q_l	-	Load Reactive Power
P_{gsc}	-	GSC Active Power
Q_{gsc}	-	GSC Reactive Power
V_w	-	Wind Speed in m/s
ω_r	-	Rotor Speed in rad /s
ω^*_r	-	Reference Rotor Speed in rad/s
θ_e	-	Angle of Grid Voltage Vector
θ_r	-	Electrical rotor angle
V_{dc}	-	DC Link Voltage
T_{em}	-	Electromagnetic torque
T_m	-	Shaft mechanical torque
J	-	Inertia coefficient
H	-	system Inertia constant
F	-	Friction factor
R_{blade}	-	Blade radius of rotational turbine
C_p	-	Performance coefficient
λ	-	Tip speed ratio
β	-	Blade pitch angle
P_p or P	-	No of Pole Pairs
R_s	-	Stator resistance
L_s	-	Total stator and rotor inductances

LIST OF ABBREVIATIONS

WECS	-	Wind Energy Conversion System
HAWT	-	Horizontal Axis Wind Turbines
VAWT	-	Vertical Axis Wind Turbines
FSWT	-	Fixed Speed Wind Turbine
SCIG	-	Squirrel Cage Induction Generator
WRIG	-	Wound Rotor Induction Generator
PCC	-	Point Of Common Connection
DFIG	-	Doubly Fed Induction Generator
RSC	-	Rotor Side Converter
GSC	-	Grid Side Converter
PMSG	-	Permanent Magnet Synchronous Generator
LPF	-	Low Pass Filter
SCR	-	Silicon Controlled Rectifier
MOSFET	-	Metal Oxide Field Effect Transistor
IGBT	-	Insulated Gate Bipolar Transistor
SG	-	Synchronous Generator
WRSG	-	Wound Rotor Synchronous Generator
IWGC	-	Indian Wind Grid Code
GW	-	Giga Watt
PID	-	Proportional Integrator and Differentiator
MW	-	Mega Watt
VSC	-	Voltage Source Converter
CSC	-	Current Source Converter
PWM	-	Pulse Width Modulation
LVRT	-	Low Voltage Ride Through
PLL	-	Phase Lock Loop
GTO	-	Gate Turn Off Device
PI	-	Proportional Integrator

CHAPTER 1

INTRODUCTION

1.1 PROVOCATION:

Renewable energy sources have led to set a paradigm to accumulate the requirement of energy for our needs. Renewable energy sources are clean, pollution free, naturally refill, unlimited in availability. The interest of research in the field of renewable energy sources like solar, wind, geothermal, tidal, ocean temperature difference and wave are increasing progressively, and this is happening because of the decrement in the deposition of fossil fuels and increment in environmental concern. Renewable energy resources are used for electricity generation, transportation and rural energy supply [1-2]. Advancement of the technology cost reduction, government financial aids, and environmentalist demand for clean energy, wind energy is most preferable than the other renewable energy resources but also with the conventional hydrocarbon deposition based power generation [3].

Wind energy is a major source of energy for mankind from hundreds of years to sailing the ship across ocean, pump water, and grid grain. The electricity production from the wind energy started during the 1880s with 12 kilowatt (kW) using direct current (DC) generator. As per the passage of time there have many researches carried out to improve the design of mechanical and electrical of wind turbines (WT) for producing the electricity more efficiently. The size of WTs has gradually increases and reached up to 10-15 MWs. In the 1980s the diameter of WTs is 15m but today the size of diameter is 150m (twice the length of Boeing 747) because of larger WTs diameter extracted more power from wind [4].

In an extended area the group of WTs formed a wind farm and they connected to an electric grid. The wind farm can be formed on the land called onshore wind farm or in the sea called offshore wind farm. The onshore wind farm has various advantages such as easy access, lower maintenance cost, easy and cost effective installation, easy connectivity with transmission lines [5-6]. The cost of initial installation and maintenance of offshore wind farms are higher than the onshore wind farms because it require stronger foundation and the connection to the onshore grid done with the help of submarine cables [7-8]. The linking of onshore and offshore wind farm to the electrical power system done with the help of various types of series/parallel and AC/DC and high voltage ac and dc (HVAC and HVDC) transmission system, these system developed by various turbine manufactures [9-11].

The various innovations in WTs and power converters design and configuration have been taken to achieve fixed speed, semi variable speed and full variable speed operations. In fixed speed wind turbine (FSWT) operation the power converters uses for the start up process (soft start). The power converters in variable speed wind turbines (VSWT) work as power processor, enhance the wind energy conversion efficiency, power quality improvement, and makes compatible with grid codes. The electrical control system is developed to control the generator and power converter, extract maximum energy from wind and enhance power quality. These electrical control system implemented by digital control system such as microcontroller based, digital signal processor (DSP) based, field programmable gate array (FPGA) or finite control set model predictive control (FCS-MPC) [11-12].

Wind is ambient in nature, it require the variable speed operated WTs for extracting maximum power. For variable speed operation the doubly fed induction generator (DFIG) based wind energy conversion system (WECS) dominating the market with reduced power converter rating, 30% approximately (maximum slip) of the rated power of generator. Wound rotor synchronous generator (WRSG) and permanent magnet synchronous generator (PMSG) require full capacity of power converter to operate on variable speed [11], [13].

In this chapter, the focus is not only on the motive of this work, the chapter divided into sections. The sections cover the various points, to easily visualise the view of this chapter. The glimpse of status of wind power in the world and status of wind power in India further projected in this chapter, also the objective of this work and structure of this thesis mentioned further.

1.2 WIND ENERGY SCENARIO ACROSS WORLD

The wind energy installations progressively expand with the passage of time. Wind energy established as a part of global worldwide energy system. In 2016, there is a total of 54 GW was installed globally but it is decrement of 14.0% from previous year due to the dropping of installation in China from 30.293GW in 2015 to 23.328GW in 2016. This installed capacity in 2016 brings new cumulative wind capacity up to 486,831 MW, an annual increment of 12.1% [14].The installed capacity of WTs cumulative and annually across the world are shown in figures 1.1 and 1.2 respectively. The worldwide installed wind power categorize in regions is shown in figure 1.3. The top ten countries of installing the new WTs during the time January 2017 to December 2017 is shown in figure 1.4 and table 1.1. These data are based on the Global wind statistics 2017 [15], and [16].

1.2.1 Key Highlights

- (a) As per the figure 1.1, the cumulative installed capacity in 2017 increased exponentially from 6.1 GW in 1996 to 539.6 GW in 2017.
- (b) As per the figure 1.2, the annually installed capacity in 2017 is 52.6 GW, a decrement of 3.66% from the year 2016, 54.6 GW.
- (c) Asia emerged as growing marking market for wind power; it is indicate from figure 1.3, total installed capacity in 2017 is 24.4 GW.

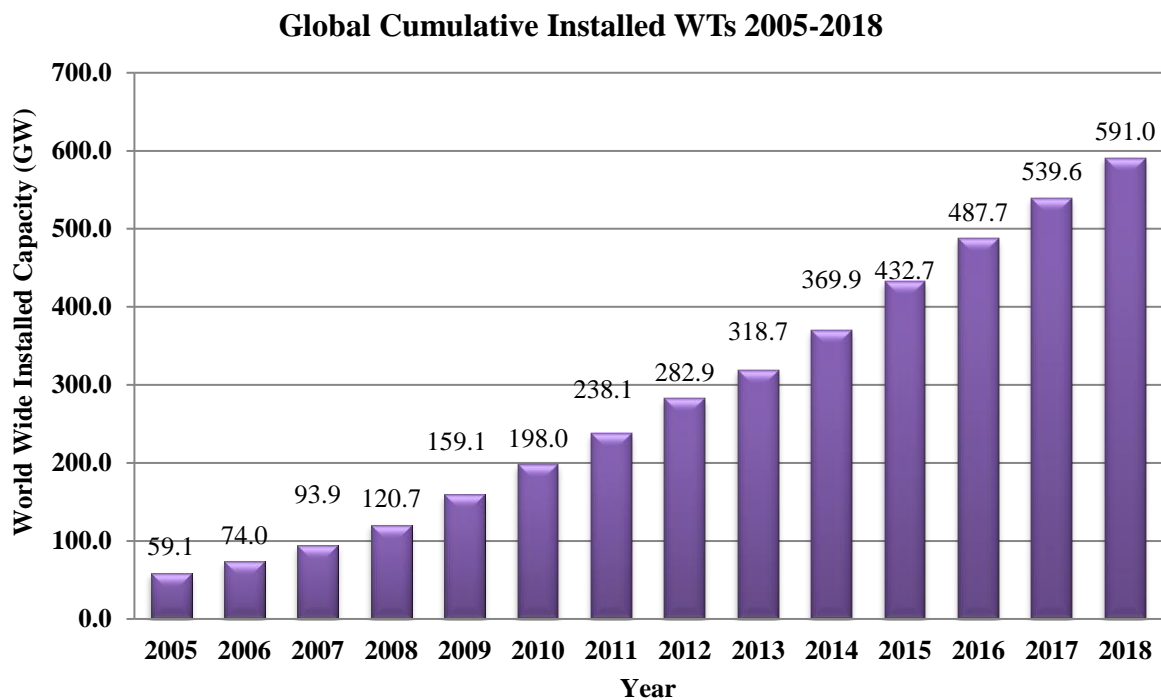


Figure 1.1 Global cumulative installed wind power capacity (2005-2018)

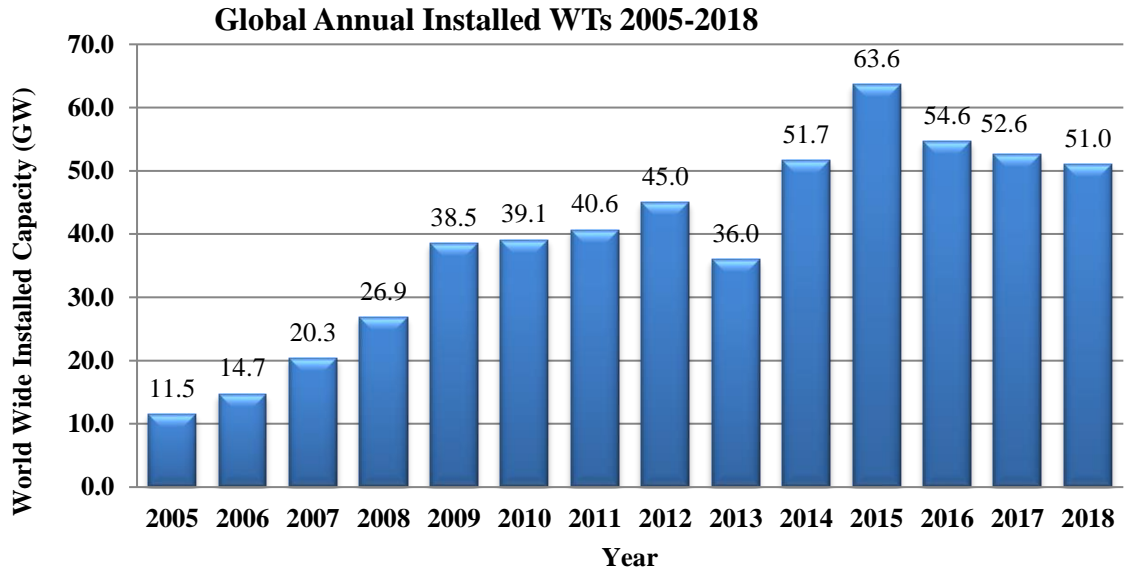


Figure 1.2 Global annual installed wind power capacities (2005-2018)

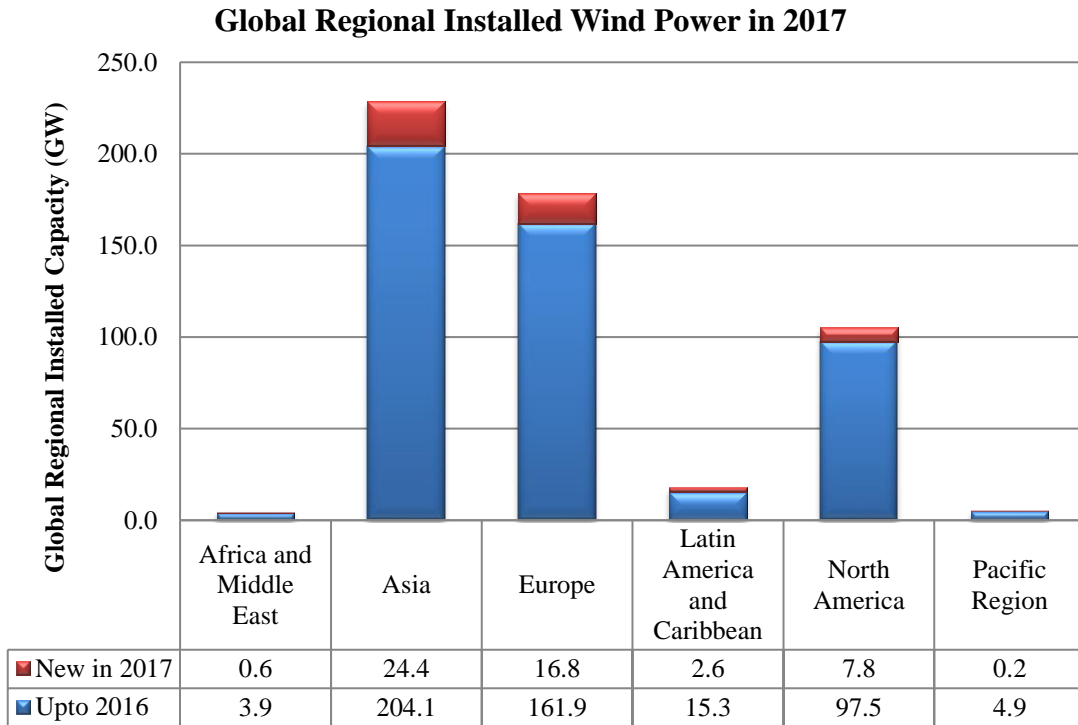


Figure 1.3 Worldwide regional WTs installation capacity in 2017.

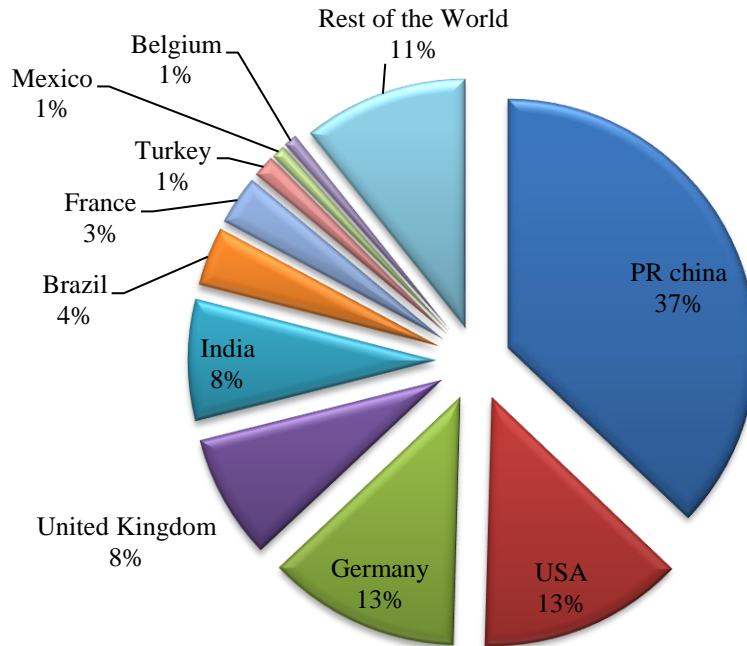


Figure 1.4 Top ten countries installed capacities in duration January - December 2018

Table 1.1 Top Ten Countries Installed WTs Jan-Dec 2018

Country	MW	% Share
PR China	19,500	37
USA	7,017	13
Germany	6,581	13
United Kingdom	4,270	8
India	4,148	8
Brazil	2,022	4
France	1,694	3
Turkey	766	1
Mexico	478	1
Belgium	467	1
Rest of the World	5,630	11
World Total	52,573	100

- (a) China has led the wind market of energy production by 37 %, followed by USA 13%, India has 5 position with 8% (4,148 MW).
- (b) Asia and Europe are the leading in wind energy market with 46.56% and 32.06% of global wind power capacity, respectively.

1.3 WIND ENERGY IN INDIA

The energy is the only factor for India's development goals achievement for supporting the chop-chop development in the economy. India is the 5th largest wind market in the world and having installed capacity of 32.79GW at end of March 2018. India has a target to achieve 60GW by 2022 as the incremental rate of 5 GW annually. Still, 20% population remains without electricity. There are available 7600 KM of coastline area of offshore for wind energy in India. Although support from central government will not enhance the wind projects due to reasons like state level power sectors are not in good economic condition, delay in payment up to 4 or 6 month is a concern, land acquisition is also a challenging factor. Wind energy integrates the maximum share of 55.75% among the renewable energy [17-18].

In India, the potential of wind energy first estimated by the National Institute for Wind Energy's (NIWE) and as a consequence the potential is 302 GW at 100 meters. India has 7,600 km coastline for offshore wind energy. Indian renewable energy development agency ltd (IREDA) gets a mini-ratna status from the ministry of new and renewable energy in 2015. IREDA provide the financial support for development of renewable energy efficiency projects. The generation based incentive (GBI) is shown in table 1.2. The data for table 1.2 collected on the IREDA website [19].

The state wise cumulative installed power in India is shown in figure 1.5. The data obtained from the IWTMA websites [18].

Table 1.2 Generation Based Incentive (GBI) Registration Status

Generation Based Incentive (GBI) Registration Status on Dec 2018		
Scheme	Period of Scheme	Capacity Registered (MW)
GBI-II	01.04.2012 - 31.03.2017	11593.5
GBI-I	17.12.2009 - 31.03.2012	2031.38
Demo	Scheme limited to first 49 MW registered	48.9

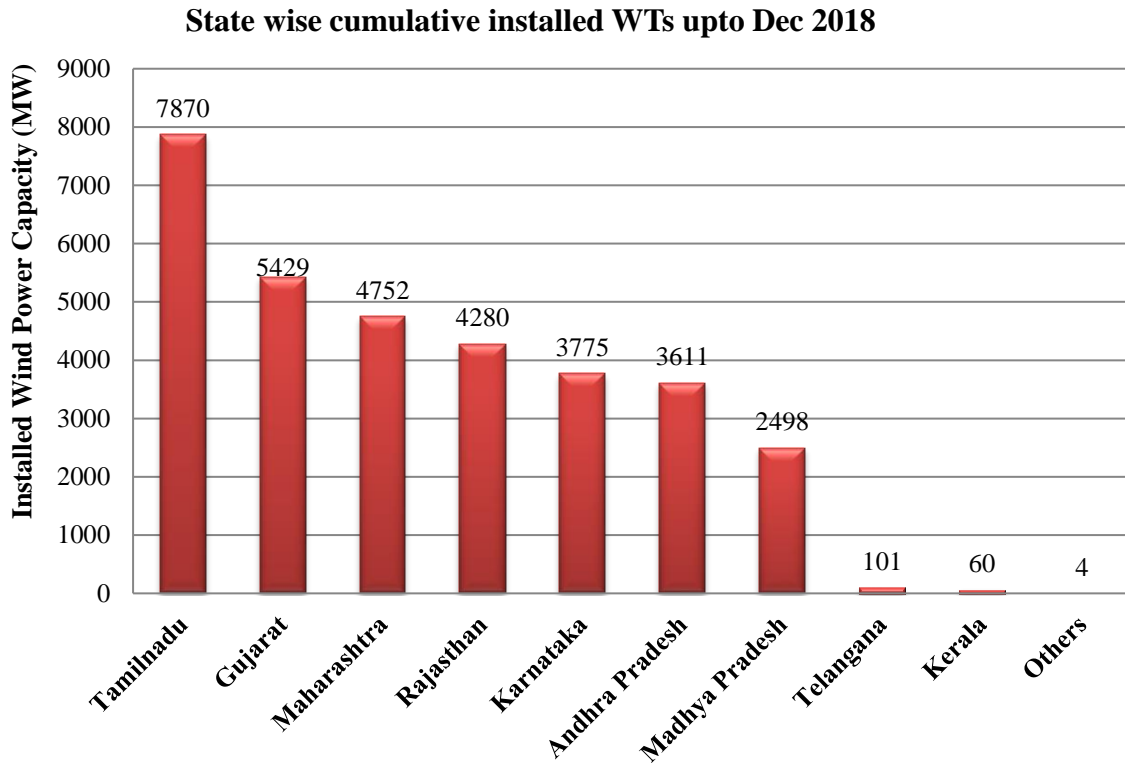


Figure 1.5 State wise installed cumulative wind power capacities up to march 2018

1.4 LITERATURE SURVEY

Several researchers have carried out work on IG based WECS for mitigating the harmonics available in the circuit. In this section there is an attempt to summaries the main theme of the some research paper which emphasise on the harmonic mitigation of the DFIG based WECS.

Shuhui Li et. al [20], the authors compare the real and reactive power controls for a DFIG using the stator voltage oriented and stator flux oriented reference frames. Authors conclude that it is easy to obtain the stator voltage space vector position as compared to the stator flux space vector position. The stator flux space vector position can calculate by just adding the 90° in the stator voltage space vector position. Controllers have the same performance in both the cases.

H. M. Hasanien [21], the author proposes the super conducting magnetic energy storage (SMES) system with a novel adaptive control scheme for the smoothing of the output power of wind farms. The author used here the set membership affine projection algorithm

(SMAPA), which provides the faster convergence and less computational complexity than normalized least mean square algorithm. In this work the SMAPA based adaptive PI controllers are used. Author concluded that SMES units are very effective tools for smoothing the wind farms output power.

G. O. Suvire et. al [22], the authors proposes a distributed static synchronous compensator (DSTATCOM) coupled with a flywheel energy storage system (FESS) is used to mitigate problems introduced by wind turbine system. The active power exchanged and control is presented in this system with controlling the DSTATCOM and FESS and mitigating the power fluctuations.

D. Somayajula et. al [23], the authors included the ultra-capacitor for power conditioning in distributed generated system (wind energy conversion system). Ultra- capacitor is helpful to tackle the grid intermittencies and the voltage sag and swell. In this work author proposes that the ultra-capacitor is integrated with dc link through a bidirectional dc-dc converter to get a stiff dc link voltage.

A. Gaillard et. al [24], the authors introduces the machine side converter control to mitigate harmonic contents and also introduces a new selectivity harmonic isolator based on self-tuning filter. Author uses the harmonic current loop in the RSC in order to inject the harmonic component in the grid at the connection point. These current components mitigate the harmonics produced by the non-linear load.

M. Boutoubat et. al [25], the authors emphasize on the reactive power exchange and active filtering capability of a WECS. The authors used the selective filtering approach to mitigate the most dominating low frequency harmonic components to avoid over ratings. In RSC the harmonics used to inject.

E. Tremblay et. al [26], the authors introduces the direct power control to control independently the active and reactive power and this control strategy applied on the rotor side converter control. Similarly the GSC is used to mitigate the harmonics with a synchronous reference frame based strategy.

G. Todeschini et. al [27], the authors compares the three controlling strategies for the WECS with three objectives as active filter and power generation, the second objective is that the compensation triple harmonics, and the last objective is the power losses due to active filter operation. In this literature the three concepts are described for harmonic mitigation generated from the non-linear loads. (i) RSC modulation is taken place; stator injects the harmonics which is equal in magnitude and 180° out of phase with the harmonics injected by the non-linear loads. (ii) LSC (load side converter) control is used to inject harmonics currents. (iii) Combine modulation of RSC and LSC to inject harmonic current.

Peng Zhan et. al [28], the authors proposed the design procedure for the back to back converter for DFIG based WECS in order to mitigate the harmonics produced by the PWM converter. Author designed the filter for the grid side converter as well as for the rotor side converter.

D. Zhou et. al [29], the author compares the current ripples and the supportive reactive power ranges between the L and LCL filter. If the reactive power is injected from the grid side converter then it considered the power losses in the converters and concluded that the energy loss is lower with the optimized filter. The required reactive power can be supplied through the GSC control or from the RSC control. It conclude that the reactive power compensation from the GSC increase the power loss of the GSC itself but lower the total loss of the whole DFIG system while the reactive power supported from the RSC will increase the RSC loss as well as the whole DFIG system loss.

M. Liserre et. al [30], the author introduces the step by step design procedure for designing the LCL filter for three phase rectifier. The LCL filter used for mitigating the harmonics. The design procedure also shows the stability factor for the LCL filter.

Parikshith. B. C. et.al [31], the authors proposes the design procedure in order to follow the filtering response as per standard such as IEEE-519-1992, and IEEE P1547.2-2003. The authors provide the design step for a high order LCL filter.

Min Huang et. al [32], the author introduces the step by step design procedure for a LLCL filter. When LCL filter design then the three phase inverter is simplified as the single phase inverter and the output phase voltage is used to calculate the inverter side current harmonics for designing the inverter side inductor. The author proposes a new designing concept of filter for three wires three phase grid tied inverter, and also compare the simulations results of three types of filters such as LCL, LLCL with single trap and LLCL with double traps. The total inductance of LLCL filter with one traps and with two traps are reduced by the 25-40% respectively.

A. Merabet et. al [33] introduces proposes the Kalman's filter as rotor flux observer and the AI adaption mechanism to estimate the rotor speed and both were used to find out the states of rotor flux and speed without any sensing device. The speed estimation by the conventional PI controller does not take into consideration of the nonlinearities in the system. The authors conclude that the ANN based system gives the better performance than PI based system. Model reference adaptive system (MRAS) method depend on the exactness of the reference model, which is sensitive to parameter variations, and there is also a consideration in MRAS that there is no parameter variation taken place during the machine operation.

Amit Kumar et.al [34], propose the ANFIS based controller for RSC control worked on direct torque control (DTC) principle, and compare the simulate result through the PI controller. The authors concluded that ANFIS based controller gives the improved settling time and peak overshoot of the response and improve its performance.

Ahmad A. Zaki Diab et.al [35] analysis the performance of DFIG based WECS with the vector control of the RSC and GSC through the ANFIS controller. The author just uses the conventional RSC and GSC controlling scheme in vector control and replaces the PI controller with the ANFIS controller, and compare the result with the traditional controller.

Arun Shankar V.K et.al [36], proposes the ANFIS based controller for the PMSM driven centrifugal pump and analyse the performance. The authors also compare the simulation result with the PI controller, Fuzzy controller and ANFIS based controller and they concluded that the ANFIS based controller has improved performance.

K. R. Angeline et. al [37], used the ANFIS based controller for performance enhancement of the DFIG based WESC. The authors show the comparison between the Fuzzy controller and the ANFIS controller and the result state that the ANFIS controller has better response than the Fuzzy controller.

N. K. S. Naidu et.al [38], proposes the novel control of the GSC for mitigating the harmonics produced by the nonlinear loads. The author proposes to control the grid current indirectly and in this method the harmonics developed in the system by the GSC to mitigate the harmonics generated by the nonlinear loads, and successfully they mitigate the harmonics within the permissible limit as per IEEE standard.

Ali M. Eltamaly et.al [39], the authors studied the behaviour of doubly fed induction generator system for wind energy conversion system during the failure of DC link electrolytic capacitor. The electrolytic capacitor failure conditions design by the short circuit and open circuit of DC link capacitor. The capacitor failure can leads to the power outages, higher transients, increase the current, increase the generator speed and the causes the low voltage at generator terminal. The active power capability is lost with the high rotor and stator current during the short circuit, GSC exchange high current than the normal value while in open circuit of DC link the active power capability is lost and the current controllers at RSC and GSC are fail. These disturbances are liable to disturb the performance of a wind farm.

A. M. Shiddiq Yunus et. al [40], the authors investigates the effect of the short circuit and open circuit faults in the DC link capacitor on the dynamic performance of DFIG and also investigates with the compliances of different grid codes such as Denmark, Spain, Nordic, and Sweden. The authors studied the performance and fault ride through for above mention countries

to compliance the grid codes under the fault scenario like successful and unsuccessful fault clearance.

Hadeed Ahmed Sher et.al [41], the authors investigate the effect of the short circuit of DC link capacitor on induction machine as well as on the freewheeling diode. The system behaviour observed by both the simulation and by the experimental. When the DC link capacitor fails and transistor becomes OFF then the high current will pass through the freewheeling diode and the diode is not designed for this extra stress.

1.5 OBJECTIVE

The main objectives of this project are listed as follows:

- (a) Study the basic terminology in Permanent Magnet Synchronous Generator.
- (b) Study and analysis of converter control schemes and use of Model Predictive control (MPC).
- (c) Study the parameter under different wind and load condition.
- (d) Study the parameter under harmonics/ fault at grid.

PMSG scheme is used as a variable speed fixed frequency topology. In this scheme, stator is directly connected to the grid through an AC/ DC/ AC back to back frequency converter. The rating of this converter is typically 100% of the total power rating of the generator. This is the main advantage of PMSG over other variable speed topologies as it provides same features with good efficiency and power to weight ratio. PMSG is basically a WRIG which has a stator and permanent magnet rotor. Stator circuit of the PMSG consist of stator frame, laminated stator core having stator slots embedded in it and balanced 3- ϕ windings placed 120° electrically apart from each other. The winding distributed in nature, are insulated and are housed in the stator slots. Stator windings may be connected in delta or star manner. The stator circuit is connected directly to grid through a bidirectional AC/DC/AC bidirectional converter.

The bidirectional AC/DC/AC converter is consists of two, 2-L full bridge converters connected in cascade by means of a DC bus. The converter which is connected to stator of machine is called machine side converter (MSC) and converter which is connected to grid side is called grid side converter (GSC). The switches used in these converters require high speed operation. So typically IGBT switches are used for this purpose. The main purpose of GSC is to regulate the DC link voltage. Apart from that, it is sometimes help to improve the power quality of grid at the point of common connection (PCC) by feeding reactive power during reactive power fluctuation in grid.

Grid side converter control is used to regulate the voltage across the DC link and sometime also to compensate harmonics. This is a two stage controller scheme which is achieved by grid voltage oriented vector control scheme i.e. by aligning the dq- axis in the direction of grid voltage. Grid converter is typically a three phase, two level voltage source converter which uses IGBT as a switching device. As we have discussed earlier, the main purpose of grid side converter control is done to regulate the DC link voltage. This is done by implementing grid voltage oriented control scheme.

The main purpose of controlling machine side converter is to control stator side active and reactive power independently.

- (a) Stator voltage drop across resistance has been neglected as the stator resistance value is quite low in value.
- (b) The DFIG is connected to stiff grid i.e. the frequency and amplitude of stator and grid voltage is assumed to be constant.
- (c) The q- axis is rotating 90° ahead of d-axis at synchronous speed in the direction of rotation.
- (d) The stator flux vector is aligned with the d-axis of the stator.

1.6 SCOPE OF WORK

1.6.1 Problem statement

In this research thesis, the control the flow of the powers of PMSG based wind energy conversion system is tested/ verified. Efforts were taken to maintain dc link voltage constant for various parameters under pure resistive load, dynamic load at grid and also under fault at grid. A vector control strategy with stator voltage orientation is applied to both the grid side converter and the machine side converter for the independent control of Active and reactive powers produced by the PMSG based wind energy conversion system. The system along with its Digital control circuit/ MPC was simulated in a Matlab/ Simulink and the results are presented and discussed.

1.6.2 Constraint

A grid connected Permanent Magnet Synchronous Generator (PMSG) based Wind Energy conversion System (WECS) with a back to back converter setup to control the PMSG. The constituents of the WECS are mathematically modelled in Matlab/ Simulink. The back to back converter set up consists of the Machine Side Converter (MSC) and the Grid Side Converter (GSC) with intermediate DC link. Decoupled control of the DC link voltage and the

grid reactive power is obtained through Voltage oriented control (VOC) of GSC. Similarly independent control of power from wind and reactive power of PMSG is carried out by machine oriented vector control of MSC.

1.6.3 Methodology

A vector control scheme has been used at machine side converter control and grid side converter control. Grid side converter control is used to regulate the voltage across the DC link and sometime also to compensate harmonics. This is a two stage controller scheme which is achieved by grid voltage oriented vector control scheme i.e. by aligning the dq- axis in the direction of grid voltage. Grid converter is typically a three phase, two level voltage source converter which uses IGBT as a switching device. As we have discussed earlier, the main purpose of grid side converter control is done to regulate the DC link voltage. This is done by implementing grid voltage oriented control scheme.

1.7 THESIS OUTLINE

This thesis organized in 7 chapters. The each individual chapter has their own significance.

The chapter 2 includes the basic theory of wind energy. This chapter covers the mathematical model of wind turbine and wind powers used to rotate the turbine. This chapter include the various types of wind energy conversion system and also highlighted the advantages and disadvantages of the different types of WECS. The power curve of wind turbine also demonstrates the relation between the wind speed and the power of turbine, and this chapter also include the MPPT scheme used for this thesis.

The chapter 3 includes the basics of PMSG and the dynamic equations of the PMSG in a rotating frame. The PMSG operating zones were also summarise in this chapter. In this chapter the MSC and GSC controlling schemes are discussed. The chapter 4 has the simulation results and analysis for Steady State Stand alone operation of PMSG.

The chapter 5 includes the LCL filter design steps and constraints alongwith Model Predictive control of PMSG. The chapter 6 includes the Model Predictive Control (MPC) controller design steps are elaborated.

The chapter 7 is last chapter which includes the conclusion of this thesis and have some points related to future works.

CHAPTER 2

THEORY OF WIND ENERGY SYSTEMS

2.1 OVERVIEW OF WIND ENERGY

Wind energy is clean and sustainable. It is one of the fastest growing renewable energy resources. The conversion of wind kinetic energy into electric energy is of a multidisciplinary nature, involving aerodynamics, mechanical systems, electric machines, power electronics, control theory, and power systems. Over the last twenty years, renewable energy sources have been attracting great attention due to the cost increase, limited reserves, and adverse environmental impact of fossil fuels. In the meantime, technological advancements, cost reduction, and governmental incentives have made some renewable energy sources more competitive in the market. Among them, wind energy is one of the fastest growing renewable energy sources.

Wind energy has been used for hundreds of years for milling grains, pumping water, and sailing the seas. The use of windmills to generate electricity can be traced back to the late nineteenth century with the development of a 12 kW DC windmill generator. It is, however, only since the 1980s that the technology has become sufficiently mature to produce electricity efficiently and reliably. Over the past two decades, a variety of wind power technologies have been developed, which have improved the conversion efficiency of and reduced the costs for wind energy production. The size of wind turbines has increased from a few kilowatts to several megawatts each. In addition to on-land installations, larger wind turbines have been pushed to offshore locations to harvest more energy and reduce their impact on land use and landscape.

This chapter provides an overview of wind energy conversion systems (WECS) and their related technologies. The aim of the chapter is to provide a background on several aspects related to this exciting technology and market trends such as installed capacity, growth rate, and costs.

2.1.1 Stand-Alone and Grid-Connected Applications

The wind turbines can operate as stand-alone units of small power capacity to power villages, farms, and islands where access to the utility grid is remote or costly. Since the power generated from the wind is not constant, other energy sources are normally required in stand-alone systems. It is common that a stand-alone wind energy system operates with diesel generators, photovoltaic energy systems, or energy storage systems to form a more reliable

distributed generation (DG) system. Due to its limited applications, stand-alone wind power constitutes only a small fraction of the total installed wind capacity in the world.

2.1.2 On-Land and Offshore Applications

Large capacity wind farms have traditionally been placed on land for several reasons: easy construction, low maintenance cost, and proximity to transmission lines. On the other hand, offshore wind farms are also commercially viable. One of the main reasons for the offshore wind farm development is the lack of suitable wind resources on land. This is particularly the case in densely populated areas such as in some European countries. Another important reason is that the offshore wind speed is often significantly higher and steadier than that on land. Considering that the energy obtained by wind turbines is proportional to the cube of the wind speed, the turbines can capture more energy when operating offshore. Moreover, the environmental impact, such as audible noise and visual impact, is minimal in offshore applications. These factors are the primary drivers for the development of offshore wind turbine technology. The increase of turbine power capacity and reduction of maintenance costs are crucial for offshore wind farms. The average power rating of installed offshore wind turbines was around 2.9 MW as of 2009, and the power rating of the generators for offshore applications is expected to increase in the next decade. To reduce the maintenance cost, direct-driven wind turbines using low-speed permanent magnet synchronous generators (PMSGs) is a viable technology. The maintenance costs for these turbines are reduced due to elimination of the gearbox and brushes. For offshore wind farms, the foundation and transmission cable add significantly to the total project costs. The wind resources, capital/maintenance costs, and energy production are the critical factors to be considered in the development of offshore wind farms.

2.2 WIND TURBINE TECHNOLOGY

The wind turbine is one of the most important elements in wind energy conversion systems. Over the years, different types of wind turbines have been developed. This section provides an overview of wind turbine technologies, including horizontal/ vertical-axis turbines and fixed/variable-speed turbines.

2.2.1 Horizontal- and Vertical-Axis Wind Turbines

Wind turbines can be categorized based on the orientation of their spin axis into horizontal- axis wind turbines (HAWT) and vertical-axis wind turbines (VAWT). In horizontal-axis wind turbines, the orientation of the spin axis is parallel to the ground. The tower elevates the nacelle to provide sufficient space for the rotor blade rotation and to reach better wind conditions. The nacelle supports the rotor hub that holds the rotor blades and also houses the

gearbox, generator, and, in some designs, power converters. The industry standard HAWT uses a three blade rotor positioned in front of the nacelle, which is known as upwind configuration. However, downwind configurations with the blades at the back can also be found in practical applications. Turbines with one, two, or more than three blades can also be seen in wind farms.

In vertical-axis wind turbines, the orientation of the spin axis is perpendicular to the ground. The turbine rotor uses curved vertically mounted airfoils. The generator and gearbox are normally placed in the base of the turbine on the ground. The rotor blades of the VAWT have a variety of designs with different shapes and number of blades. The VAWT normally needs guide wires to keep the rotor shaft in a fixed position and minimize possible mechanical vibrations.

2.2.2 Fixed- and Variable-Speed Turbines

Wind turbines can also be classified into fixed-speed and variable-speed turbines. As the name suggests, fixed-speed wind turbines rotate at almost a constant speed, which is determined by the gear ratio, the grid frequency, and the number of poles of the generator. The maximum conversion efficiency can be achieved only at a given wind speed, and the system efficiency degrades at other wind speeds. The turbine is protected by aerodynamic control of the blades from possible damage caused by high wind gusts. The fixed-speed turbine generates highly fluctuating output power to the grid, causing disturbances to the power system. This type of turbine also requires a sturdy mechanical design to absorb high mechanical stresses. On the other hand, variable-speed wind turbines can achieve maximum energy conversion efficiency over a wide range of wind speeds. The turbine can continuously adjust its rotational speed according to the wind speed. In doing so, the tip speed ratio, which is the ratio of the blade tip speed to the wind speed, can be kept at an optimal value to achieve the maximum power conversion efficiency at different wind speeds.

2.2.3 Stall and Pitch Aerodynamic Power Controls

Turbine blades are aerodynamically optimized to capture the maximum power from the wind in normal operation with a wind speed in the range of about 3 to 15 m/s. In order to avoid damage to the turbine at a high wind speed of approximately 15 to 25 m/s, aerodynamic power control of the turbine is required. There are a number of different ways to control aerodynamic forces on the turbine blades, the most commonly used methods being pitch and stall controls. The simplest control method is the passive stall control, in which the blades of the turbine are designed such that when the wind speed exceeds the rated wind speed of about 15 m/s, air turbulence is generated on the blade surface that is not facing the wind. The turbulence reduces the lift force on the blade, resulting in a reduction in captured power, which prevents turbine

damage. Since there are no mechanical actuators, sensors, or controllers, the power control by passive stall is robust and cost-effective.

The main disadvantage of this method is the reduction in power-conversion efficiency at low wind speeds. Passive stall is normally used in small-to-medium-size WECS. Pitch control is normally used for large wind turbines. During normal operating conditions with the wind speed in the range from 3 to 15m/s, the pitch angle is set at its optimal value to capture the maximum power from the wind. When the wind speed becomes higher than the rated value, the blade is turned out of the wind direction to reduce the captured power. The blades are turned in their longitudinal axis, changing the pitch angle through a hydraulic or electromechanical device located in the rotor hub attached to a gear system at the base of each blade. As a result, the power captured by the turbine is kept close to the rated value of the turbine. are pitched completely out of the wind (fully pitched or feathered), and thus no power is captured.

This method is effective in protecting the turbine and the supporting structure from damage caused by strong wind gusts. When the blades are fully pitched, the rotor is locked by a mechanical brake, and the turbine is in the parking mode. The major disadvantages of pitch control include the extra complexity and cost due to the pitch mechanism, and the power fluctuations during strong wind gusts due to slow pitch-control dynamics. Another aerodynamic power control method is active stall control, which is essentially a pitch-control mechanism with the difference that the angle of attack of the blade is turned into the wind, causing stall (turbulence on the back of the blade), instead of being turned out of the wind. Active stall mechanism is an improvement over the passive stall, and can improve the power conversion efficiency at low wind speeds and limit the maximum captured power in high wind gusts. However, as with pitch controlled WECS, it is a complex system. Active stall methods are normally used in medium-to-large-size WECS.

2.3 WIND ENERGY CONVERSION SYSTEM CONFIGURATIONS

The generator and power converter in a wind energy conversion system are the two main electrical components. Different designs and combinations of these two components lead to a wide variety of WECS configurations, which can be classified into three groups:

- (1) fixed-speed WECS without power converter interface
- (2) WECS using reduced-capacity converters
- (3) full-capacity converter operated WECS

2.3.1 Fixed-Speed WECS without Power Converter Interface

A typical configuration of WECS without a power converter is where the generator is connected to the grid through a transformer. A squirrel cage induction generator (SCIG) is exclusively used in this type of WECS, and its rotational speed is determined by the grid frequency and the number of poles of the stator winding. For a four-pole megawatt generator connected to a grid of 60 Hz, the generator operates at a speed slightly higher than 1800 rpm. At different wind speeds, the generator speed varies within 1% of its rated speed. The speed range of the generator is so small that this system is often known as a fixed-speed WECS, as mentioned earlier.

A gearbox is normally required to match the speed difference between the turbine and generator such that the generator can deliver its rated power at the rated wind speed. This configuration requires a soft starter to limit high inrush currents during system start-up, but the soft starter is bypassed by a switch after the system is started. During normal operation, the system does not need any power converter. A three phase capacitor bank is usually required to compensate for the reactive power drawn by the induction generator.

2.3.2 Variable-Speed Systems with Reduced-Capacity Converters

Variable-speed operation has a series of advantages over fixed-speed wind systems. It increases the energy conversion efficiency and reduces mechanical stress caused by wind gusts. The latter has a positive impact on the design of the structure and mechanical parts of the turbine and enables the construction of larger wind turbines. It also reduces the wear and tear on the gearbox and bearings, expanding the life cycle and reducing the maintenance requirements. The main drawback of variable-speed WECS is the need for a power converter interface to control the generator speed, which adds cost and complexity to the system. However, the power converter decouples the generator from the grid, which enables the control of the grid-side active and reactive power.

2.4 GRID CODE

Grid codes have been developed and enforced in many countries for many years. They ensure applications of uniform standards for power systems and provide a framework for manufacturers to develop their equipment. Grid codes are usually based on the experience acquired through the operation of power systems and may vary from one utility to another. Differences in various grid codes also stem from regional and geographical conditions. However, the key elements in the different grid codes remain similar across the globe since their ultimate goal is to ensure safe, reliable, and economic operation of the power system. Due to the rapid

development of renewable energies and their integration into the grid, the grid codes in many countries have been updated to address issues related to renewable energy power generation. According to the updated grid codes, wind farms tend to be considered as power generation plants, which should perform in a similar manner to conventional power-generation plants. The main elements in the grid codes include fault ride-through requirements, active/reactive power control, frequency/ voltage regulation, power quality, and system protection.

2.5 WIND TURBINE COMPONENTS

A wind energy conversion system (WECS) transforms wind kinetic energy to mechanical energy by using rotor blades. This energy is then transformed into electric energy by a generator. The system is made up of several components, participating directly in the energy conversion process. There are also other components that assist the system to achieve this task in a controlled, reliable, and efficient way. In order to better understand the process of wind energy conversion, descriptions of the major parts of a wind turbine are given in this chapter. Since the energy source for a WECS is wind kinetic energy, wind speed plays a key role in several aspects of the conversion process, especially in relation to the maximum power output. The power output of a wind turbine can be regulated by adjusting the blade pitch angle or by controlling the generator's torque or speed. These power control methods are essential to ensure a maximum power output over a wide range of wind speeds. They also enable reliable and safe operation, protecting the mechanical and structural parts of the wind turbine from damage during strong wind gusts.

A wind turbine is composed of several parts to achieve kinetic-to-electric energy conversion. There are several variants to this layout of components, particularly for direct-drive (gearless) wind turbines. The wind kinetic energy is converted to mechanical energy by the blades mounted on the rotor hub. The rotor hub is installed on the main shaft, also known as the low speed shaft. The mechanical energy is transmitted through the drive train (shafts, bearings, and gearbox) to the generator, which converts mechanical energy into electric energy. This conversion is usually assisted by a power converter system which delivers the power from the generator to the grid. Most of the wind turbine components are enclosed in a nacelle on top of the tower. There are other parts that are not directly involved in the power conversion but are important to ensure the proper, efficient, and reliable operation of the system. Examples include the pitch system, yaw system, mechanical brake, wind speed and direction sensors, power distribution cables, heat dissipation/exchange system, lightning protection system, and structural components such as the tower, foundation, and nacelle enclosure. Large wind turbines are also equipped with an uninterruptable power supply or backup energy system that ensures uninterrupted operation of essential parts such as the control system, pitch drive, and brakes.

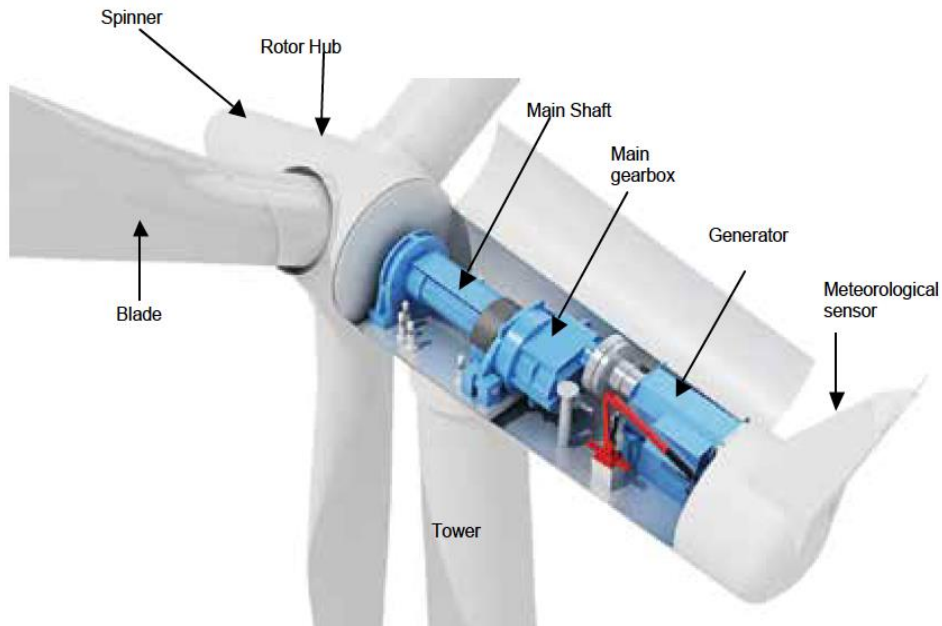


Fig.2.1 Component of wind turbine

In direct-drive (gearless) turbines, the absence of the gearbox and high-speed shaft leads to a more compact drive train and, hence, a shorter nacelle. However, the wider diameter of low-speed generators requires a taller nacelle structure. This phenomenon is more evident in wound rotor synchronous generators than permanent-magnet synchronous generators.

2.5.1 Turbine Blade

The blade is the most distinctive and visible component of a wind turbine. It is also responsible for carrying out one of the most essential tasks of the energy conversion process: transforming the wind kinetic energy into rotational mechanical energy. Blades have greatly evolved in aerodynamic design and materials from the early windmill blades made of wood and cloth. Modern blades are commonly made of aluminium, fibreglass, or carbon-fibre composites that provide the necessary strength-to-weight ratio, fatigue life, and stiffness while minimizing the weight.

Although single- and two-bladed wind turbines have found practical applications, the three-blade rotor is considered the industry standard for large wind turbines. Turbines with fewer blades operate at higher rotational speeds. This is an advantage from the drive train point of view since they require a gearbox with a lower gear ratio, which translates into lower cost. In addition, fewer blades imply lower costs. However, acoustic noise increases proportionally to the blade tip speed. Therefore, acoustic noise is considerably higher for single- and two-bladed turbines,

which is considered an important problem, particularly in populated areas. Single-blade turbines have an asymmetrical mechanical load distribution. The turbine rotors are aerodynamically unbalanced, which can cause mechanical vibrations. Moreover, higher rotational speed imposes more mechanical stress on the blade, turbine structure, and other components, such as bearings and gearbox, leading to more design challenges and lower life span.

Rotors with more than three blades are not common since they are more expensive (more blades). Operating at lower rotational speeds requires a higher gear ratio. The lagging wind turbulence of one blade can affect the other blades since they are closer to each other. Hence, the three-blade rotor presents the best trade-off between mechanical stress, acoustic noise, cost, and rotational speed for large wind turbines.

The aerodynamic operating principle of the turbine blade is similar to the wings of an airplane. It can be explained by Bernoulli's principle, which states that as the speed of a moving fluid (liquid or gas) increases, the pressure within the fluid decreases. The curved shape of the blade creates a difference between the wind speed above (v_{w1}) and below (v_{w2}) the blade. The airflow above the blade is faster than the one below ($v_{w1} > v_{w2}$), which, according to the Bernoulli's principle, has the inverse effect on the pressure ($p_{w2} > p_{w1}$). The pressure difference between the top and bottom of the blade results in a net lift force F_w on the blade. The force applied at a certain distance of a pivot (the turbine shaft) produces torque, which creates the rotational movement of the wind turbine.

One of the important parameters for controlling the lift force of the blade is the angle of attack a , which is defined as the angle between the direction of the wind speed v_w and the cord line of the blade. For a given blade, its lift force F_w can be adjusted by a . When this angle is equal to zero, no lift force or torque will be produced, which often occurs when the wind turbine is stopped (parked) for maintenance or repair.

The power of an air mass flowing at speed v_w through an area can be calculated by

$$P_w = \frac{1}{2} \rho A v_w^3 \quad (2.1)$$

where ρ is the air density in kg/m³, A is the sweep area in m², and v_w is the wind speed in m/s. The air density ρ is a function of air pressure and air temperature. At sea level and temperature of 15°C, air has a density of approximately 1.2 kg/m³. The wind power captured by the blade and converted into mechanical power can be calculated by

$$P_m = \frac{1}{2} \rho A v_w^3 C_p \quad (2.2)$$

Where, C_p is the power coefficient of the WT. This coefficient has a theoretical maximum value of 0.59 according to the Betz limit. With today's technology, the power coefficient of a modern turbine usually ranges from 0.2 to 0.5, which is a function of rotational speed and number of blades. For a three-blade turbine with a rotor diameter of 82 m and power coefficient of $C_p = 0.48$, the captured power is 2 MW at a wind speed of 12 m/s and air density of $\rho = 1.225 \text{ kg/m}^3$.

Additional blade requirements, such as lightning protection, audible noise reduction, transportation, optimum shape and weight, as well as manufacturability, make the blade design a challenging task. Blade manufacturing is a tedious process and requires careful planning and large factory space. It is a combination of automated and manual processes. Considering that the blade length of a 5 MW wind turbine is as long as a Boeing 747. The blade transportation and installation are other great challenges. The transportation and related costs are one of the reasons why the size of the blade are expected to increase at a slower pace in the future compared to the rapid developments experienced in the last decade.

2.5.2 Pitch Mechanism

The pitch mechanism in large wind turbines enables the rotation of the blades on their longitudinal axis. It can change the angle of attack of the blades with respect to the wind, by which the aerodynamic characteristics of the blade can be adjusted. This provides a degree of control over the captured power to improve conversion efficiency or to protect the turbine. When the wind speed is at or below its rated value, the angle of attack of the blades is kept at an optimal value, at which the turbine can capture the maximum power available from the wind. When the wind speed exceeds the rated value, the pitch mechanism is activated to regulate and limit the output power, thus keeping the power output within the designed capability. For this purpose, a pitch range of around 20 to 25 degrees is usually sufficient. When the wind speed increases further and reaches the limit of the turbine, the blades are completely pitched out of the wind (fully pitched or feathering), and no power will be captured by the blades. The wind turbine is then shut down and protected. The pitch mechanism can be either hydraulic or electric. Electric pitch actuators are more common nowadays since they are simpler and require less maintenance. Traditionally, all blades on the rotor hub are pitched simultaneously by one pitch mechanism. Modern wind turbines are often designed to pitch each blade individually, allowing an independent control of the blades and offering more flexibility. The pitch system is usually placed in the rotor hub together with a backup energy storage system for safety purposes (an accumulator for the hydraulic type or a battery for the electric type).

2.5.3 Gearbox

The rotor of a large three-blade wind turbine usually operates in a speed range from 6-20 rpm. This is much slower than a standard 4- or 6-pole wind generator with a rated speed of 1500 or 1000 rpm for a 50 Hz stator frequency and 1800 or 1200 rpm for a 60 Hz stator frequency. Therefore, a gearbox is necessary to adapt the low speed of the turbine rotor to the high speed of the generator. The gearbox conversion ratio (r_{gb}), also known as the gear ratio, is designed to match the high-speed generator with the low-speed turbine blades. For a given rated speed of the generator and turbine, the gearbox ratio can be determined by

$$r_{gb} = \frac{n_M}{n_m} = \frac{(1-s).60.f_s}{P.n_M} \quad (2.3)$$

Where n_m and n_M are the generator and turbine rated speeds in rpm, s is the rated slip, f_s is the rated stator frequency in Hz, and P is the number of pole pairs of the generator. The rated slip is usually less than 1% for large induction generators, and zero for synchronous generators. Considering the rated slip of 1% for an induction generator, the gear ratio as a function of the rated turbine speed for different pole numbers and rated stator frequencies.

2.5.4 Rotor Mechanical Brake

A mechanical brake is normally placed on the high-speed shaft between the gearbox and the generator, but there are some turbines in which the brake is mounted on the low-speed shaft between the turbine and gearbox. The main advantage of placing the brake on the high-speed shaft is that it handles much lower braking torque. The brake is normally used to aid the aerodynamic power control (stall or pitch) to stop the turbine during high speed winds or to lock the turbine into a parking mode during maintenance. Hydraulic and electromechanical disc brakes are often used.

To minimize the wear and tear on the brake and reduce the stress on drive train during the braking process, most large wind turbines use the aerodynamic power control to reduce the turbine speed to a certain level or zero, and then the mechanical brake to stop or lock the wind turbine. However, the mechanical brake should be able to bring the turbine rotor to a complete stop at any wind speeds.

2.5.5 Generator

The conversion of rotational mechanical energy to electric energy is performed by the generator. Different generator types have been used in wind energy systems over the years. These include the squirrel cage induction generator (SCIG), doubly fed induction generator

(DFIG), and synchronous generator (SG) (wound rotor and permanent magnet) with power ratings from a few kilowatts to several megawatts. The SCIG is simple and rugged in construction. It is relatively inexpensive and requires minimum maintenance. Traditional direct grid-connected wind energy systems are still available in today's market. All these turbines use SCIGs and operate at a fixed speed. Two-speed SCIGs are also commercially available, in which a tapped stator winding can be adapted to change the pole pairs to allow two-speed operation. The SCIGs are also employed in variable-speed wind energy systems. To date, the largest SCIG wind energy systems are around 3.5 MW in offshore wind farms. The DFIG is the current workhorse of the wind energy industry. The stator of the generator is connected to the grid directly, while the rotor is interfaced with the grid through a power converter system with reduced power capacity. The DFIG typically operates about 30% above and below synchronous speed, sufficient for most wind speed conditions. It also enables generator-side active power control and grid-side reactive power control. The reduced-capacity converter is less expensive and requires less space, which makes the DFIG WECS popular in today's market.

2.5.6 Yaw Drive

The main function of the yaw drive is to maximize the captured wind energy by keeping the turbine facing into the wind. It usually consists of more than one electric motor drive, yaw gear, gear rim, and bearing, as can be observed in Fig.2.5, where a four drive yaw system is illustrated. A set of yaw brakes are disposed around the yaw rim to lock the position of the turbine when facing the wind or during maintenance. The yaw drive uses a planetary gear to lower the rotating speed of the yaw gear. All the motors are commanded by the same signals and lock after turning the wind turbine into the desired position. The yaw system typically needs to generate torque from 10,000 to 70,000 Nm to turn the nacelle.

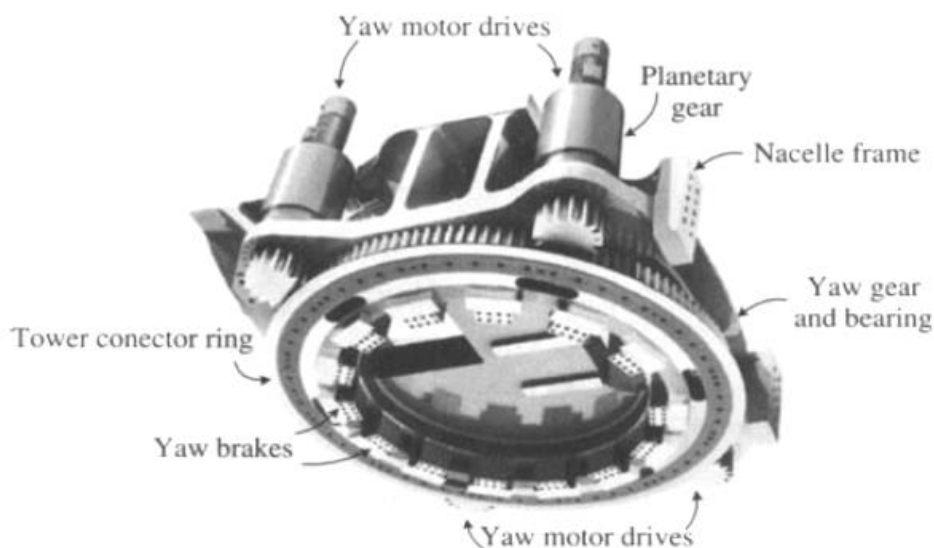


Fig.2.2 Yaw drive of wind turbine

2.5.7 Tower and Foundation

The main function of the tower is to support the nacelle and the turbine rotor, and provide the rotor with the necessary elevation to reach better wind conditions. Most towers for wind turbines are made of steel. Concrete towers or towers with a concrete base and steel upper sections are sometimes used as well. The height of the tower increases with the turbine power rating and rotor diameter. In addition, the tower must be at least 25 to 30 m high to avoid turbulence caused by trees and buildings. Small wind turbines have towers as high as a few blade rotor diameters.

However, the towers of medium and large turbines are approximately equal to the turbine rotor diameter as shown in Fig.2.6. The highest tower to date is a 160 m steel lattice tower for a 2.5 MW wind turbine. The tower also houses the power cables connecting the generator or power converters to the transformer located at the base of the tower. In some cases, the transformer is also included in the nacelle and the cables connect the transformer to the wind farm substation. In large multi megawatt turbines, the power converters may be located at the base of tower to reduce the weight and size of the nacelle. The stairs to the nacelle for maintenance are often attached along the inner wall of the tower in large wind turbines.

2.5.8 Wind Sensors (Anemometers)

The pitch/stall and yaw control systems require wind speed and direction measurements, respectively. The pitch/stall control needs the wind speed to determine the angle of attack of the blade for optimal operation. The yaw control requires the wind direction to face the turbine into the wind for maximum wind power capture. In addition, in variable speed turbines, the wind speed is needed to determine the generator speed for maximum power extraction.

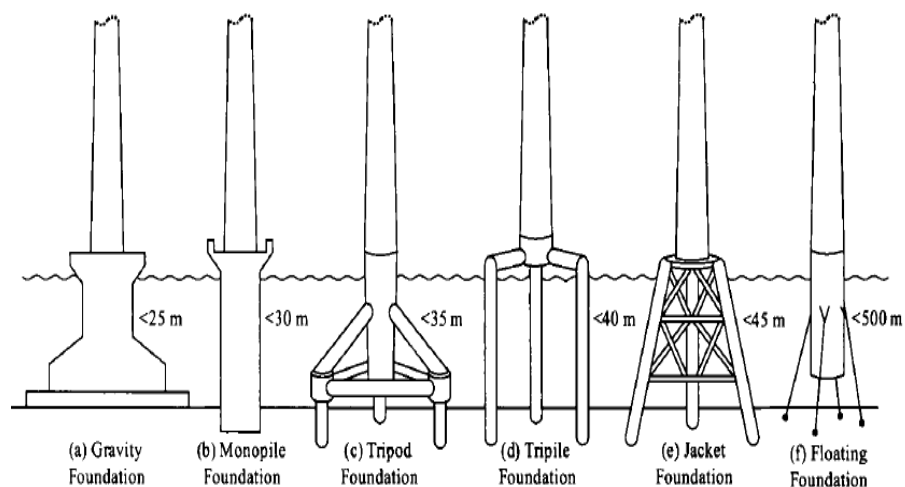


Fig.2.3 Foundations for off shore wind turbines

Most large wind turbines are equipped with sensors, also referred to as anemometer, for wind data collection and processing. The wind speed sensor is usually made of a three-cup vertical-axis micro turbine driving an optoelectronic rotational speed transducer. The wind direction is measured by a wind vane connected to an optoelectronic angle transducer. These are the main components of a wind measurement system, and are usually located on the top back part of the nacelle. More than one sensor system may be used in a wind turbine for more reliable and accurate measurements. Ultrasonic anemometers are also used in practical wind turbines. They measure the wind speed by emitting and receiving acoustic signals through the air and monitoring the transmission time. Several emitters and receptors are disposed in such a way that a three-dimensional measurement can be made. The transmission time is affected by both wind speed and direction. With a given physical distribution of the sensors, the wind speed and direction can be computed from the propagation times. The ultrasonic anemometers are more accurate and reliable than the mechanical ones with moving parts. However, they are more expensive. An ultrasonic anemometer is situated on the top of the nacelle of a modern wind turbine.

2.6 WIND ENERGY CONVERSION SYSTEM CONFIGURATION

In the wind energy conversion system (WECS) there are two main electrical components, one is generator and the other is power converters. According to these two components the various configuration of WECS are formed and classified in to five groups [11].

- (a) Type 1: Fixed Speed ($\pm 1\%$) WECS with squirrel cage induction generator (SCIG).
- (b) Type 2: Semi Variable Speed ($\pm 10\%$) WECS with wound rotor induction generator (WRIG)
- (c) Type 3: Semi Variable Speed ($\pm 30\%$) WECS with doubly fed induction generator (DFIG)
- (d) Type 4: Full Variable Speed (0-100%) WECS with SCIG, wound rotor induction generator (WRSG) and permanent magnet synchronous speed (PMSG)
- (e) Type 5: Full Variable Speed (0-100%) WECS with WRSG

2.6.1 Type 1: Fixed Speed ($\pm 1\%$) WECS Configuration

In this configuration system the generator is connected to the grid through a soft starter. This is the oldest and very old technology, developed in 1970s, called 'Danish' concept. The generator speed varies within 1% around the synchronous speed at different wind speed. After the starting of system, the soft startup system is bypassed by a switch and system run over without power converter. The type 1 configuration is shown in figure 2.1.

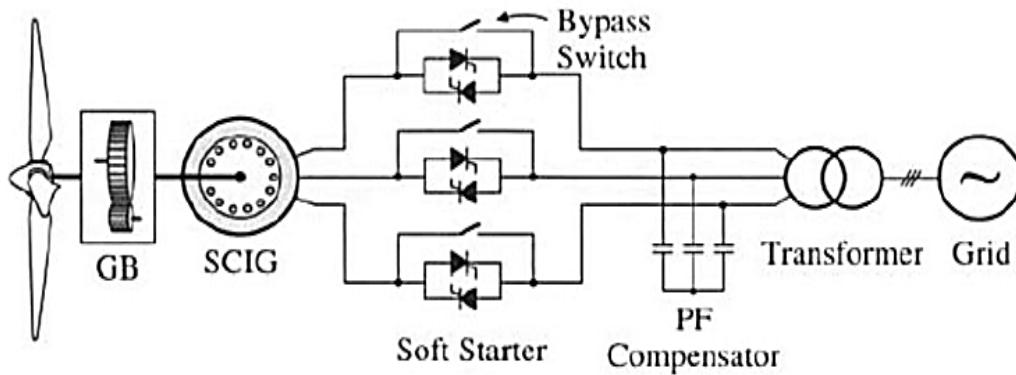


Figure 2.4 Type 1: Fixed Speed ($\pm 1\%$) WECS with SCIG

Advantages-

- (a) Low Initial Cost
- (b) Simple construction
- (c) Reliable operation

Disadvantages-

- (a) Wind Speed variations effect the grid
- (b) Conversion efficiency is low
- (c) Severe mechanical stress on the mechanical components during grid faults
- (d) Additional hardware require to comply with the grid codes.

2.6.2 Type 2: Semi Variable Speed ($\pm 10\%$) WECS Configuration

The variable Speed ($\pm 10\%$) of its rated speed can achieve by varying the rotor resistance, which affects the speed and torque characteristic. This system is also called 'Optislip control'. The rotor resistance can made variable with the power converter (diode rectifier and chopper). The type 2 WECS configuration is shown in figure 2.2.

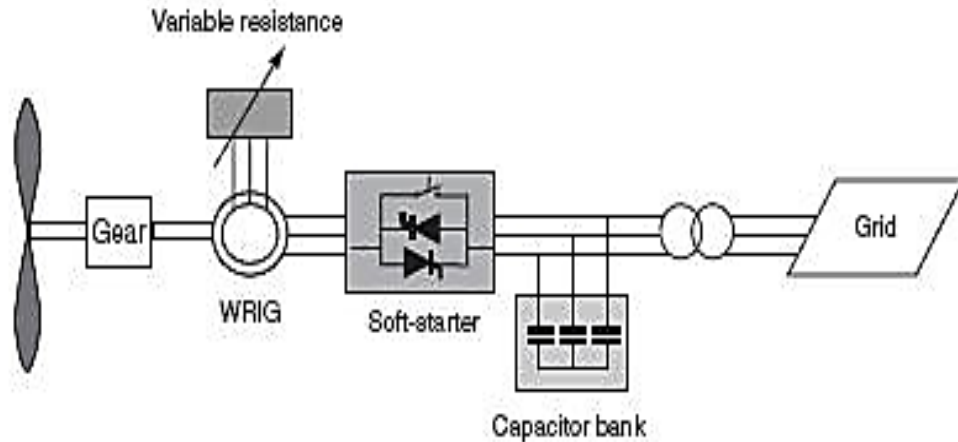


Figure 2.5 Type 2: Semi-variable speed ($\pm 10\%$) WECS with WRIG

Advantages-

- (a) Conversion efficiency increase
- (b) Mechanical stress reduce due to wind gust
- (c) Reduce the maintenance require
- (d) Increase the life cycle

Disadvantages-

- (a) Energy losses in rotor resistance
- (b) Limited speed of operation
- (c) Low energy conversion efficiency

2.6.3 Type 3: Semi Variable Speed ($\pm 30\%$) WECS Configuration

This is the configuration which is extensively used in current scenario of wind market (more than 50% share). In this configuration the DFIG used for conversion, and the power flow from the generator is fed to grid through both the stator and rotor windings. Power converter with rated 30% of generator power rating embedded with rotor circuit to maintain the bidirectional power flow in the rotor circuit and increase the speed range of generator. The type 3 WECS configuration is shown in figure 2.3. The power converter connected to the rotor windings through slip rings and brushes.

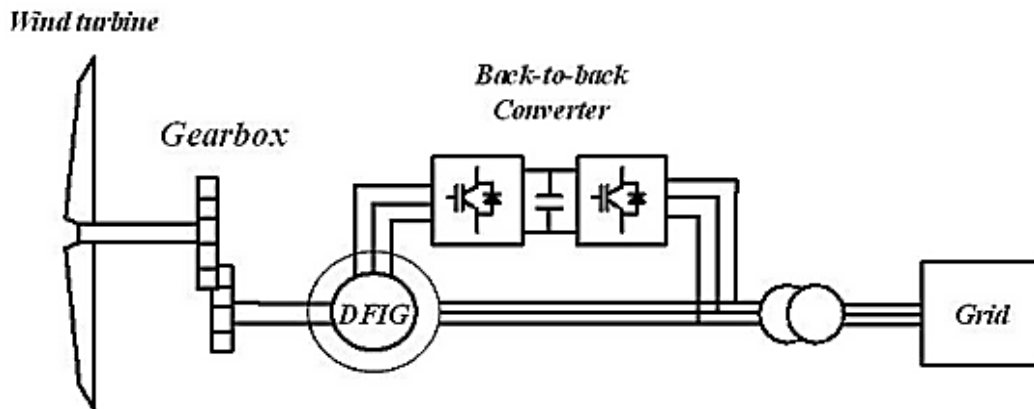


Figure 2.6 Type 3: Semi variable speed ($\pm 30\%$) WECS configuration with DFIG

Advantages-

- (a) Extended speed range as compare to type 1 and type 2 WECS
- (b) Robustness against power system turbulence
- (c) Improved dynamic performance

Disadvantages-

- (a) Fault ride through capability is limited due to limited rated power converters.
- (b) Regular maintenance require due to average life (6-12 months) of brushes.

2.6.4 Type 4: Full Variable Speed (0-100%) WECS Configuration

In this type of configuration the PMSG, WRSG, and SCIG generators are applicable with 100% power converter ratings. The 100% rating of power converters increase the size, cost and complexity of system. The power converters also handle the reactive power compensation and smooth grid connection. This configuration is shown in figure 2.4.

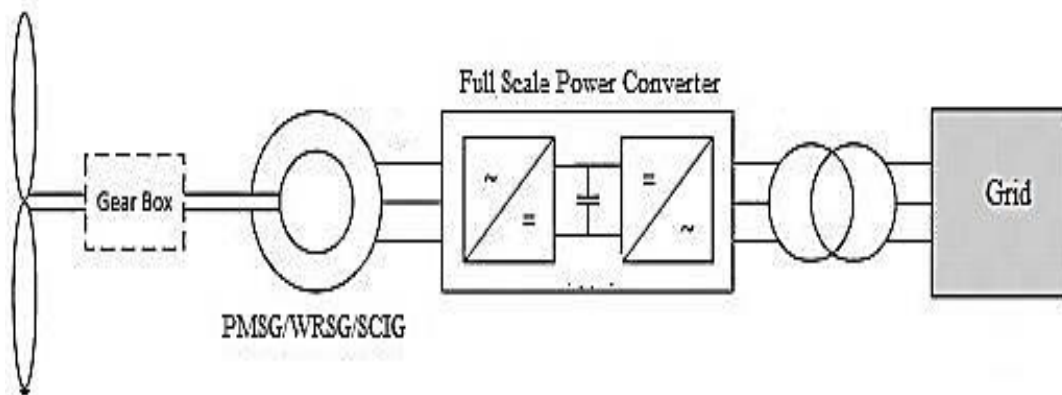


Figure 2.7 Type 4: Full variable speed (0-100%) WECS Configuration

The distributed drive train concept can be used in current scenario for megawatts turbines. The gear box drives multiple generators at high speeds and the higher power density can achieve due to this distributed drive train and multiple generators.

Advantages-

- (a) Higher wind energy conversion efficiency
- (b) FRT compliance good without any external hardware
- (c) Robustness high as compared to type 1, 2, and 3

Disadvantages-

- (d) Complexity increase
- (e) Power converter losses increase

2.6.5 Type 5: Full Variable Speed (0-100%) WECS Configuration with WRSG

This is the concept for replacing the electrical converter by mechanical converter, it is an old concept. In this configuration the mechanical converter is used to achieve the variable speed operation of the system. The generator is directly connected to grid. The Torque/speed converter converts the variable speed of wind turbine to a fixed speed and it is also known as variable ratio transmission (VRT). The figure 2.5 shows the full variable speed WECS with WRSG.

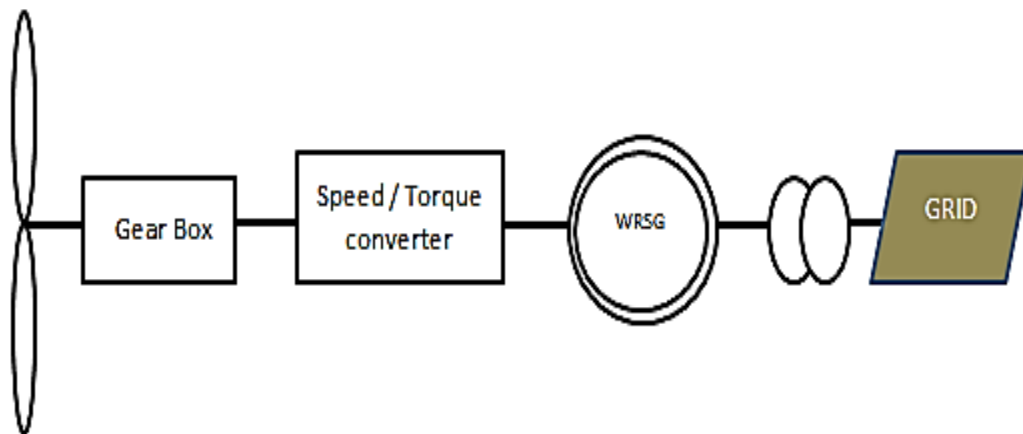


Figure 2.8 Type 5: Full variable speed (0-100%) WECS configuration with WRSG

Advantages-

- (f) Require mechanical converter instead of electrical converter
- (g) High energy conversion efficiency
- (h) Lower system cost and space due to mechanical converter

Disadvantages-

- (i) Limited knowledge of mechanical converter

2.7 MATHEMATICAL EXPRESSION OF WIND POWER AND WIND TURBINE POWER

Wind turbines generate electric power from the wind power, by driving the electrical generator. Wind strikes the wind turbine blade, creating the lift force which rotates the blade and this rotating blade rotates the generator through the shaft and gear box combinations. The gearbox increases the rotational speed to match the high rotational speed of the generator shaft.

A wind turbine extracts the kinetic energy of the wind through the blade of wind turbine as per the given formula [45, 42].

$$P_{wind} = 0.5\rho_{air}\pi R^2V_{wind}^3 \quad (2.1)$$

Where P_{wind} =Wind power; ρ_{air} =air density approximately 1.225 Kg/m³; R=Radius of wind turbine blade; and V_{wind} = speed of wind in m/s.

The equation 2.1 shows the power available in the wind, while the actual require for for wind energy conversion is the power to drive the turbine i.e. turbine power (P_m) which can be estimated by the coefficient called power coefficient C_p .

$$C_p = \frac{P_m(\text{wind turbine power})}{P_{wind}} \quad (2.2)$$

$$P_m = P_{wind} * C_p \quad (2.3)$$

The maximum value of C_p is obtained by theoretically and is called the Betz's limit, and this limit define that a turbine can never extract power from wind energy more than 59.3%. In practical the C_p values varying as per manufactures, in general it lies between the 25-48%. C_p is a function of Blade tip ratio λ and pitch angle β . The blade tip speed ratio λ defined as

$$\lambda = \frac{\omega_{turb}*R}{V_{wind}} \quad (2.4)$$

Where ω = rotational speed of wind turbine. And, C_p function may vary as per manufacturers, here taken accordingly [43].

$$C_p(\lambda, \beta) = C_1 \left(\frac{C_2}{\lambda_i} - C_3\beta - C_4 \right) e^{-\left(\frac{C_5}{\lambda_i}\right)} + C_6 \quad (2.5)$$

$$1/\lambda_i = \left(\frac{1}{\lambda + 0.08\beta} \right) - \frac{0.035}{\beta^3 + 1} \quad (2.6)$$

Where $C_1=0.5176$; $C_2=116$; $C_3=0.4$; $C_4=5$; $C_5=21$; $C_6=0.0068$.

The curve between C_p and λ at distinct values of β shown in figure 2.6. From the figure 2.6 it is clear that the maximum value of power conversion coefficient C_p obtain at $\beta=0$. At the point where the maximum value of C_p obtained known as optimal λ . From figure 2.6 the $C_{p,max}=0.48$ obtained at $\lambda_{opt}=8.1$ at pitch angle $\beta=0$.

The mechanical power of wind turbine converted to torque to be applied is converted by the given equation (2.7) with the help of turbine rotational speed.

$$T_m = P_m / \omega_{turb} \quad (2.7)$$

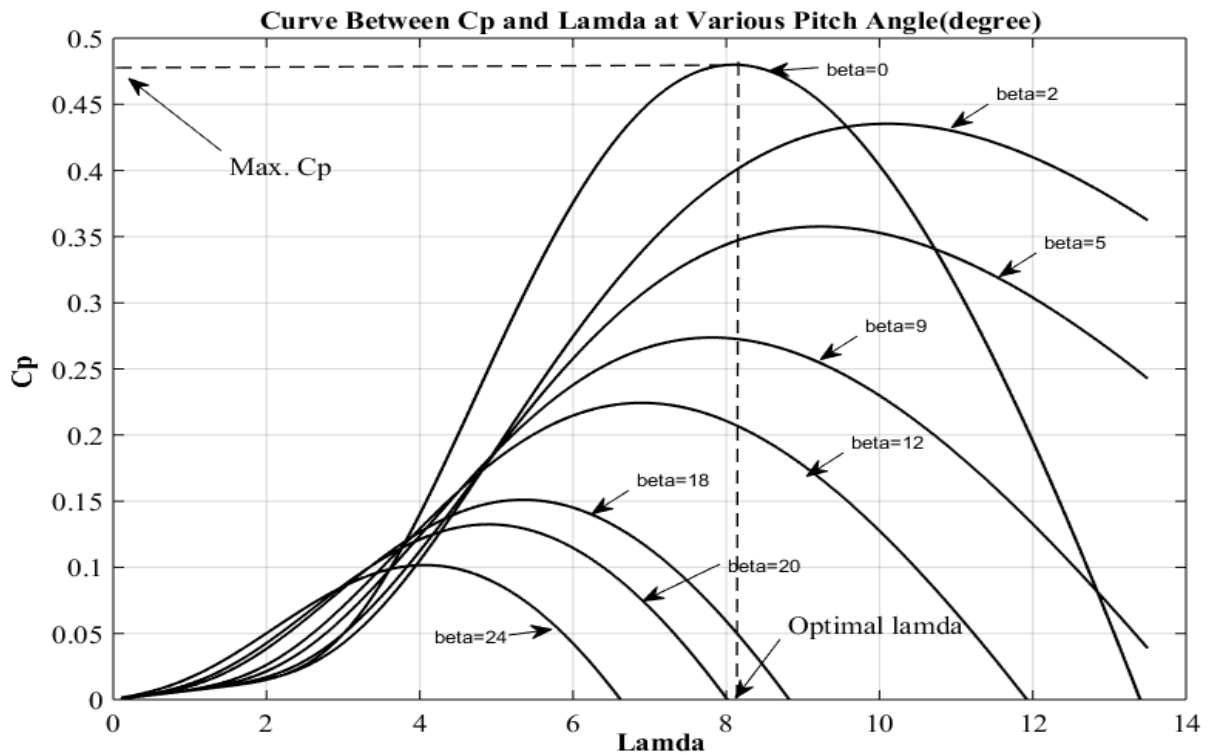


Figure 2.9 Curve between the C_p and Lamda (λ , tip speed ratio) at various Pitch angles

2.8 POWER CHARACTERISTIC OF A WIND TURBINE

The power characteristic of a wind turbine is the curve between the mechanical power of wind turbine and the wind speed. The wind power characteristics provided by the manufacturers and it is a type of certificate for the guaranteed performance of wind turbine [16]. A typical wind power characteristic has the three wind speed property says it cut-in wind speed, rated wind speed and cut-out wind speed. The power curve of a 3MW turbine [22] (ECO 100 Alstom-Ecotecnia) is shown in figure 2.7. The four operating zones of wind turbine are defined as per figure 2.7.

The cut-in wind speed is the speed where turbine starts to operate and deliver power. Below the cut-in speed the turbine is in parking mode (Region-1), no operation of turbine takes place. The rated wind speed is the point at which the turbine delivers the rated power. Region-2, start from the cut-in wind speed to rated wind speed is also known for the point tracking region, in this region the control of generator is main factor. Cut-out wind speed is the point before turbine is in operating condition but after this point turbine should be in parking mode to prevent the damage of turbine with high wind speed/gust, which is the region-4.

The region-3 is the region of aerodynamic control of blades, when the wind speed increase from the rated wind speed then the aerodynamic control of turbine blades are require maintaining the rated output power. Aerodynamic controls have the techniques like passive stall control, active stall control, and pitch control.

In this thesis the focus is on the maximum power tracking control also known as maximum power point tracking (MPPT).

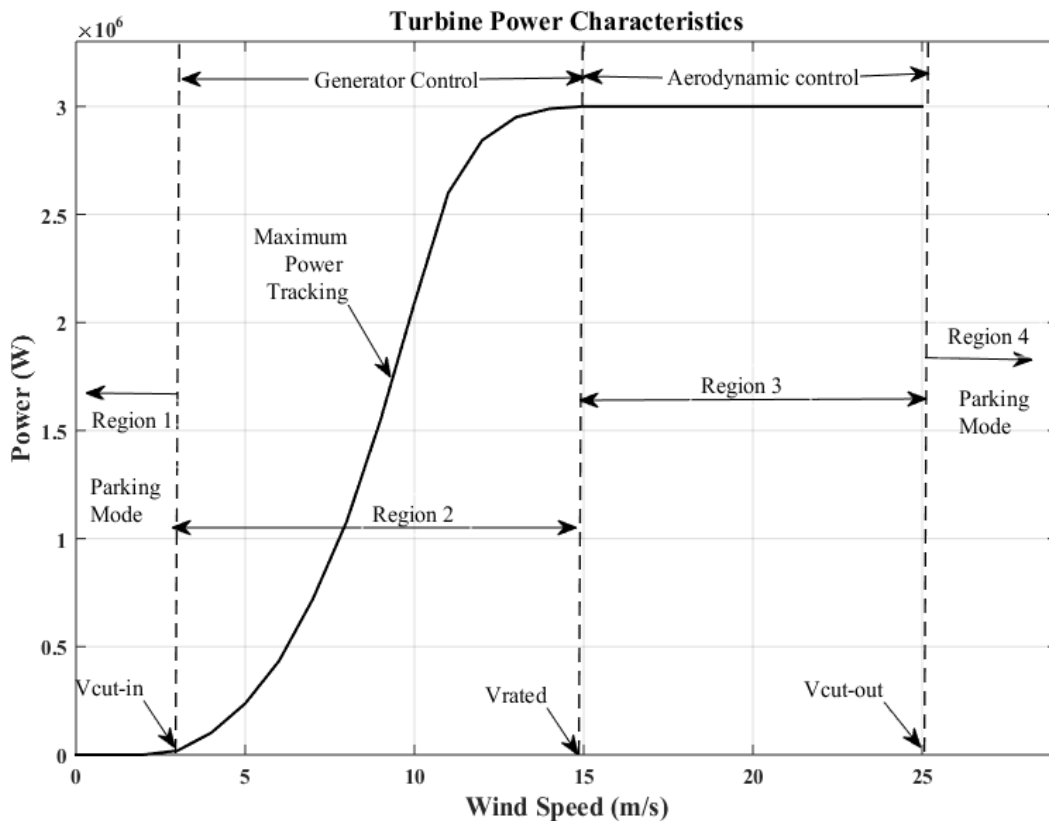


Figure 2.91 Turbine power characteristic of 3MW wind turbine

2.9 MAXIMUM POWER POINT TRACKING (MPPT) CONTROL

The control of the variable speed wind turbine below the rated wind speed is obtained by the tracking of maximum power point through the controlling of generator. The optimal speed and desired torque can be calculated by the relation of mechanical power, wind speed, and rotational speed of turbine to control the generator and to achieve the MPP. There are various controlling scheme for achieving the MPPT [11,16,44], like as-

- (a) MPPT with turbine power profile.
- (b) 2-MPPT with optimal tip speed ratio (Direct speed controller).
- (c) 3-MPPT with optimal torque control (Indirect speed controller).
- (d) Power signal feedback control.
- (e) Hill climbing search control.

And, there are many other advance technique based on artificial intelligent. In this thesis optimal tip speed ratio control technique is apply to achieve MPPT.

2.10 MPPT with Optimal Tip Speed Ratio

MPPT is a vital issue for a variable speed wind energy configuration to extract maximum wind energy. For a given wind speed, the reference speed of generator estimate accordingly to the optimal tip speed ratio, as per the mention relations.

$$\omega_m^* = \frac{\lambda_{opt} * V_{wind}}{R} \quad (2.8)$$

And,

$$\omega_m = N * \omega_{turb} \quad (2.9)$$

Where, ω_m^* is reference rotational speed of generator (mechanical), N is the ratio of gear to manipulate the low speed shaft to high speed shaft, and ω_{turb} is the rotational speed of wind turbine (low speed). The optimal tip speed ration control is shown in below figure 2.8.

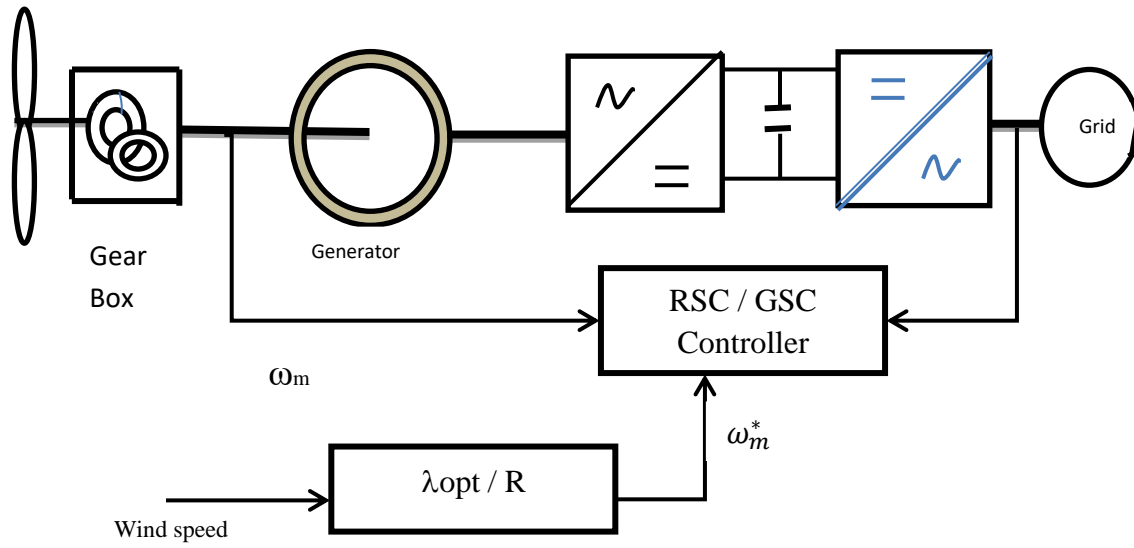


Figure 2.92 MPPT with optimal tip speed ratio

Chapter - 3

PERMANENT MAGNET SYNCHRONOUS GENERATOR

3.1 PMSG

In the PMSG, the rotor magnetic flux is generated by permanent magnets, and these generators are, therefore, brushless. Because of the absence of the rotor windings, a high power density can be achieved, reducing the size and weight of the generator. In addition, there are no rotor winding losses, reducing the thermal stress on the rotor. The drawbacks of these generators lie in the fact that permanent magnets are more expensive and prone to demagnetization.

Depending on how the permanent magnets are mounted on the rotor, the PMSG can be classified into surface-mounted and inset PM generators. In the surface-mounted PMSG, the permanent magnets are placed on the rotor surface. Figure 3-1 shows such a generator, where 16 magnets are evenly mounted on the surface of the rotor core, separated by non ferrite materials between two adjacent magnets. Since the permeability of the magnets is very close to that of the non ferrite materials, the effective air gap between the rotor core and stator is uniformly distributed around the surface of the rotor. This type of configuration is known as a non salient-pole PMSG.

3.1.1 Surface Mounted PMSG

The main advantage of the surface-mounted SG is its simplicity and low construction cost in comparison to the inset PMSG. However, the magnets are subject to centrifugal forces that can cause their detachment from the rotor and, therefore, the surface mounted PMSGs are mainly used in low-speed applications. In a direct-driven WECS, the synchronous generator with a high number of poles is used. The surface-mounted PMSG can have an external rotor in which the permanent magnets are attached to the inner surface of the rotor. In this case, the centrifugal forces help to keep the magnets attached to the rotor core.

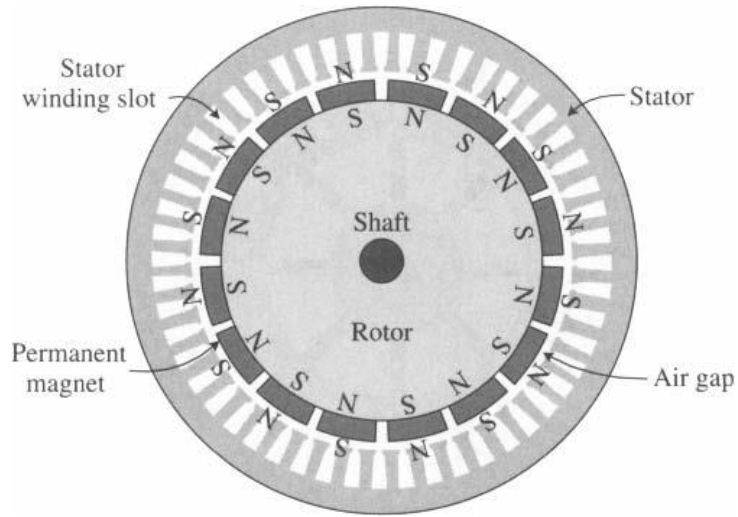


Fig 3-1 Surface-mounted non salient PMSG (sixteen-pole configuration)

3.1.2 Inset PMSG

In the inset PMSG, the permanent magnets are inset into the rotor surface as shown in Figure 3-2. The saliency is created by the different permeability of the rotor core material and magnets. This configuration also reduces rotational stress associated with centrifugal forces in comparison to the surface-mounted PMSG and, therefore, this type of generator can operate at higher rotor speeds.

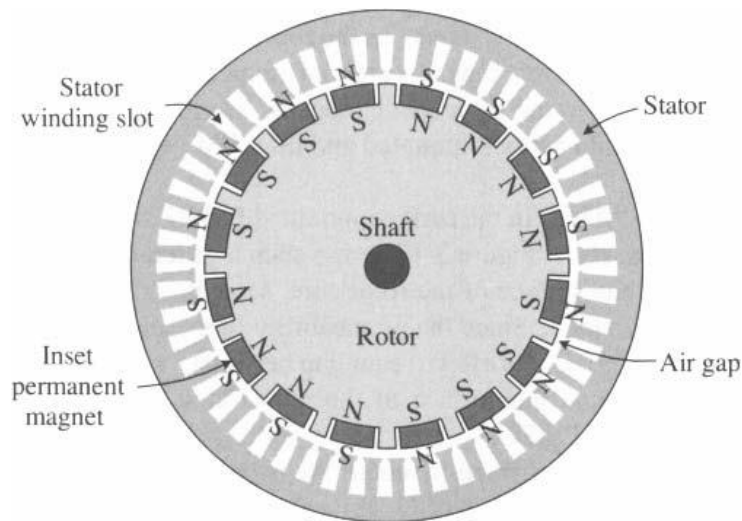


Fig 3-2 Inset PMSG with salient poles (four-pole configuration)

3.2 MATHEMATICAL MODELING OF PMSG

The general dq-axis model of a PMSG is used to simplify the analysis; the SG is normally modelled in the rotor field synchronous reference frame. The stator circuit of the dq-axis model is essentially the same as that of the induction generator, except that

- (a) The speed of the arbitrary reference frame ω in the IG model is replaced by the rotor speed ω_r in the synchronous frame.
- (b) The magnetizing inductance L_m is replaced by the dq-axis magnetizing inductances L_{dm} and L_{qm} of the synchronous generator. In a non-salient SG, the d- and q-axis magnetizing inductances are equal ($L_{dm} = L_{qm}$), whereas in the salient pole generators, d-axis magnetizing inductance is normally lower than the q-axis magnetizing inductance ($L_{dm} < L_{qm}$).
- (c) The dq-axis stator currents, i_{ds} and i_{qs} , flow out of the stator. This is based on the generator convention since most synchronous machines are used as generators.

To model the rotor circuit, the field current in the rotor winding is represented by a constant current source I_f in the d-axis circuit. In the PMSG, the permanent magnet that replaces the field winding can be modelled by an equivalent current source I_f with a fixed magnitude.

To simplify the SG model, the following mathematical manipulations can be performed. The voltage equations for the synchronous generator are given by

$$V_{ds} = -R_s * i_{ds} - \omega_r * \lambda_{qs} + p * \lambda_{ds}$$

$$V_{qs} = -R_s * i_{qs} - \omega_r * \lambda_{ds} + p * \lambda_{qs}$$

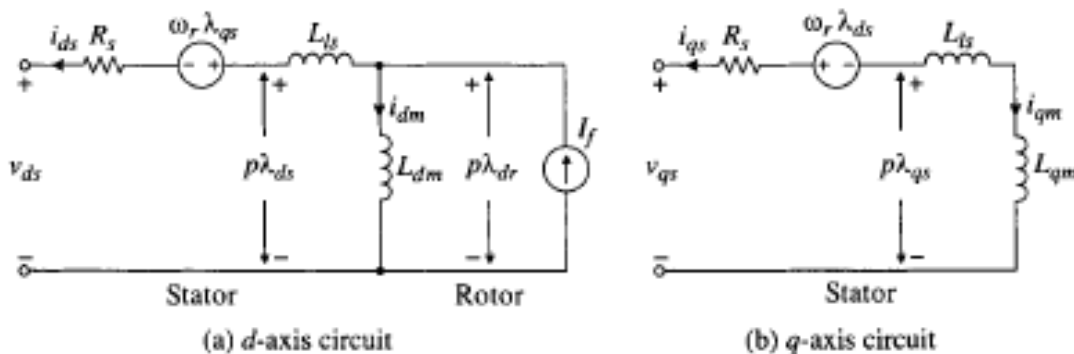


Fig 3-3 General dq-axis model of SG in the rotor field Synchronous reference frame

Where λ_{ds} and λ_{qs} are d and q axis stator flux linkages, given by

$$\begin{aligned}\lambda_{ds} &= -L_{ls} * i_{ds} + L_{dm}(I_f - i_{ds}) \\ &= -(L_{ls} + L_{dm})i_{ds} + L_{dm} * I_f - L_d * i_{ds} + \lambda_r\end{aligned}$$

$$\lambda_{qs} = -(L_{ls} + L_{qm})i_{qs} = -L_q * i_{qs}$$

Where λ_r is the rotor flux and L_d and L_q are the stator dq-axis self inductance, defined by

$$\lambda_r = L_{ds} * I_f$$

$$L_d = L_{ls} + L_{dm}$$

$$L_q = L_{ls} + L_{qm}$$

Substituting above equation and considering d of $\lambda_r/dt = 0$ for constant field current, I_f in the WRSG and constant λ_r in the PMSG, we have

$$V_{ds} = -R_s * i_{ds} - \omega_r * L_q * i_{qs} - L_d * p * i_{ds}$$

$$V_{qs} = -R_s * i_{qs} - \omega_r * L_d * i_{ds} + \omega_r * \lambda_r - L_d * p * i_{qs}$$

A simplified model for the synchronous generators, which is derived based on above equations. It should be pointed out that:-

(a) The simplified mode is as accurate as the general model. Since no assumption was made during the derivation of the simplified model. The performance analysis based on the general and simplified models should give identical results.

(b) The SG model is valid for both wound-rotor and permanent-magnet synchronous generators. For a given field current I_f in the WRSG, the rotor flux can be calculated by $\lambda_r = L_{dm} I_f$. For the PMSG, the rotor flux λ_r is produced by permanent magnets and its rated value can be obtained from the nameplate data and generator parameters.

(c) The model is also valid for both salient- and non-salient-pole synchronous generators. For a non-salient generator, the dq-axis synchronous inductances, L_d and

L_d , are equal, whereas they are different for a salient-pole generator. The d-axis synchronous inductance of PMSG is usually lower than that of the q-axis ($L_d < L_q$).

The electromagnetic torque produced by the SG can be calculated by the same equation for the IG given in equation above, that is,

$$\mathbf{T_e} = \frac{3}{2} \mathbf{p}(\mathbf{i_{qs}} * \lambda_{ds} - \mathbf{i_{ds}} * \lambda_{qs})$$

Or

$$\mathbf{T_e} = \frac{3}{2} \mathbf{p}(\lambda_r * \mathbf{i_{qs}} - (\mathbf{L_d} - \mathbf{L_q})\mathbf{i_{ds}} * \mathbf{i_{qs}})$$

The rotor speed ω_r is governed by motion equation as under:-

$$\omega_r = \frac{p}{J_s} * (\mathbf{T_e} - \mathbf{T_m})$$

To derive the SG model for dynamic simulation of synchronous generators, equations is rearranged as under:-

$$\mathbf{i_{ds}} = \mathbf{1/S}(-\mathbf{V_{ds}} - \mathbf{R_s} * \mathbf{i_{ds}} + \omega_r * \mathbf{L_q} * \mathbf{i_{qs}})/\mathbf{L_d}$$

$$\mathbf{i_{qs}} = \mathbf{1/S}(-\mathbf{V_{qs}} - \mathbf{R_s} * \mathbf{i_{qs}} + \omega_r * \mathbf{L_d} * \mathbf{i_{ds}})/\mathbf{L_q}$$

Based on the above three equations, the block diagram for computer simulation of the SG/ PMSG is derived. The input variables of the SG model are the dq-axis stator voltages v_{ds} and v_{qs} , the rotor flux linkage λ_r and the mechanical torque T_m , whereas the output variables are the dq-axis stator currents i_{ds} and i_{qs} , the rotor mechanical speed ω_m , and the electromagnetic torque T_e .

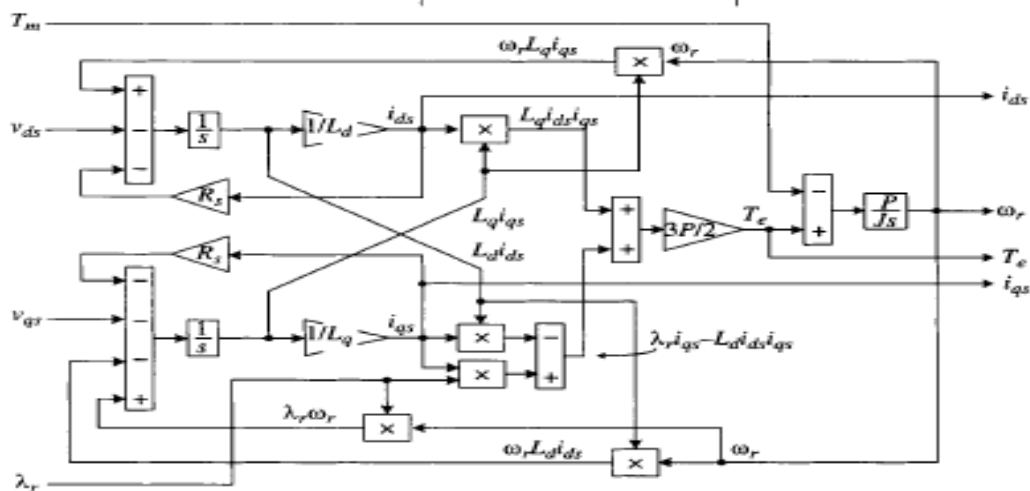


Fig 3-4 Matlab Block diagram for dynamic simulation of synchronous generators.

Chapter - 4

STUDY OF PERMANENT MAGNET SYNCHRONOUS GENERATOR STAND ALONE OPERATIONS

4.1 STAND ALONE OPERATION OF PMSG

The main purpose of this case study is to:

- (a) Investigate the operation of a stand-alone SG wind energy system feeding a three-phase resistive load.
- (b) Illustrate how to effectively use the simulation model for the simulation of synchronous generators.
- (c) Reveal the relationship between the three-phase abc variables in the stationary frame and the dq variables in the synchronous frame.

The generator used in the study is a 2.45 MW, 4000 V, 53.33 Hz, 400 rpm non salient pole PMSG, whose parameters are as under:-

PMSG 2.45 MW, 4000V, 53.33Hz		
Type	Non Salient Pole	
Rated Mechanical Power	2.4487 MW	1.0 pu
Rated Apparent Power	3.419 MVA	1.0 pu
Rated Line to Line Voltage	4000 V (rms)	1.0 pu
Rated Phase Voltage	2309.4 V (rms)	1.0 pu
Rated Stator Current	490 A (rms)	1.0 pu
Rated Stator Frequency	53.33 Hz	1.0 pu
Rated Power Factor	0.7162	1.0 pu
Rated Rotor Speed	400 rpm	1.0 pu
Number of Pole Pairs	8	-
Rated Mechanical Torque	58.4585 kN-m	1.0 pu
Rated Rotor Flux Linkage	4.971 Wb (rms)	
Stator Winding Resistance R_s	24.21 m Ω	
d-axis Synchronous Inductance L_d	9.816 mH	
q-axis Synchronous Inductance L_q	9.816 mH	
Base Flux Linkage λ_s	6.892 Wb (rms)	1.0 pu
Base Impedance Z_s	4.6797 Ω	1.0 pu
Base Inductance L_s	13.966 mH	1.0 pu
Base Capacitance C_s	637.72 μ F	1.0 pu

Table 4.1 - 2.45 MW, 4000V, 53.33Hz non salient pole PMSG parameters

The generator is loaded with a three-phase balanced resistive load R_L and operates at 320 rpm (0.8pu) at a given wind speed. The loading of the generator can be changed by switch S . When S is closed, the load resistance is reduced to $R_L/2$ per phase. It is assumed that the combined moment of inertia of the blades, rotor hub, and generator are very large such that the rotor speed is kept constant at 320 rpm during the transients caused by the changes in load resistance. The motion equation is then not needed. Since the rotor speed ω_r is known, it becomes the system input variable. The SG simulation algorithm is slightly modified accordingly.

The block diagram for the simulation of the SG stand-alone operation is shown below. The dq-axis stator currents, i_{ds} and i_{qs} , in the synchronous frame rotating at the synchronous speed of ω_r are calculated by the SG model. They are then transformed into the abc-axis stator currents, i_{as} , i_{bs} , and i_{cs} , in the stationary frame through the dq/abc transformation. The calculated load voltages, v_{as} , v_{bs} , and v_{cs} , which are also the stator voltages, are transformed to the dq-axis voltages v_{ds} and v_{qs} in the synchronous frame, which are then fed back to the SG model.

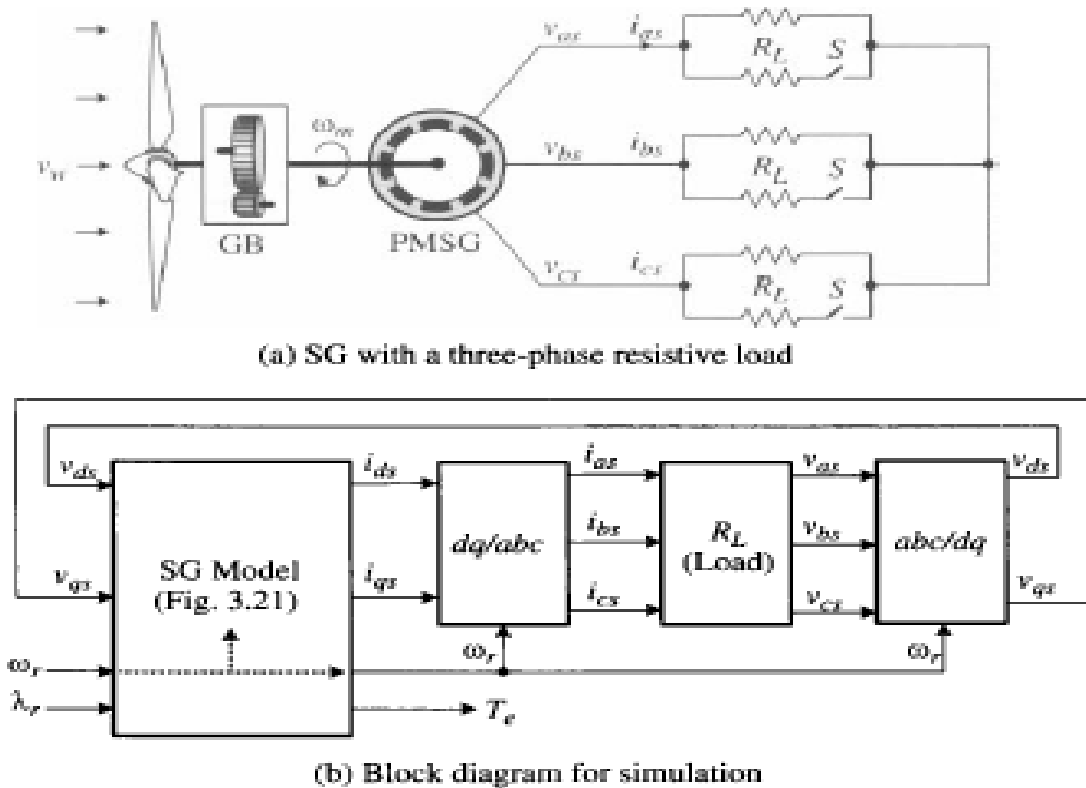


Fig 4-1

A simple test for the synchronous generator in stand-alone operation is carried out, and results are given in Figure 3-23. The generator initially operates in steady state with a resistive load of RL . The load resistance is reduced to $RL/2$ by closing switch S at $t = 10.0$ sec. After a short transient period, the system reaches a new steady-state operating point. The dq-axis stator currents, i_{ds} and i_{qs} , in the synchronous frame are DC variables, whereas the aèc-axis stator currents, i_{as} , i_{bs} , and i_{cs} , in the stationary frame are sinusoids in steady state. The magnitude of the stator current is given by $I_s = \text{square root of addition of square of } i_{qs} \text{ and } i_{ds}$, represents the peak value of i_{as} , i_{bs} , and i_{cs} .

A similar phenomenon can be observed for the stator voltages. A decrease in the load resistance results in an increase in the stator currents, but the stator voltages are reduced mainly due to the voltage drop across the stator inductances. The electromagnetic torque T_e and stator active power P_s are increased accordingly when the system operates at the new operating point.

For the non-salient synchronous generator, its dq-axis inductances are equal ($L_q = L_d$). The torque equation can then be simplified to The above equation indicates that the d-axis current i_{ds} in the non-salient SG does not contribute to the torque production and, therefore, the electromagnetic torque is proportional to the q-axis stator current for a given rotor flux λ_{r} . This can be confirmed by comparing the waveforms of i_{qs} and T_e .

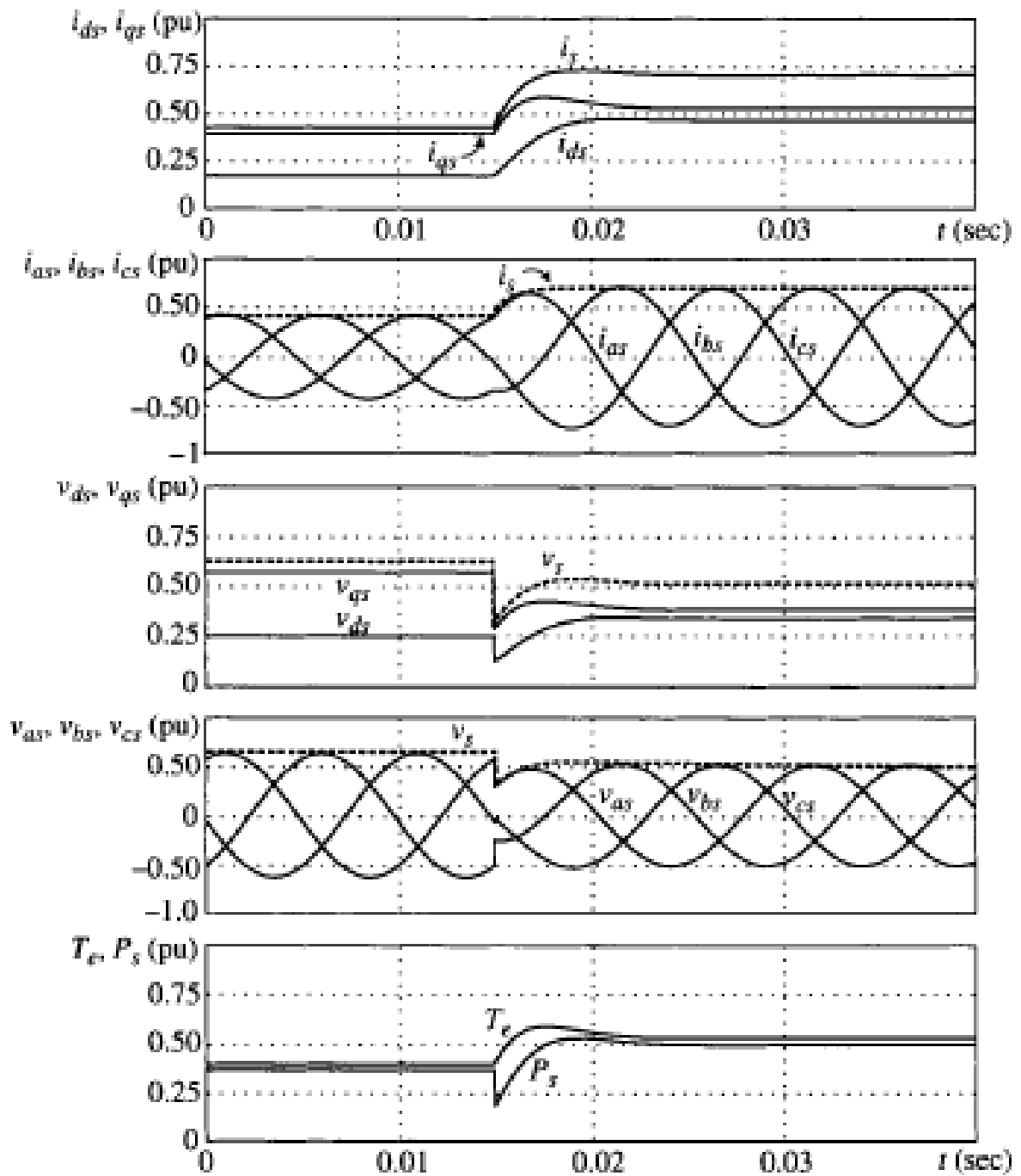


Fig 4-2 - Simulated waveforms for a stand-alone PMSG system with resistive load.

4.2 SIMULINK RESULTS AND CONCLUSION:

4.2.1 Block Diagram

The complete block diagram as shown below of PMSG in standalone mode is as under:-

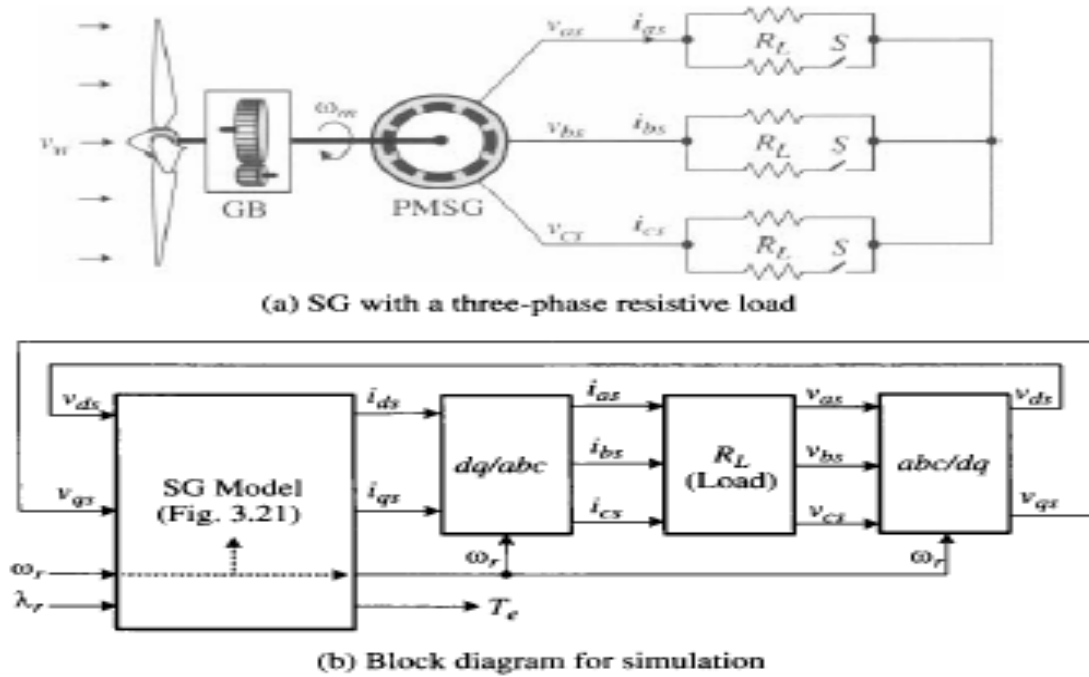


Fig 4-3 – Block diagram PMSG

4.2.2 SIMULINK MODEL OF SYSTEM

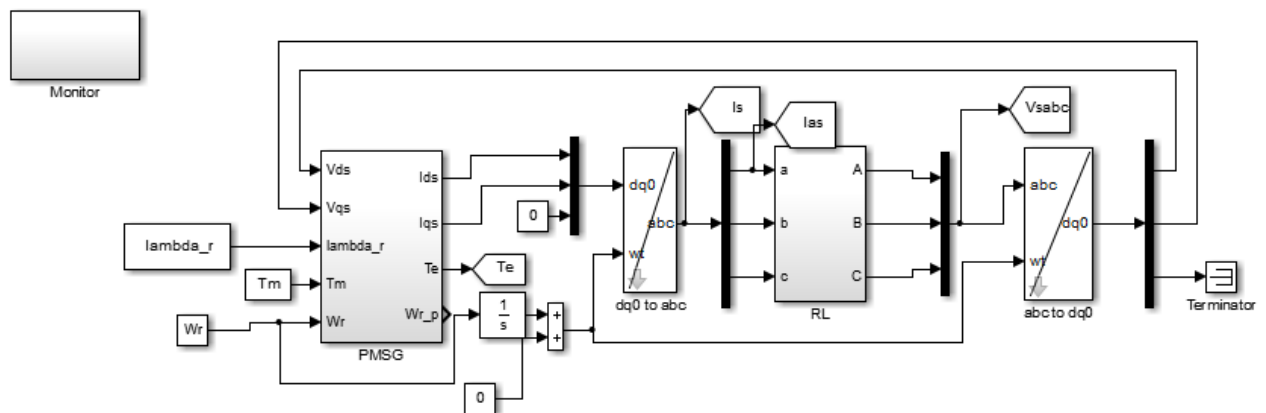


Fig 4-4 – Simulink Model of PMSG with resistive load in standalone mode

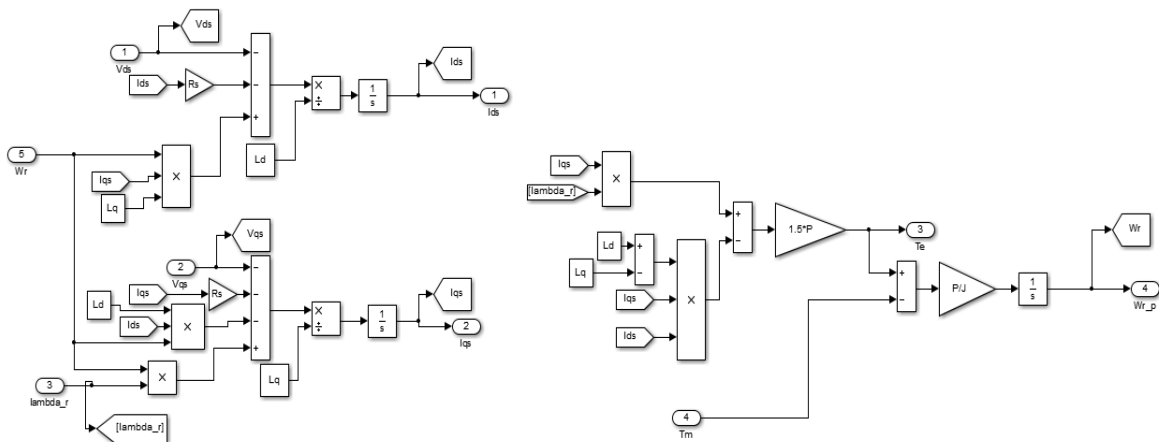


Fig 4-5 – Modeling of PMSG

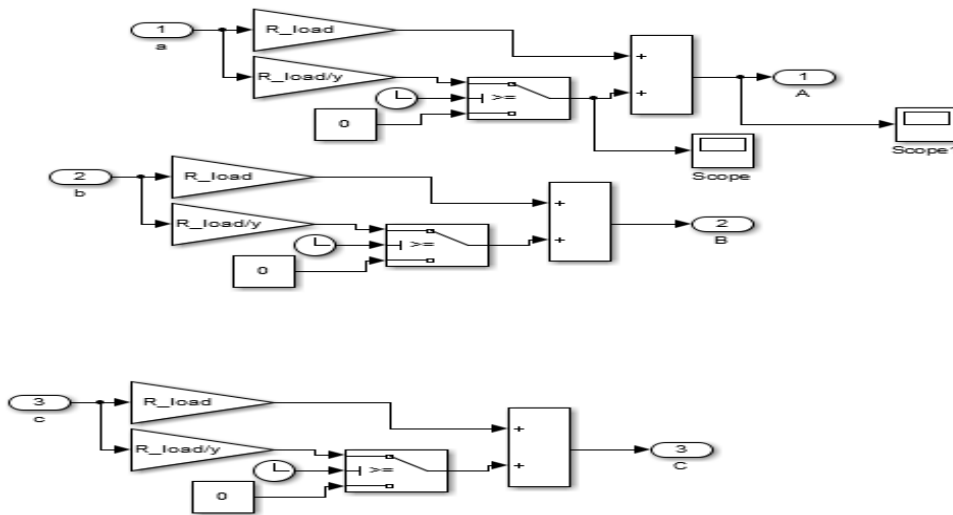


Fig 4-6 – Simulink subsystem of PMSG With load and switches

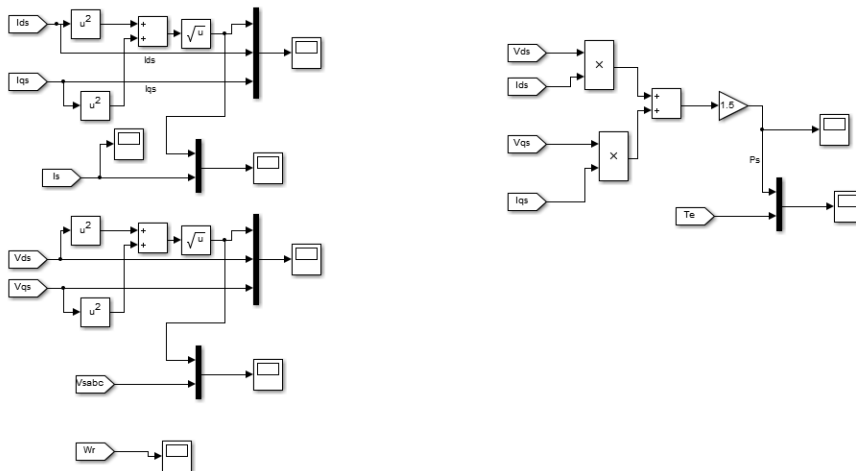


Fig 4-7 – Simulink Scope for Results

4.2.3 RESULTS

Switch was connected to reduce the resistive load at $t = 10$ sec.

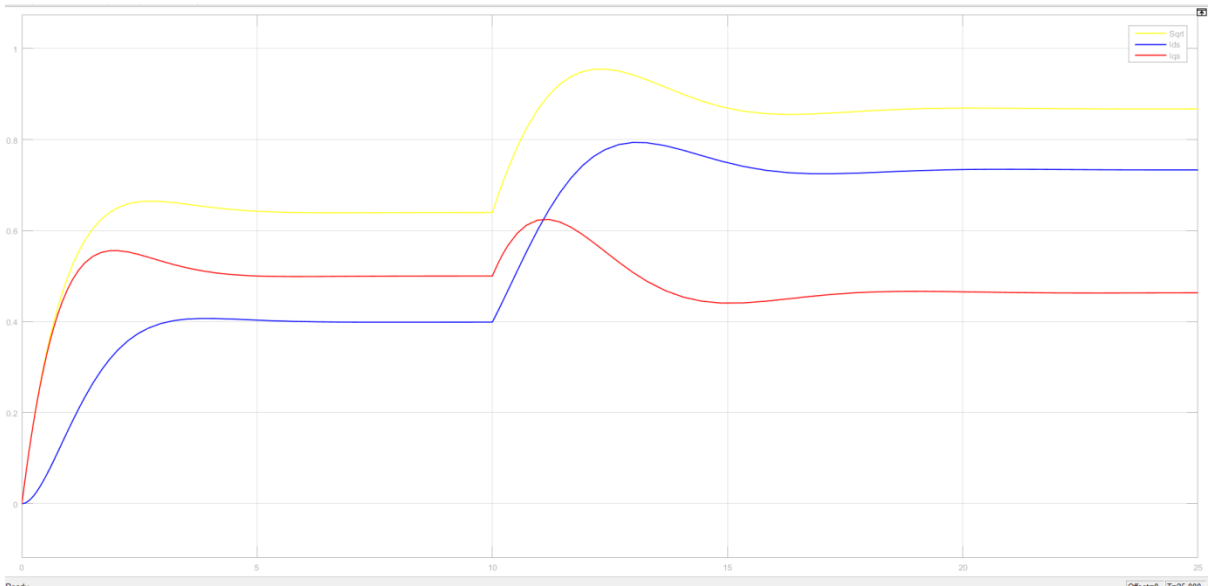


Fig 4-8 – I_{ds} , I_{qs} and I_s

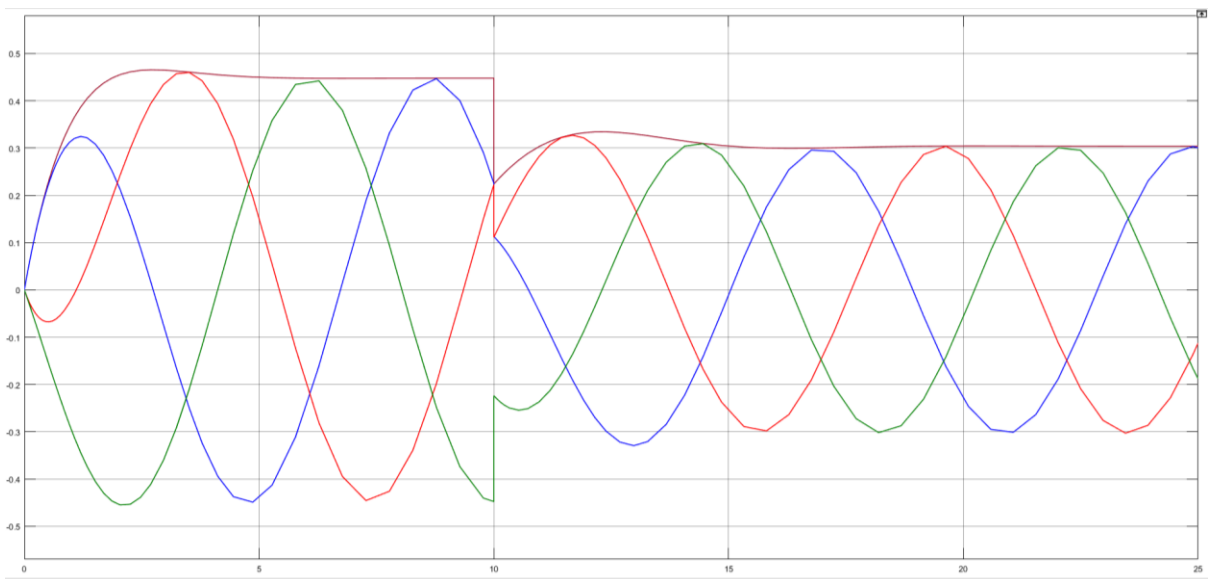


Fig 4-9 – I_{as} , I_{bs} and I_{cs}

4.3 CONCLUSION

The SG model is modified to act as PMSG and the post connecting it with resistive load its various out puts were studied. This PMSG model in standalone operations has been simulated using MATLAB/ Simulink environment and results were collaborated with the IEEE Paper. These results were analyzed and found correct.

CHAPTER 5

DIGITAL CONTROL/ MODEL PREDICTIVE CONTROL AND MODELLING OF 2L - BACK TO BACK CONVERTOR

5.1 CONTROL OF WECSs

Control theory has evolved as an important discipline in modern WTs and WFs. Control schemes enforce WECS to achieve the desired operation, increase wind energy conversion efficiency, reduce energy cost, increase the lifespan of WT components, decrease structural loading, decrease turbine down times, and provide a superior dynamic and steady-state performance.

The block diagram of the overall control scheme for a modern variable-speed WECS is shown in Figure 5.1. The analysis given in this section is applicable for Type 3 and 4 WECS. The stator and rotor connections of Type 3 DFIG WECS are shown by the dotted lines. The power conversion system in Type 3 and 4 WECS is realized by RSC + GSC and MSC + GSC, respectively. The WECS mainly consists of six control levels, wherein the Level I control loop involves fast varying variables and the Level VI control loop comprises by slow-varying variables. The tight control of variables in Level I loop is important to fulfill the active and reactive power commands imposed by the TSO/ DSO in the Level VI control loop. The control loops also consider normal and abnormal operation for WECS.

During grid faults, the FRT control in the Level IV loop issues a fault enable signal S_f . The mechanical and electrical control systems in the Level I to IV loops coordinate for better control performance during grid faults. For example, during grid faults, the GSC stops injecting active power and produces reactive power to the grid, the pitch control system starts working to decrease power extraction, and the DC chopper starts functioning to prevent the DC-bus voltage from exceeding the upper threshold limit.

The feedback signals from the WECS such as grid voltages \mathbf{v}_g , grid currents \mathbf{i}_g , generator voltages \mathbf{v}_s , generator currents \mathbf{i}_s , DC-link voltage v_{dc} , generator angular speed ω_m , rotor position angle θ_m , and wind speed v_w are used by various control loops. The control requirements are met by generating optimal gating signals s_r , s_i , and s_{ch} for the MSC/RSC, GSC, and DC chopper, respectively. The three-phase variables are represented by an equivalent vector, for example, $\mathbf{x}_y = [x_{ay} \ x_{by} \ x_{cy}]^T$. The main variable \mathbf{x} denotes the voltage, current, or switching signal ($\mathbf{x} \in \{\mathbf{v}, \mathbf{i}, \mathbf{s}\}$). The subscript y represents the source (generator), grid, rectifier, or inverter

($\mathbf{y} \in \{\mathbf{s}, \mathbf{g}, \mathbf{r}, \mathbf{i}\}$). The vector variables are denoted by a double line arrow (\Rightarrow), and the scalar variables are represented by a single line arrow (\rightarrow).

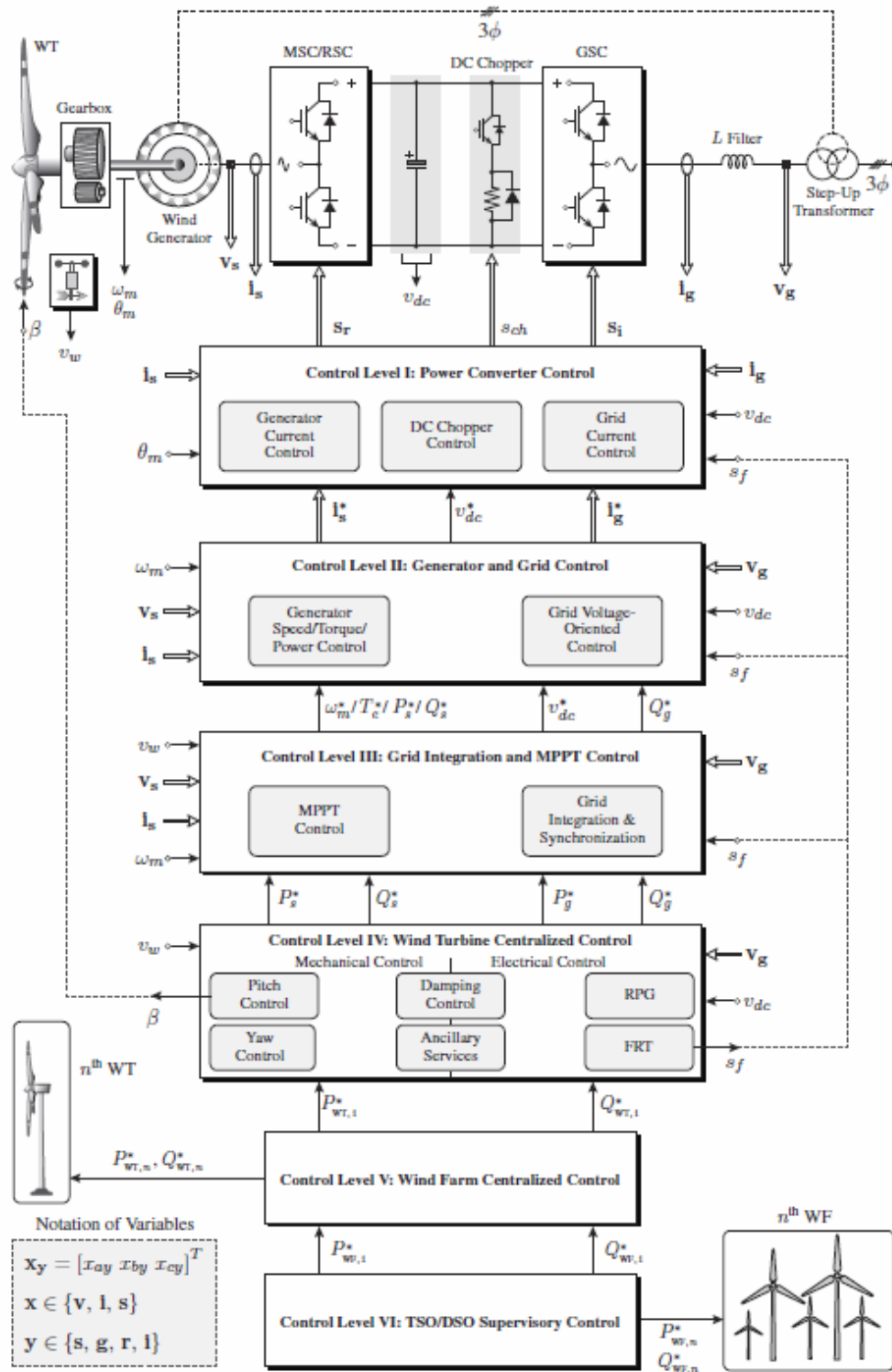


Fig 5-1 - Block diagram of the overall control scheme for variable-speed WECS

5.1.1 TSO/DSO Supervisory Control (Level VI)

The power output from the WT or WF is highly variable depending on wind-speed conditions. The variable energy in the existing energy mix brought serious reliability and security issues because of the intensive penetration of large-scale WECS into the existing power system. With the efforts made through strict grid codes, large scale wind farms changed their operations over the years from being passive power generation sources to active generation units with grid support characteristics.

Large-scale wind farms are connected to the TSO/DSO dispatch centers through communication networks to continuously share information about active and reactive power generation statuses. The top-level TSO/DSO supervisory control (Level VI) sends active and reactive power commands to each wind farm (similar to conventional power plants) connected to the power system.

5.1.2 Wind Farm Centralized Control (Level V)

The power commands from the Level VI control is received from the WF centralized control. The WTs are connected to the WF centralized control by communication links to share the active and reactive power generation statuses. The supervisory control and data acquisition system is used for WF monitoring. The WF centralized control defines the active and reactive power requirements for each WT. The first WT is commanded with P^*_{WT1} and Q^*_{WT1} and the n th WT is supplied with the P^*_{WTn} and Q^*_{WTn} commands. The active and reactive power references are calculated such that the frequency and voltage at the PCC are maintained at the desired values.

If the WF centralized control learns that the WTs cannot meet the RPG requirement, the wind farm static compensators such as STATCOM or SVC are initiated to support the WTs. The WF centralized control takes every possible effort to command the WTs such that the P and Q references imposed by the superior Level VI control loop are met all the time. The aerodynamic interaction of the WTs is also surpassed by the WF centralized control.

5.1.3 WT Centralized Control (Level IV)

As shown in Figure 5.1, the WT centralized control includes both mechanical and electrical controls. The pitch control and yaw control is solely involved in mechanical control, whereas RPG and FRT correspond to electrical control. The damping control includes both mechanical and electrical aspects: mechanical damping control lessens the mechanical resonances in the tower and torsional vibrations in the drive train, whereas electrical damping control provides damping for electrical subsynchronous resonances in the grid.

The electrical ancillary services include electrical energy storage, uninterruptible power supply (UPS), and power quality. The UPS unit with battery energy storage forms an emergency power supply backup for pitch and yaw drives. Inertia emulation, spinning reserve, and kinetic energy storage are included in mechanical ancillary services [30]. The grid voltage magnitude is continuously monitored by the FRT subsystem. When the grid voltage falls below or above the preset magnitude, it sends a fault enable signal, sf . This fault signal is sent to the other control loops and other functions inside the Level IV control loop. By coordinating various mechanical and electrical control systems, the WT centralized control provides active power reference P^*s for WT MSC (P^*s and reactive power reference Q^*s for RSC), along with P^*g and Q^*g to the GSC. During normal grid conditions, Q^*g is set to zero to maintain unity grid PF in Type 4 WECS.

When the wind speed is lower than the rated value, the pitch angle β is kept constant at zero degrees to extract the maximum possible energy from the wind. When the wind speed is higher than the rated value, the proportional-integral (PI) controller produces β such that the generator output power is limited to its rated value. As pitch angle increases, C_p decreases along with the extracted wind power, and the generator power comes back to the nominal value. In practice, the pitch control system is realized by a high performance μC , generator output voltage and current sensors, three DC/AC power converters, three electric motors, and a backup power supply. The μC generates gating signals for power converters on the basis of wind-speed data, measured generator output power, preset power rating, and so on. Power converters change the speed of the three independent electric motors according to the instructions given by the μC .

5.1.4 Grid Integration and MPPT Control (Level III)

The Level III control loop includes the peak power extraction, also called MPPT, grid integration, and synchronization. By employing a grid synchronization algorithm, the phase angle between grid currents and grid voltages can be adjusted accurately with the grid PF requirement. Grid synchronization is performed by zero-crossing detection, grid voltage filtering, or phase-locked loop (PLL). The latter is preferred because of its robustness against grid voltage harmonics and digital control platform friendliness [30]. The control system for a GSC helps in grid synchronization and integration by employing a PLL. The output of the grid integration subsystem is the reference DC-bus voltage v^*_{dc} and reference grid reactive power Q^*g . For a given grid voltage magnitude v^*_{dc} is usually set constant according to the required modulation index of a GSC.

With the random nature of wind speed v_w , the peak power extraction is important in variable-speed WECS because it increases energy conversion efficiency. For a given v_w value, the MPPT control attempts to obtain the maximum possible power from the wind. The maximum power point (MPP) trajectory changes with respect to the wind speed. According to

this curve, the operating region for the MPPT control is the cut-in wind speed to the rated wind speed. The various control schemes are as under:

- (a) Optimal Tip Speed Ratio Control
- (b) WT Power Curves-Based Control
- (c) Optimal Torque Control
- (d) Power Signal Feedback Control:
- (e) Speed Sensor less Control
- (f) Other MPPT Algorithms:

5.15 Power Converter, Wind Generator, and Grid Control (Level I and II)

The block diagram of the overall control scheme depicted in Figure 1.22 indicates that the Level II control loop is related to the wind generator and grid control, and the Level I control loop corresponds to the power converter control. The Level I and II control loops are shown as two different blocks to clearly indicate the flow of the control variables. However, in reality, the Level I and II control loops are closely intertwined; thus, distinguishing them is difficult. To simplify the discussion, Level I is introduced first followed by Level II. To achieve high-energy conversion and feed the power to the grid, the following control objectives must be fulfilled in high-power WECS:

- (a) MPPT under all wind-speed conditions.
- (b) Net DC-bus voltage control to ensure proper operation for the GSC.
- (c) RPG to meet the grid codes.

An accurate control of wind generators and power converters is necessary to fulfill the above control objectives. The first objective is achieved by the MSC/RSC, whereas the GSC handles last two objectives. Level II control produces the reference generator and grid currents (i_s^* and i_g^*), and the Level I control produces switching signals (s_r and s_i), such that the measured generator and grid currents (i_s and i_g) follow their references (i_s^* and i_g^*) closely.

The power flow between the wind generator and utility grid is also tightly regulated by the Level I control during both normal and grid fault conditions. In grid faults, the surplus energy between the generator and utility grid is dumped to the resistive load through a DC chopper, thus converting the kinetic energy of the turbine rotation into heat. The control system of the DC chopper dynamically adjusts the amount of energy to be dumped to the resistor. The DC chopper control subsystem reads the fault signal s_f value and generates the switching signal s_{ch} to the DC chopper such that the DC-link voltage v_{dc} never exceeds the upper threshold limit v_{dc}^{max} .

5.1.5.1 Power Converter Control (Level I)

Classical control techniques are well established and are widely employed to control converters, variable-speed drives, and energy conversion systems. The recent developments in digital control platforms such as μC , DSP, and FPGA enabled a designer/ industry to develop more complex control algorithms to obtain optimal system performance. With the exponential increase in the computational capacity of digital control platforms, often expressed as million instructions per second (MIPS), the designer need not worry about the high number of calculations involved in the control algorithm. For example, the computational capacity offered by the TMS320C14 DSP in 1983 was limited to 10 MIPS, whereas the modern dSPACE DS1103 control platform can perform 2500 MIPS. The advanced control techniques improve the overall system performance by just software reconfiguration.

5.1.5.2 Wind Generator and Grid Control (Level II)

The design, construction, operation, and control of a wind generator and electric motor are similar. Based on the sign of mechanical input torque T_m , an electric machine can be used as a generator or motor (negative T_m for generator and positive T_m for motor). All theories and practical developments in electric motor control can therefore be attributed to wind generator control. In comparison to electric motors control, the wind generators employ additional MPPT control loop to generate reference speed ω^*_m , reference torque T^*_e , or reference power P^*_s . Wind generator control schemes are broadly classified into two classes: classical control and predictive control.

Scalar and vector control techniques are part of classical control schemes, and these are extensively used in electric drives and the wind energy industry. **In scalar control**, only the magnitude and frequency of space vector (voltage, current, or flux linkage) is adjustable; therefore, **an acceptable performance is guaranteed during steady-state operation**. **In vector control**, in addition to magnitude and frequency, the instantaneous position (phase angle) of the space vector is controlled; as a result, **a high-performance operation is obtained in both steady-state and transient conditions**.

Vector control of a wind generator is a general and decoupled control philosophy that can be further classified as FOC, DTC, DPC, and other forms, such as feedback linearization control and passivity-based control. Vector control schemes are implemented by transforming the generator dynamic equations into field coordinates that rotate in synchronism with the rotor or stator flux or voltage vector.

FOC and DTC are two frequently-used methods in the present industry to obtain high control performance. In the FOC scheme, wind generator three-phase currents are **transformed into two orthogonal components that define the magnetic flux and electromagnetic torque**. To force the measured currents to follow their reference currents, two PI controllers are used to generate a reference voltage vector for the modulation stage. The modulation stage compares the reference voltages with the carrier waveform and generates switching signals for the power converter. FOC is a linear control method, and its switching frequency is constant (set by modulator). FOC schemes are available in two forms:

- (a) Direct or feedback FOC (DFOC or Blaschke control)
- (b) Indirect or feed-forward FOC (IFOC or Hasse control).

The latter is widely used because of its simplicity throughout the speed range. **The rotor field-oriented FOC is used to control SCIG, stator field-oriented FOC is employed in DFIG, and rotor flux-oriented maximum torque per ampere control (essentially FOC scheme) is used in PMSG.**

DTC represents a viable alternative to the FOC scheme. Instead of a decoupled generator current control, the **DTC scheme directly controls the generator stator flux and electromagnetic torque** by employing hysteresis comparators and a lookup table. The required flux and torque are computed on the basis of measured generator voltages and currents. In comparison with FOC, the DTC scheme is relatively simple and eliminates the need for coordinate transformation, PI controllers, and pulse-width modulation. However, the number of online calculations with DTC is higher than FOC, thus making DTC a highly computational intensive control. **Classical DTC is a nonlinear control and operates with variable-switching frequency.**

DTC control is available in two forms based on the selection of switching sectors: circular stator flux DTC (*Takahashi* and *Noguchi* control) and hexagonal stator flux (Depenbrock control). The DTC technique has been applied to SCIG, DFIG, and interior PMSG (IPMSG).

The operating principles of FOC, DTC, and DPC vector control schemes are used by FCS-MPC to design predictive current control (PCC), predictive torque control (PTC), and predictive power control (PPC), respectively. All control variables of FOC, DTC, and DPC are regulated by PCC, PTC, and PPC without employing any internal PI or hysteresis controllers.

All model predictive control schemes are modulation-stage free; thus switching frequency is variable. In both classical and predictive control schemes, the outer speed control loop employs a PI controller to regulate the generator speed at its reference value. The PCC, PTC, and PPC schemes only replace the internal control loops of FOC, DTC, and DPC schemes respectively that need faster control actions than the sluggish outer speed control loop.

5.2 FINITE CONTROL-SET MODEL PREDICTIVE CONTROL

FCS-MPC offers several advantages that make it suitable for the optimal control of power converter-based energy processing applications. FCS-MPC is an attractive solution which can easily be applied to a wide range of power converters with different output harmonic filter configurations, adjustable-speed motor drives, power quality, HVDC, and wind and PV energy conversion applications. These features come with few technical challenges (**research opportunities**) that need to be addressed. In this section, the main features and challenges of FCS-MPC are analyzed in detail.

5.2.1 Main Features of FCS-MPC

The main features of the FCS-MPC are classified into eight categories. A brief description of these main features is presented below.

(a) **Simple and Easy to Understand:** FCS-MPC uses a simple concept, and it is easy to understand. Regardless of control application, FCS-MPC always uses four main subsystems, as given below:

(i) **References Calculation:** This subsystem calculates the reference control variable $\mathbf{x}^*(k)$ (\mathbf{x}^* voltage, current, power, torque, flux, etc.) according to the type of application. The references calculation is common designs step for classical and MPC schemes.

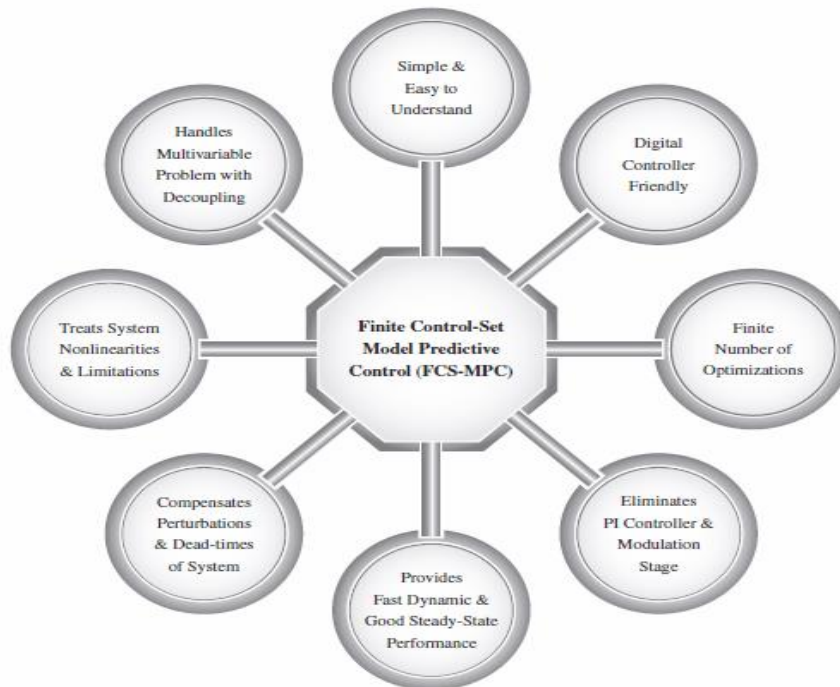


Fig 5-2 – Features MPC

(ii) **Extrapolation:** In this subsystem, the future value of the reference control variable $\mathbf{x}^*(k+1)$ is estimated based on the present and past sample values ($\mathbf{x}^*(k)$, $\mathbf{x}^*(k-1)$, etc.), or based on present sample value and angle of reference frame ($\mathbf{x}^*(k)$ and $\theta^*(k)$).

(iii) **Predictive Model:** Possible future values of control variables $\mathbf{x}^p(k+1)$ are predicted by this subsystem based on DT model and parameters of system, feedback signal values, and converter switching state combinations, $\mathbf{s}(k)$.

(iv) **Cost Function Minimization:** The error between the predicted and extrapolated control variable $\mathbf{g}=\mathbf{x}^*(k+1)-\mathbf{x}^p(k+1)$ is calculated by this subsystem. The switching state $\mathbf{s}(k)$ that produces the ‘**minimum**’ cost function error is elected as an optimal actuation (output) of FCS-MPC, and the output is applied to the power converter directly.

(b) **Digital Controller Friendly:** The inherent and discrete nature of power converters is considered in the design of a “predictive model” subsystem of FCS-MPC. Simulation models of FCS-MPC execute the algorithm with a discrete step size; consequent analysis of the control scheme is conducted in a DT domain. Real-time implementation of FCS-MPC by digital control platforms is, therefore, intuitive and natural. Hence, the time required for a designer to switch from a simulation stage to a real-time implementation stage is negligible; thus the overall FCS-MPC design framework is simple.

(c) **Finite Number of Optimizations:** FCS-MPC is a model-based optimization algorithm that performs a set of calculations during each sampling period. The number of iterations in the optimization algorithm is determined according to the possible number of converter switching states $\mathbf{s}(k)$. The power semiconductor switch in any converter possesses two discrete states: turn-on (‘1’) or turn-off (‘0’). Thus the number of switching combinations (switching states) in any converter is limited to a finite set. For example, 8 and 27 switching states are available for 2L-VSC and NPC converter, respectively. Optimizations are greatly simplified because of the finite number of switching states, making it possible to implement FCS-MPC by digital control platforms available in the market.

(d) **Eliminates PI Controller and Modulation Stage:** FCS-MPC uses the DT model of system to predict the future behavior of control variables for every possible actuation sequence. Cost function minimization is used as an optimization criterion to evaluate system performance for all possible switching states. An optimal switching state that minimizes the cost function is directly applied to the converter. This approach eliminates the need for linear PI controllers, hysteresis regulators, intermediate

modulation stage, and the lookup table in the control loop. FCS-MPC is a nonlinear control method, and it provides a better approach to control the power converters that are also nonlinear in nature.

(e) **Provides Fast Dynamic and Good Steady-State Performance:** Linear control techniques, such as FOC and VOC, treat the power converter as a linear actuator. The nonlinear nature of the power converter becomes more predominant at a lower switching frequency operation. Under such conditions, FCS-MPC provides better control in dynamic response and steady-state reference tracking. The resultant dynamic performance of FCS-MPC is superior to linear control because of the elimination of the low-bandwidth modulation stage.

(f) **Compensates Perturbations and Dead-Times of System:** Power conversion system perturbations, power converter dead-times, and on-state voltage drop of semiconductor switches are easily compensated by FCS-MPC. Although the output harmonic filter and internal DC-link filter parameters change, the controller can mitigate the perturbations by choosing a switching state that produces the minimal cost function error. Reference tracking is slightly affected by system perturbations; however, the transient response remains fast compared with linear control.

(g) **Treats System Nonlinearities and Limitations:** FCS-MPC treats various power converter topologies as discontinuous and nonlinear actuators that are the closest approximations to a real-time scenario. One of the best features of FCS-MPC is that the nonlinearities and limitations of the power converter can be incorporated directly into the system model. The cost function definition is flexible; several constraints and technical requirements such as maximum current limitation, switching frequency reduction, spectrum shaping, common-mode voltage minimization, power losses reduction, THD, boundary limits for electrical and mechanical variables, etc., can be incorporated in the design and operation of the controller to achieve a safe and reliable operation.

(h) **Handles Multivariable Problem with Decoupling:** For a wide variety of systems, FCS-MPC handles multivariable control problems in a decoupled manner without employing compensation terms outside the control loop. The “soft constraint” and “hard constraint” handled in a multivariable control framework is naturally accommodated by FCS-MPC through proper selection of weighting factors. This feature is particularly preferred in electromechanical energy conversion applications where both electrical and mechanical control variables need to be handled by FCS-MPC.

5.2.2 Challenges of FCS-MPC

Despite the simplicity and benefits of FCS-MPC, several challenges exist in state-of-the-art research that include, but not limited to:

- (a) **Large Number of Calculations:** FCS-MPC performs a large number of online calculations during each sampling interval, thus leading to higher computational burden than the linear control scheme

- (b) **Variable-Switching Frequency:** The main drawback of FCS-MPC compared with the linear control is that the converter switching frequency varies with respect to the operating conditions. This finding leads to spread spectrum in the control variable harmonic profile. The cost function can be penalized to control the switching frequency to some extent. For example, the average switching frequency of the converter can be regulated between two close boundary limits by the online adjustment of weighting factors.

- (d) **Heuristic Selection of Weighting Factors:** The cost function in FCS-MPC includes several control objectives (variables) simultaneously. The relative importance of one objective over the other can be set through the weighting factors. Control variables possess different physical natures (current, voltage, power, etc.), and these variances lead to coupling effects; thus the selection of suitable weighting factors becomes tedious. The numerical procedure for the weighting factor selection is still an open research topic.

- (e) **Need for Accurate Model of System:** The control performance obtained by the FCSMPC depends greatly on the DT system model and prediction horizon. In the field of power electronics, CT mathematical models of various power converters and wind generators that are highly accurate and precise are readily available. Mapping CT models to the DT models is a mature subject matter in the field of control theory. For linear time-varying CT (for example, induction, and synchronous machine) models, calculation of corresponding exact DT models is impossible. In such cases, approximate models with high precision improve the system performance.

5.3 Model Predictive Control of WECS

The block diagram of the predictive current control scheme for a 2L-VSR-based PMSG WECS is shown in Figure 5.2. The control scheme is very easy to understand. It consists of four main subsystems: reference currents calculation, extrapolation, predictive model, and cost function minimization. Notation of variables, calculation of reference speed ω_m^* , and reference currents i_{ds}^* and i_{qs}^* is similar to the ZDC control discussed earlier. Once the reference currents are obtained in $(k)^{\text{th}}$ instant, these are extrapolated to $(k+1)$ sampling instant for use with the cost function. The PCC scheme replaces the decoupled PI controller, dq/ $\alpha\beta$ transformation, and SVM stage. PCC considers one-sample-ahead prediction horizon to simplify the analysis.

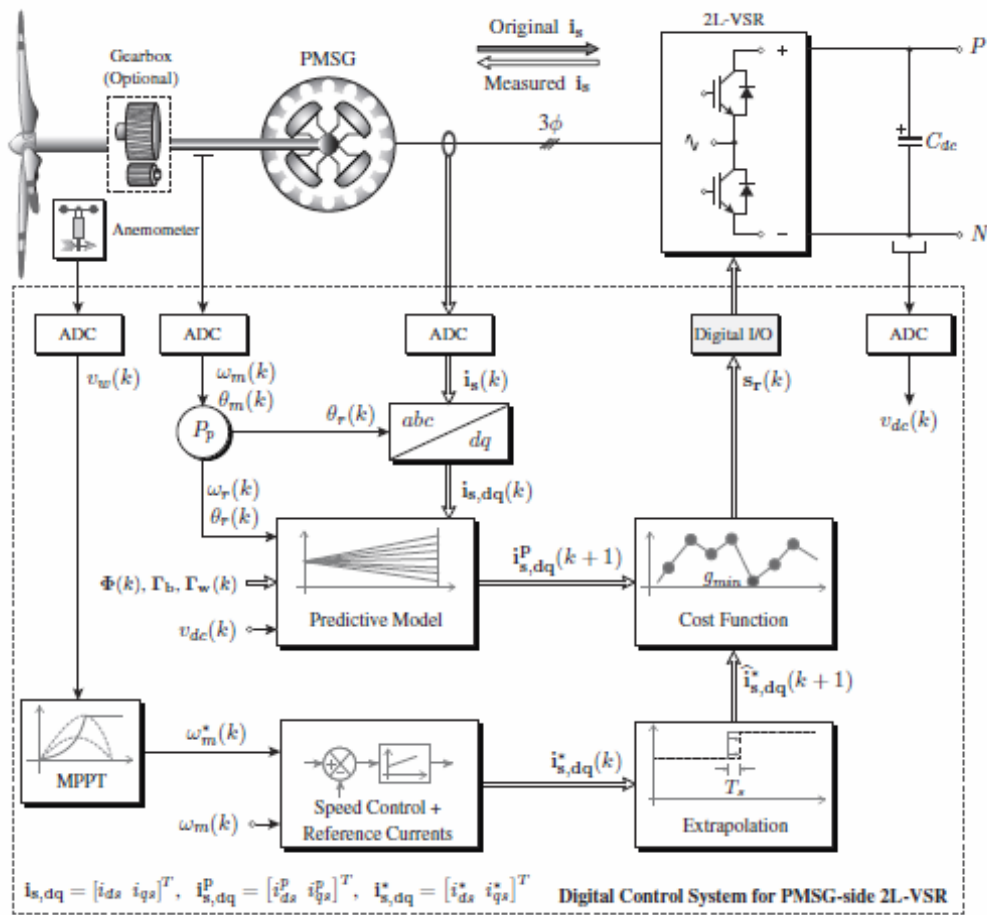


Fig 5-3 - Predictive current control of 2L-VSR-based PMSG WECS

The control objective is to regulate i_{ds} and i_{qs} at their reference values i_{ds}^* and i_{qs}^* , respectively. As the final stage, a cost function is defined to fulfill the control objective:

$$\mathbf{g}(\mathbf{k}) = [\mathbf{i}^*_{ds}(\mathbf{k} + 1) - \mathbf{i}^p_{ds}(\mathbf{k} + 1)]^2 + [\mathbf{i}^*_{qs}(\mathbf{k} + 1) - \mathbf{i}^p_{qs}(\mathbf{k} + 1)]^2$$

The ideal minimum of the cost function is zero that represents the perfect regulation of the generator currents. During each sampling instant, switching signals that minimize the cost function in are chosen and applied to the 2L-VSR directly. Additional constraints such as generator current limitation during transient condition, switching frequency minimization, common-mode voltage mitigation, etc., can also be included in the cost function with suitable weighting factors. A fast dynamic response is guaranteed by PCC because it eliminates the linear PI controllers and SVM stage.

5.4 Comparison of Classical and Model Predictive Control

Classical and model predictive control schemes are compared based as discussed above. The digital control schemes are compared based on the nature of controller, critical design stage, requirement for modulation stage, control complexity, computational burden (number of online calculations), nature of converter switching frequency, and performance during transient conditions. Switching frequency is constant with classical FOC, and all other control schemes operate with variable-switching frequency. The steady-state response obtained in all the methods is more or less same. The dynamic response obtained by predictive control schemes is better compared to classical FOC and DTC. In general, the model predictive control provides opportunities for a designer or industry to control wind generators and power converters in a simple manner.

Table 5.1 Summary of comparison between classical and predictive control schemes

Control Scheme	Classical FOC	Classical DTC	Predictive FOC (PCC)	Predictive DTC (PTC)
Nature of Controller	Linear	Nonlinear	Nonlinear	Nonlinear
Critical Design Stage	PI + Modulation	Lookup Table	Cost Function	Cost Function
Modulation Stage	PWM/ SVM	Not Required	Not Required	Not Required
Control Complexity	Very High	High	Low	Low
Computational Burden	Moderate	Very High	High	High
Switching Frequency	Fixed	Variable	Variable	Variable
Transient Response	Moderate	Good	Excellent	Excellent

CHAPTER 6

CONTROLLER DESIGN FOR PMSG BASED WIND GENERATOR WITH LCL FILTER FOR WIND ENERGY CONVERSION SYSTEM BASED ON PERMANENT MAGNET SYNCHRONOUS GENERATOR.

6.1 ABSTRACT

This chapter introduces a **design** and **analysis** of the **grid side converter controller** for Permanent Magnet Synchronous Generator (PMSG) based variable speed wind generator connected to a grid through LCL filter. Although use of the **LCL filter** at the grid side converter, reduces the harmonics injected in grid system but same can also lead to stability problem due to resonance at high frequency. Therefore the design parameters of the controllers should be planned considering the attrition caused by various elements of LCL filter.

In this study, a model of directly driven PMSG based variable-speed WECS, along with dynamic model of the LCL filter is developed and imitated in **MATLAB/ SIMULINK** environment. By use of bode diagram and step response of the system, the combination of gain controller and damping resistance parameters are selected. The proposed method has been implemented on the grid side controller design for 2.5 MW PMSG based variable speed wind generator. The simulation results show that the proposed method is useful and good response performance under wind speed variation of the control system can be achieved.

The proposed control technique helps in controlling back-to-back converter in a wind turbine system based on PMSG. The effectiveness of the proposed control approach is validated through extensive simulation results.

6.2 INTRODUCTION

Due to the problem of global warming, utilization of distributed generation system which is connected with distribution grid system has gained interests and received considerable attention. The distributed generation can be located close to load consumers. It can have some merits, likewise: Increasing the available power, Improving the overall system reliability, lower costs, reduced emissions, and expanding their energy options [1]. The wind power is one of the distributed resources. Connecting wind turbine generator to distribution grid system leads stability problem. Therefore, it is very important to analyze a suitable control design for wind generators connected to the grid with enhanced stability.

The VSWT-PMSG system is designed to achieve maximum aerodynamic efficiency, increase energy capture, and reduce mechanical stress on the wind turbine [2]. The generator can be directly driven by a wind turbine without gear transmission. In addition, the permanent magnet machines have large air gaps which reduce flux linkage although with multi magnetic poles [3], [4]. However, this type of wind generator has more complicated controller system compared with other types. Therefore, the analysis method to design controller system of the generator still needs to be improved.

The VSWT-PMSG is, in general, connected to the utility power system through the voltage source power converters. The converter permits very flexible control of active and reactive power flows to the grid system. The full power converter totally decouples the PMSG from the grid, and hence grid disturbances have no direct impact on the generator. However, the converter is operated at high switching frequencies between 2-15 kHz, resulting high order harmonics which can disturb devices on the grid and generate power losses [5], [6].

In order to reduce harmonic currents injected to the grid, LCL filter is an attractive solution due many advantages such as higher harmonic attenuation and smaller inductances compared with L-filter [7]. However, resonance at high frequency caused by the filter can lead to stability problem. To avoid the resonance problem, a passive damping resistance should be adopted in the LCL filter although this method can reduce the filter effectiveness and increase losses [6]. Selection of a damping resistance should also be taken into account of the controller design of VSC as well as the filter for their effectiveness and losses.

In this paper design and analysis of the controller for 2.5 MW class of the VSWT-PMSG connected to distribution network is discussed. This study is presents investigations of the stability performance of current controlled grid side converter (GSC) connected to the grid through LCL filter. The controller is designed based on the synchronous d-q reference frame. A simple dynamic model for LCL filter including damping resistance is proposed as plant system in which the configuration of the filter can be accurately represented. Analytical expressions and plots are given to show the system stability performance. Simulation results show that the controller system is very effective to control power delivered to the grid with small total harmonics distortion.

6.3 VSWT-PMSG MODELLING SYSTEMS

The block diagram of control system for VSWT-PMSG considered in this paper is shown in Fig. 1. The VSWT- PMSG has following components: a direct drive PMSG, two levels back to back converters composed of machine side converter (MSC) and grid side converter (GSC), a DC-link circuit with a capacitor (C_{dc}), stator side controller, and grid side controller.

The MSC is connected to the stator of PMSG, and it converts the three phase AC voltage generated by PMSG to DC voltage. The three phase voltage and current sensors are attached on the stator terminal of PMSG. The rotor speed of PMSG is measured from the rotor of wind turbine.

The GSC is connected to the grid system through LCL filter and a step up transformer. The grid current and the grid voltage sensors are attached on converter side and grid side of the LCL filter, respectively. The DC voltage (V_{dc}) across the DC capacitor is detected. The voltage reference of grid side voltage source converter for modulation is controlled by using the grid side controller.

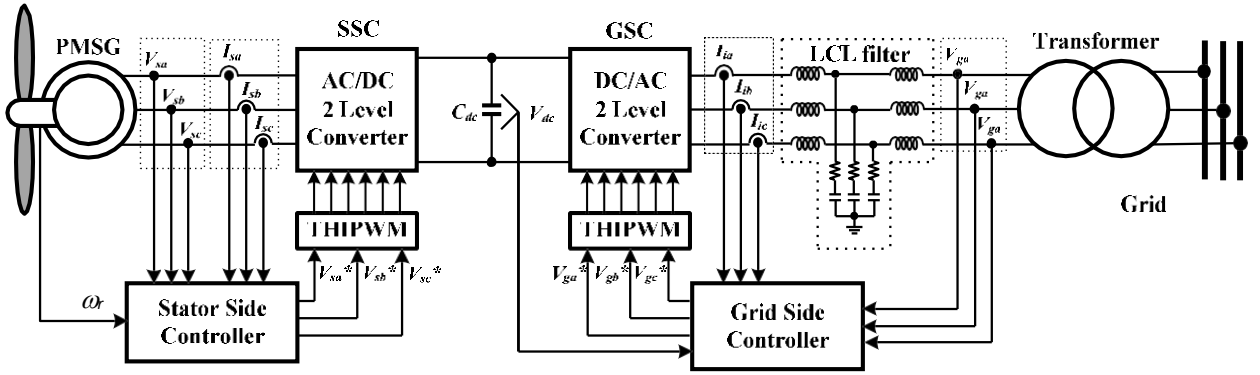


Fig. 6.1. Model and control system of PMSG based variable speed wind turbine

In modulation technique, Third Harmonic Injection Pulse Wave Modulation (THIPWM) is used in this work. Injection of third harmonic in the reference voltage makes it possible to utilize the voltage reference without over modulation. In addition, the THIPWM can maximize fundamental component of the output voltage [8].

6.3.1 Wind Turbine Model

The mechanical power output of wind turbine captured:

$$P_w = 0.5\rho\pi R^2 V^3 C_p(\lambda, \beta) \quad (6.1)$$

Where P_w is the captured wind power (W), ρ is the air density (Kg/m^3), R is the radius of rotor blade (m), V_w is wind speed (m/s), and C_p is the power coefficient. The value of C_p is dependent on tip speed ratio (λ) and blade pitch angle (β) based on the turbine characteristics as follows [9]:

$$C_p(\lambda, \beta) = (C_1(C_2/\lambda_1) - C_3\beta - C_4)e^{-C_3/\lambda_1} + C_6\lambda \quad (6.2)$$

$$1/\lambda_1 = 1/(\lambda - 0.08\beta) - ((0.035/\beta^3) + 1) \quad (6.3)$$

Where C_1 to C_6 denote characteristic coefficients of wind turbine and have values

$$(C_1=0.5176, C_2=116, C_3=0.4, C_4=5, C_5=21 \text{ and } C_6=0.0068).$$

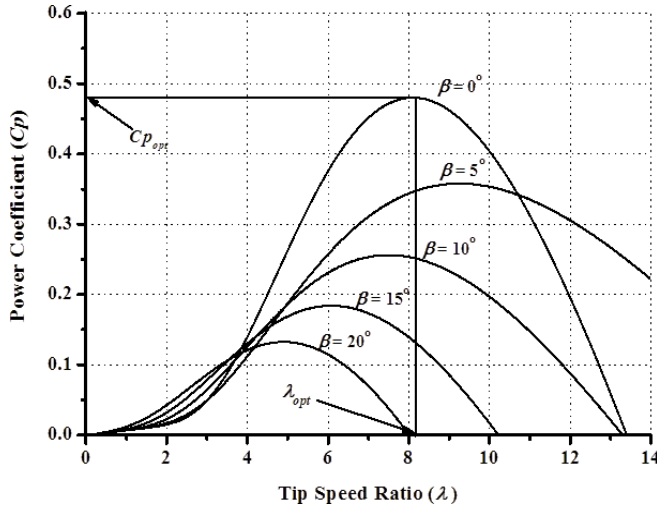


Fig. 6.2 $C_p - \lambda$ characteristic for different pitch angle

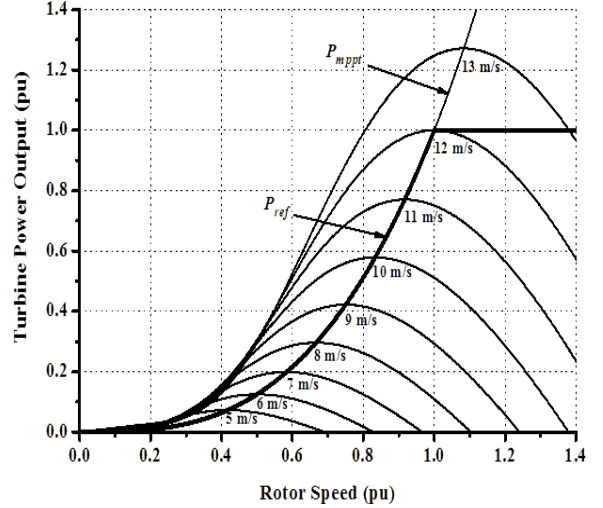


Fig. 6.3 Turbine power characteristic (for $\beta = 0^\circ$)

The $C_p - \lambda$ performance characteristics for different values of β are shown in Fig. 2. It is seen that the optimum value of C_p ($C_{popt} = 0.48$) is achieved at $\lambda = 8.1$ with $\beta = 0^\circ$. This value of λ is set as the optimal value (λ_{opt}). Fig. 3 depicts the characteristic between the turbine power output and the rotor speed for different wind speeds where the blade pitch angle is set at 0 deg. **The maximum power output (1 pu) of wind turbine is obtained at 12 m/sec of wind speed and 1 pu of rotational speed.**

In variable speed wind turbine system, the rotor speed of wind turbine (ω_r) is measured in order to determine the Maximum Power Point Tracking (MPPT). In general, it is difficult to measure the wind speed accurately, and hence the maximum power (P_{mppt}) should be calculated without measuring the wind speed as expressed in (4) [10]. The reference power (P_{ref}) is limited within the rated power of generator.

$$P_{mppt} = 0.5 \rho \pi R^2 (\omega_r R / \lambda^{opt})^3 C_{popt} \quad (6.4)$$

6.3.2 Dynamic Model of PMSG

The dynamic model of PMSG in the d-q rotating reference frame is expressed by the following (5) and (6).

$$d\psi_{sd}/dt = -V_{sd} - R_s * I_{sd} - \omega_e * \psi_{sd} \quad (6.5)$$

$$d\psi_{sq}/dt = -V_{sq} - R_s * I_{sq} - \omega_e * \psi_{sq} \quad (6.6)$$

With

$$\Psi_{sd} = L_{sd} I_{sd} + \Psi_m \quad (6.7)$$

$$\Psi_{sq} = L_{sq} I_{sq} \quad (6.8)$$

Where V_{sd} and V_{sq} are stator voltages, R_s is the stator winding resistance, I_{sd} and I_{sq} are stator currents, ω_e is the generator rotational speed, ψ_{sd} and ψ_{sq} are the stator flux linkages, L_{sd} and L_{sq} are inductances of the stator winding and ψ_m is the permanent magnet flux linkage.

By substituting (7) and (8) into (5) and (6), the differential equations of PMSG can be obtained as follows:

$$L_{sd} * \frac{dI_{sd}}{dt} = -V_{sd} - R_s * I_{sd} - \omega_e * L_{sq} * I_{sq} \quad (6.9)$$

$$L_{sq} * \frac{dI_{sq}}{dt} = -V_{sq} - R_s * I_{sq} - \omega_e * L_{sd} * I_{sd} + \omega_e * \psi_m \quad (6.10)$$

6.3.3 Mathematical Model of LCL Filter

As previously mentioned, utilization of the LCL filter can lead to stability problem due to resonance. To avoid the resonance a passive damping resistance should be allocated in series with a filter capacitor in the filter. However, adopting a damping resistance can cause power losses and then decrease the filter efficiency. Therefore, in designing the voltage source converter controller system, a passive damping resistance should be taken into account in the plant system model.

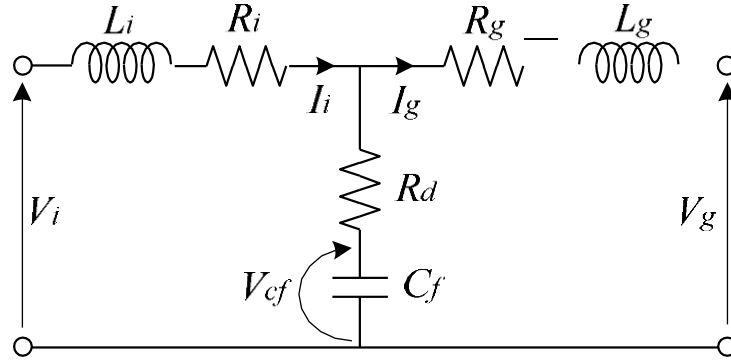


Fig. 6.4 Single phase LC filter equivalent circuit

Single phase LCL filter equivalent circuit is shown in Fig. 4. The LCL filter is composed of an inverter side inductance (L_i) and its parasitic resistance (R_i), a grid side inductance (L_g) and its parasitic resistance (R_g), a filter capacitor (C_f), and a damping resistance (R_d). V_i and I_i are voltage and current on the converter side of the LCL filter. V_g and I_g are voltage and current on the grid side of the LCL filter. It should be noted that V_{cf} is a voltage on the filter capacitor (C_f). The differential equation of LCL filter in stationary reference frame can be written as follows:

$$L_i * \frac{dI_i}{dt} = V_i - V_{cf} - (R_i + R_d)I_i + R_d * I_g \quad (6.11)$$

$$L_g * \frac{dI_g}{dt} = V_{cf} - V_g - (R_g + R_d)I_g + R_d * I_i \quad (6.12)$$

$$C_f * \frac{dV_{cf}}{dt} = I_i - I_g \quad (6.13)$$

From (6.11) to (6.13) differential equations in the d-q rotating reference frame are obtained:

$$L_i * \frac{dI_{id}}{dt} = V_{id} - V_{cfd} - (R_i + R_d)I_{id} + R_d * I_{gd} \quad (14)$$

$$L_i * \frac{dI_{iq}}{dt} = V_{iq} - V_{cfq} - (R_i + R_d)I_{iq} + R_d * I_{gq} \quad (15)$$

$$L_g * \frac{dI_{gd}}{dt} = V_{cfd} - V_{gd} - (R_g + R_d)I_{gd} + R_d * I_{id} \quad (16)$$

$$L_g * \frac{dI_{gq}}{dt} = V_{cfq} - V_{gq} - (R_g + R_d)I_{gq} + R_d * I_{iq} \quad (17)$$

$$C_f * \frac{dV_{cfd}}{dt} = I_{id} - I_{gd} + \omega * C_f * V_{cfq} \quad (18)$$

$$C_f * \frac{dV_{cfq}}{dt} = I_{iq} - I_{gq} - \omega * C_f * V_{cfd} \quad (19)$$

The dynamic block diagram of the grid connected LC filter in the d-q rotating reference frame can be derived as shown in Fig. 6, where s denotes a Laplace operator.

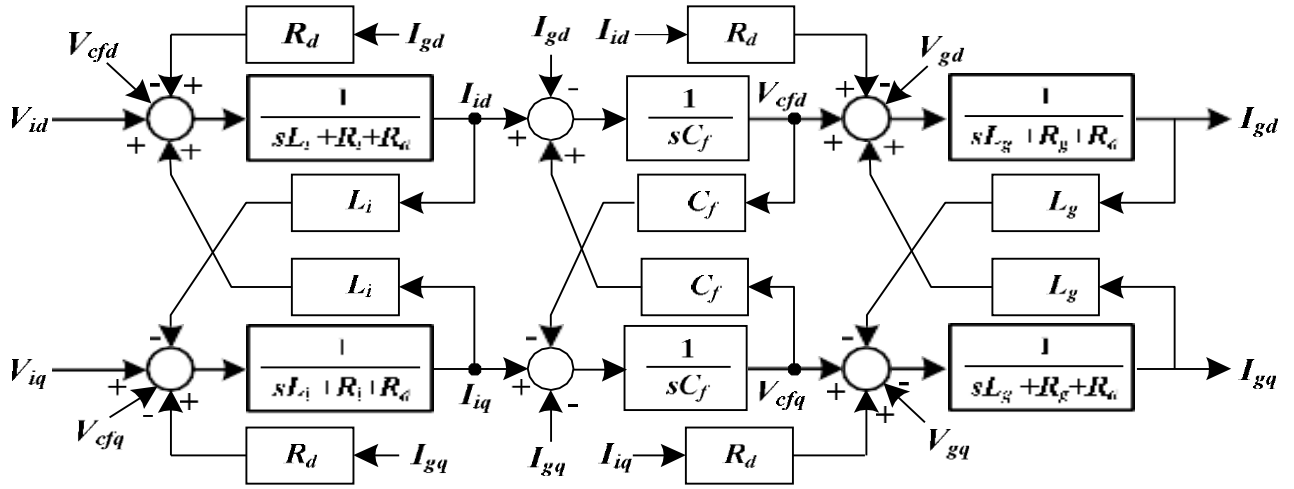


Fig. 6.5 Block diagram of LC filter in the d-q rotating reference frame

6.4. VSWT-PMSG CONTROLLER MODELLING SYSTEMS

6.4.1 Machine Side Controller

Machine side controller system (MSC) is presented in a block diagram shown in Fig. 7. The aim of the machine side controller is to control active and reactive power output of the PMSG. The current control loop is designed based on the d-q rotating reference frame. Then rotor angle position (θ_r) used in the transformation between abc and dq variables is obtained from the rotor speed of generator. The active power (P_s) and reactive power (Q_s) of the generator are controlled by the d-axis current (I_{sd}) and the q-axis current (I_{sq}), respectively.

The value of active power reference (P_{ref}) is determined by MPPT method of the WT as shown in Fig. 3. The reactive power reference (Q_s^*) is set to zero for unity power factor operation. The cross couplings $I_{sd} \cdot \omega_e \cdot L_{sd}$ and $I_{sq} \cdot \omega_e \cdot L_{sq}$ should be compensated at the output of the current controllers in order to improve tracking capability. To design controller parameters, the plant transfer function is represented as $1/(R+Ls)$ for d/ q current loop. By using the pole placement method, the gain of the PI controller can be tuned.

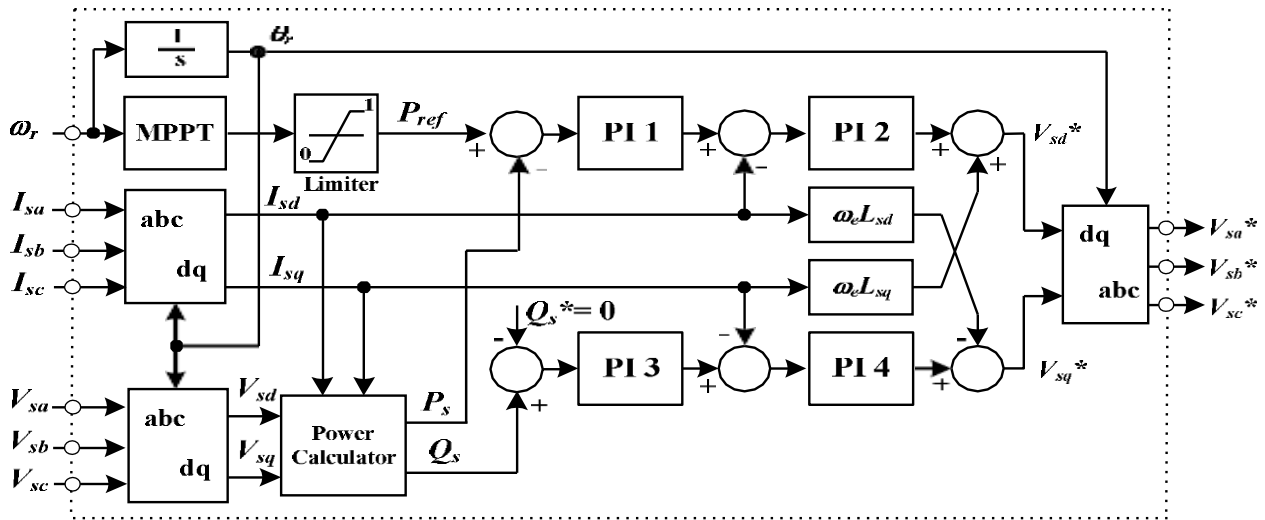


Fig. 6.6 Stator side controller system

6.4.2 Grid Side Controller

Grid side Controller is essential in design of control system because it can dominate the performance of VSWT- PMSG connected to a grid system. The aims of VSC control are: (a) to maintain DC link circuit voltage; (b) to control the reactive power exchange with the grid system as well as maintain the power factor to be unity [12].

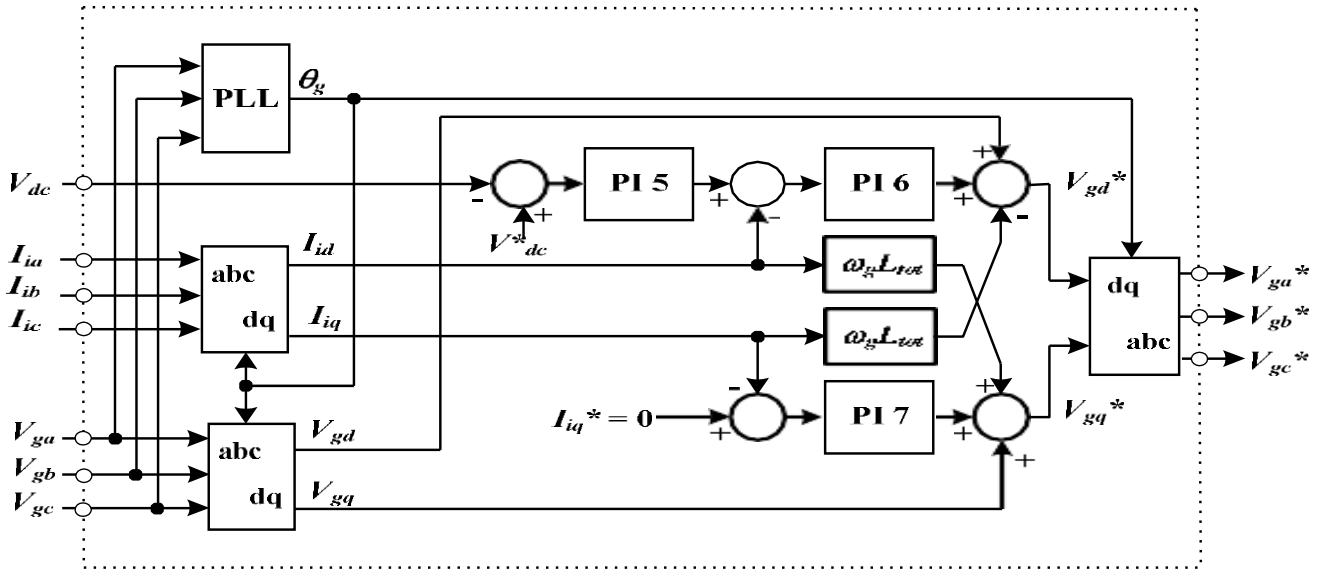


Fig. 6.7 Grid side controller system

Fig. 8 shows a block diagram of the grid side control system. In this control strategy, control system is based on the d-q rotating reference frame, which has same rotational speed as the grid voltage, is implemented. By the use of Phase Locked Loop (PLL) the grid side phase angle (θ) for the d-q transformation is obtained. In this paper PLL block introduced in [13] is used. When grid voltages on the stationary reference frame are transformed into the d-q rotating reference frame, V_{gd} becomes constant and V_{gq} becomes zero. Therefore, the active and reactive power delivered to the grid can be controlled separately by the d- axis current (I_{id}) and the q-axis current (I_{iq}), respectively.

In order to assure the active power exchange between PMSG and the grid, the voltage of DC-link capacitor (V_{dc}) is maintained constant. Hence, the d-axis current reference signal (I_{id}^*) is determined from output of the DC-voltage controller. For unity power factor operation, the q-axis current reference signal (I_{iq}^*) is also set to zero. To improve tracking capability of control system, the cross coupling terms could be canceled by adding ωL_{tot} at the output of the current controllers, where L_{tot} is total series inductances of the filter and transformer. The output of current controller (V_{gd}^* and V_{gq}^*) is transformed into the stationary reference frame (V_{ga}^* , V_{gb}^* , V_{gc}^*) which is used as reference signal for pulse wave modulation.

6.4.3. LCL Filter Parameters

In order to obtain the LCL filter parameters, the system conditions shown in Table I are considered. There are many methods that may be considered in determining the filter parameters. However, in this paper procedure and limitations of LCL filter parameters presented in [6] are considered.

TABLE – 6.1
Parameters PMSG System (Along with LCL Filter)

Component	Parameter	Value
PMSG	Rating	2.5 MW
	Rs	0.01 (pu)
	Lsd	1.0 (pu)
	Lsq	0.7 (pu)
	ψ_m	1.4 (pu)
	H	3.0 (sec)
AC/DC/AC Power Converter	SSC frequency Switching	1 kHz
	GSC frequency Switching	4 kHz
	Grid Frequency	50 Hz
	DC Link capacitor	25000 μ F
	DC Link voltage	1.75 kV
Transformer	Total winding inductance (L_t)	0.040 pu
	Total winding resistance (R_t)	0.016 pu
	Converter side voltage	1.0 kV
	Grid side voltage	6.6 kV

According to the parameters in Table - I, 0.4Ω base impedance, $1.3mH$ base inductance, and $8000\mu F$ base capacitance are calculated. As the inductance on the inverter side (L_i), 5.0% of base inductance is adopted. In order to calculate the grid side inductance (L_g), the transformer inductance (L_t) should be considered. 4% of base inductance has been adopted as transformer inductance. Adding a small value of grid side inductance (L_g), total 4.1% of base inductance is obtained. The initial value for filter capacitor (C_f) is set to maximum limitation (5%). The resonance frequency of LCL filter is around 1.4 kHz.

6.5 SIMULATION AND SYSTEM STUDY

Validity of the design and analysis method explained above has been evaluated using the model system shown in Fig. 9. A VSWT- PMSG rated at 2.5 MW is connected to 6.6 kV distribution system through converters composed of stator side and grid side VSCs, a LCL filter, a 1.0/6.6 kV step up transformer, and a double circuit transmission line. A local load

rated at 1 MW is installed near the wind generator. In the figure, impedances of the transmission line are shown in the form of $R+jX$, where R and X represent the resistance and reactance, respectively. System base power is 100 MVA.

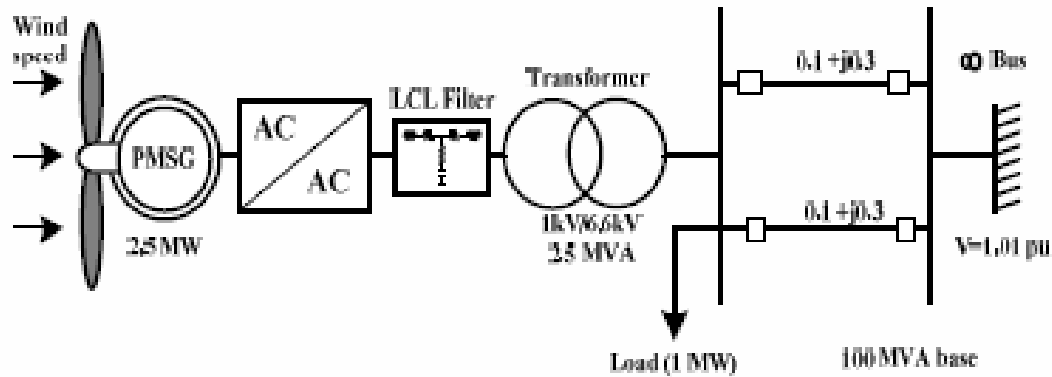


Fig. 6.8 Model system

In order to evaluate the dynamic performances of the proposed system, simulations were performed by using MATLAB. Fig. 10 depicts the pitch angle response of the VSWT-PMSG, which is activated when the wind speed exceeds the rated value. The active power reference (P_{ref}), the active power output of PMSG (P_s), and the active power delivered to the grid (P_g) are shown in Fig. 10. It is seen that P_s and P_g follow P_{ref} very well. The reactive power outputs of the generator and the grid side converter are kept almost zero as shown in Fig 11. The response of the DC link voltage is shown in Fig. 12. It is seen that the DC voltage can also be maintained constant at rated value (1.75 kV).

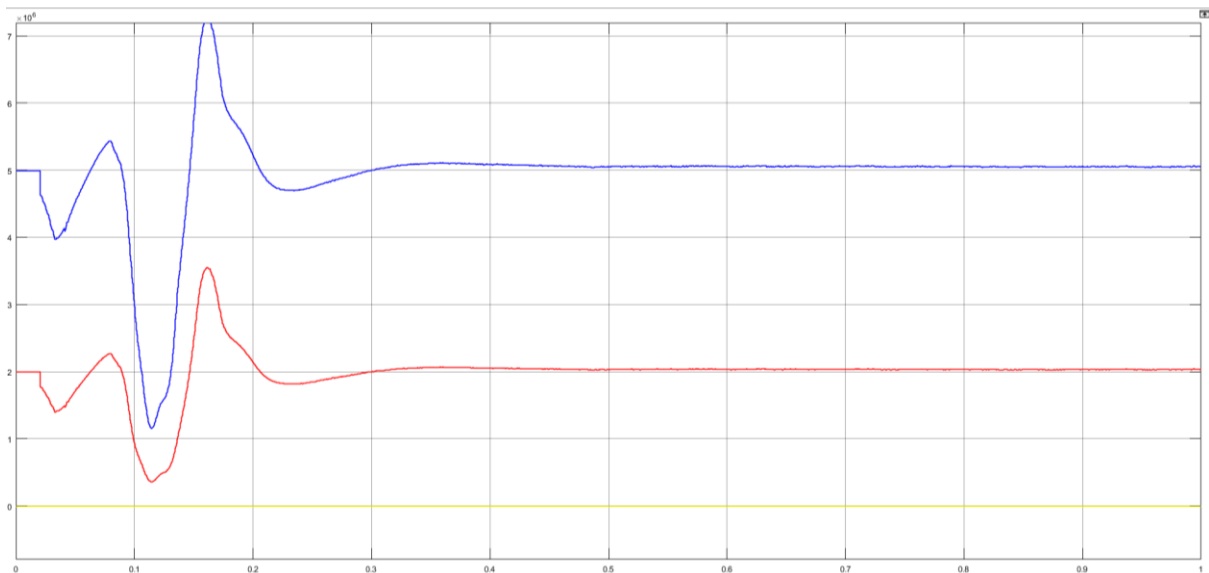


Fig. 6.9. Power Output

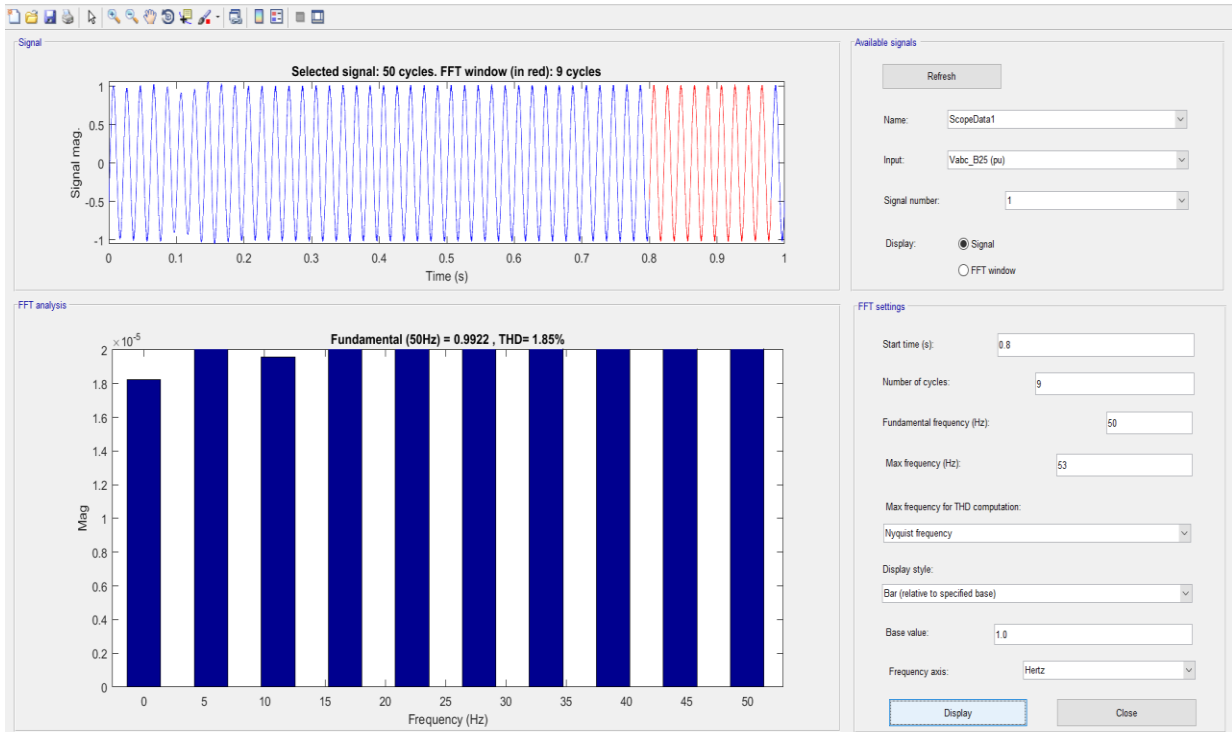


Fig. 6.10 THD Calculation

6.6 CONCLUSION

In this paper, design and analysis of the control system for 2.5 MW class of VSWT-PMSG connected to a distribution grid system through LCL filter is presented. Design and analysis of the grid side current controlled voltage source converter is focused, in which passive damping resistance of the filter and gains of PI controllers of VSC are selected based on frequency response of the bode diagram and dynamic step response. According to the simulation results it is concluded that the controller system is effective to control active and reactive power delivered to the grid. Moreover, the LCL filter is very effective to attenuate the harmonic distortions.

6.7 Appendix

Table II shows PI controller parameters used in the simulation analyses. The parameters for PI 1 to PI 4 (PI controllers for the stator side controller) are selected by using the pole placement method. The parameters for DC link voltage controller of the grid side controller (PI 5) can be selected same as those of PI 6 and PI 7.

TABLE – 6.2

PI Controller Gains

PI Controller	K_p	T_i
PI 1	0.1	0.02
PI 2	0.4	0.05
PI 3	0.1	0.02
PI 4	0.4	0.0497
PI 5	0.2	0.0497
PI 6	0.2	0.0497
PI 7	0.2	0.0497

CHAPTER 7

DIGITAL CONTROL/ MODEL PREDICTIVE CONTROL STRATEGY FOR WIND ENERGY CONVERSION SYSTEM BASED ON PERMANENT MAGNET SYNCHRONOUS GENERATOR

7.1 ABSTRACT

This review paper introduces a **Model Predictive Control (MPC)** strategy for **Variable Speed-Wind Energy Conversion System (VS-WECS)** based **Permanent Magnet Synchronous Generator (PMSG)**. The optimal operation of a PMSG wind turbine (WT) can be achieved through the predictive control. To harvest the maximum power available from the WECS, **three-phase back-to-back (BTB) converter** can be used to tie the **PMSG** and **utility grid**. Control algorithm can applied to the **Machine side Converter (MSC)** to harvest the maximum power available from the **WECS**. **Grid side Converter (GSC)** is applied to achieve the dc-link voltage regulation.

A model of directly driven PMSG based variable-speed WECS is developed and imitated in **MATLAB/ SIMULINK** environment. The MPC gives good dynamic performance under wind speed variation. The effectiveness of the proposed control approach is validated through extensive simulation results. The proposed MPC uses the model of the converter- based system to forecast the possible future behaviour of the controlled variables. It allows selection of the voltage vector that leads to a minimum error by minimizing, a predefined cost function. The low current THD and robustness against parameters variations features the MPC.

The proposed control technique helps in controlling back-to-back converter in a wind turbine system based on PMSG. Results of Simulation (under Matlab-Simulink software environment) are presented to show the performances of the considered control strategies.

7.2 INTRODUCTION

Growth of renewable energy systems in recent years is due to the following reasons [1]:-

- (a) Efforts for minimising carbon dioxide emissions to reduce environmental pollution.
- (b) Increasing cost of electricity from non-renewable sources.

Taking in view the above mentioned fact the global energy demands, wind energy systems have emerged as most promising and growing renewable energy sources [2]. This growth will continue with the expansions of renewable action plans of the countries. As a result, production of wind energy will further increase globally. Several configurations of WECS are being used for the purpose of generating cleaner and greener energy. Among them, the Doubly Fed Induction Generator (DFIG) based on VS-WECS has taken the prominent place in the market [3]. Where, DFIG acts as a source of real and reactive powers. Besides, it can operate with partial scale power converter “approximately 30% of machine rating” [4]. On the other hand, other configurations of VS-WECS are used which have features such as larger capacity, economical cost, and higher reliability. Among different generator types, the use of PMSG seems to be the most promising and successful configuration of wind energy systems. It has many advantages such as high power density, high degree of precision, variable speed operation, lesser maintenance, increased reliability due to absence of gear boxes and good grid compatibility [5]. The VS_WECS consists of a PMSG directly coupled to the WT. The stator windings of the PMSG are tied to the utility grid through a back-to-back (BTB) full scale converter, which is composed of two parts connected through a dc-link capacitor.

The implementation of advanced control schemes increases the VS-WECS performance. Among various advanced control schemes, fuzzy logic control and model predictive control (MPC) is the most common [6]. It can be predicted by using the system model to predict the behaviour of the controlled variables. A cost function is used as a criterion to select the voltage vector that minimizes the error between the controlled variable and its reference. MPC has several advantages such as, it can be used with a variety of systems and contrarians, nonlinearities can be easily included, and multi-variable case can be considered. Moreover, it depends on its own predictions for the next step.

The WT mechanical output power changes with the wind speed. As a result, different MPPT algorithms are used to maintain maximum mechanical power at all wind speed conditions. In this paper, a MPC strategy for PMSG VS-WECS is proposed. The PMSG is tied to the utility grid at the point of common coupling (PCC) via a three-phase back-to-back (BTB) converter. Two control schemes are developed for machine and network side converters. A shunt capacitor is used as a dc-link between the two converters. The MPC is applied in the MSC to extract maximum power. MPC is also used in the GSC to add only active power into the grid. A tip speed ratio (TSR/ λ) algorithm is used to maintain the mechanical power to its optimal value. The system dynamics are tested/ assessed with the help of MATLAB/ SIMULINK. This research work is subdivided as following:-

- (a) Section 2 presents the WECS modelling and
- (b) MPPT technique applied is discussed in section 3.
- (c) Control of the MSC and GSC is discussed in section 4.
- (d) The principles of MPC for MSC and GSC are discussed in section 5.
- (e) The system results are depicted/ analyzed in section 6.

(f) Conclusions of the work are given in section 7.

7.3 WIND ENERGY CONVERSION SYSTEM

The structure of the WECS is discussed in this section. It consists of a three-phase PMSG. A BTB converter is connected to the PMSG and grid as shown in Fig. 1. The MSC uses the MPC to extract maximum power as well as to add active power into the grid for unity power factor operation.

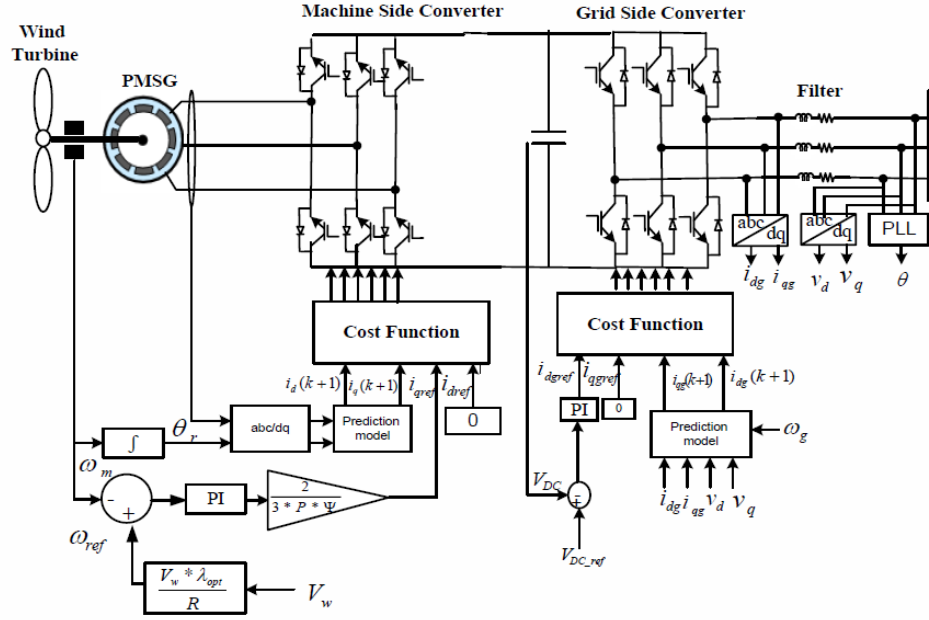


Fig. 7.1 PMSG Wind Energy Conversion System Configuration

7.3.1 Wind Turbine Model

When wind is applied to the turbine the output mechanical power drives the rotor of the generator. For a variable speed WT, the output mechanical power and torque are given by the following expressions:

$$\mathbf{P}_m = 1/2\rho A C_p(\lambda, \beta) V_w^3 \quad \text{Eq.(7.1)}$$

$$\mathbf{T}_m = \mathbf{P}_m / \omega_m \quad \text{Eq.(7.2)}$$

Where turbine output power (in Watts) is symbolized by \mathbf{P}_m , mechanical torque of turbine is denoted by \mathbf{T}_m (in Nm), C_p is the turbine power coefficient (dimensionless), ρ is the air density (in kg/m³), A is the area swept by the turbine blades (in m²), V_w is the wind velocity (in m/s), and ω_m is the mechanical angular speed of the turbine (in rad/s).

The turbine power coefficients C_p , describes the power extraction efficiency of the WT. It is a nonlinear function of both tip speed ratio λ and the blade pitch angle β . The tip speed ratio λ is a variable expresses the ratio of the linear speed of the tip of blades to rotational speed of WT, as follows:

$$\lambda = \omega_m R / V_w \quad \text{Eq.(7.3)}$$

Where, R is the radius of the turbine blade. There are many different versions of the fitted equations for C_p . This paper defines C_p as follows:

$$C_p(\lambda, \beta) = C_1 (C_2/\lambda_1 - C_3\beta - C_4) e^{-C_5/\lambda_1} + C_6 \lambda \quad \text{Eq.(7.4)}$$

$$1/\lambda_1 = 1/(\lambda + 0.08\beta) - 0.035/(1 + \beta^2) \quad \text{Eq.(7.5)}$$

The relation between C_p and λ when β is equals to zero degree is shown in Fig. 2.

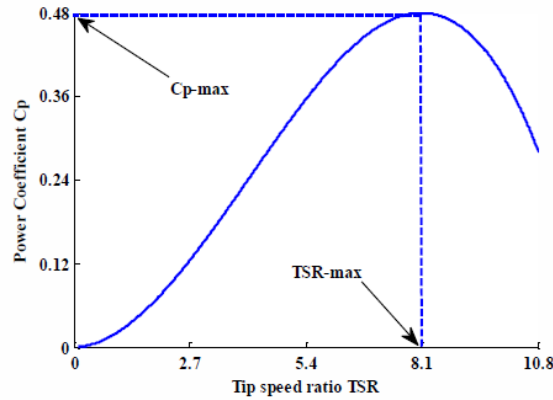


Fig. 7.2 Power Coefficient(C_p) vs. Tip Speed Ratio (TSR/ λ)

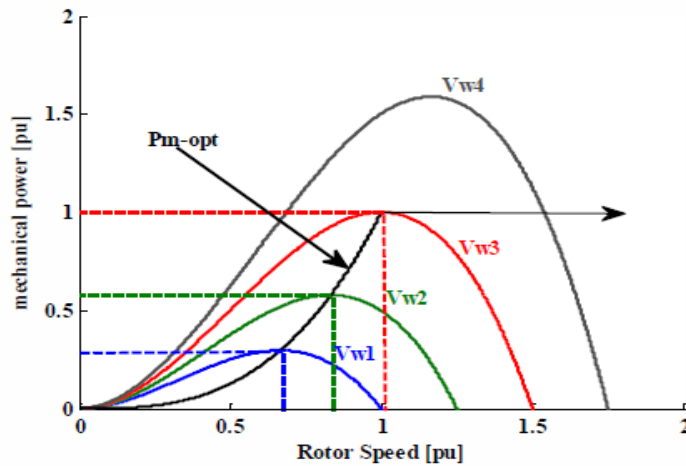


Fig. 7.3 Generated Mechanical Power vs. Rotor Speed at different Wind Speed

7.3.2 Permanent Magnet Synchronous Generator Model

The voltage equations of a three-phase PMSG in the rotor reference frame using an extended Park transformation are as follows:

$$\mathbf{V}_{ds} = \mathbf{R}_s \mathbf{i}_{ds} - \omega_r \psi_{qs} = \mathbf{R}_s \mathbf{i}_{ds} - \omega_r \mathbf{L}_{qs} \mathbf{i}_{qs} \quad \text{Eq.(7.6)}$$

$$\mathbf{V}_{qs} = \mathbf{R}_s \mathbf{i}_{qs} + \omega_r \psi_{ds} = \mathbf{R}_s \mathbf{i}_{qs} + \omega_r \mathbf{L}_{ds} \mathbf{i}_{ds} + \omega_r \psi_r \quad \text{Eq.(7.7)}$$

Where \mathbf{V}_{ds} and \mathbf{V}_{qs} denotes the stator voltages in the (d, q) axis, \mathbf{i}_{ds} and \mathbf{i}_{qs} symbolize the currents in the (d, q) axis, \mathbf{R}_s represents stator resistance, \mathbf{L}_{ds} , \mathbf{L}_{qs} represent the (d, q) axis inductances, $\omega_e = p_p \omega_r$ (p_p is number of pole pairs, ω_m represents the turbine rotor angular speed) and ψ_s is the permanent flux linkage.

The developed torque of the PMSG can be expressed as:

$$\mathbf{T}_e = 3/2 p_p \psi_s \mathbf{i}_s \quad \text{Eq.(7.8)}$$

The mechanical equation of the PMSG is given by:

$$\mathbf{T}_m = \mathbf{T}_e + \mathbf{f} \omega_m + \mathbf{J} d \omega_m / dt \quad \text{Eq.(7.9)}$$

Where f is the friction coefficient, J is the total moment of inertia, \mathbf{T}_m is the mechanical torque produced by a WT and \mathbf{T}_e is electromagnetic torque of PMSG.

Steady state dq-axis stator flux linkage

The flux equations of a three-phase PMSG expressed in the rotor reference frame using an extended Park transformation are as follows:

$$\psi_{ds} = \mathbf{L}_{ds} \mathbf{i}_{ds} + \psi_r, \quad \psi_{qs} = \mathbf{L}_{qs} \mathbf{i}_{qs} \quad \text{Eq.(7.10)}$$

Stator output active, reactive and apparent power

The power (real and apparent) equations of a three-phase PMSG expressed in the rotor reference frame using an extended Park transformation are as follows:

$$\mathbf{P}_s = 3 \mathbf{V}_s \mathbf{I}_s \cos \phi_s = 1.5 (\mathbf{V}_{ds} \mathbf{i}_{ds} + \mathbf{V}_{qs} \mathbf{i}_{qs}) \quad \text{Eq.(7.11)}$$

$$\mathbf{Q}_s = 3 \mathbf{V}_s \mathbf{I}_s \sin \phi_s = 1.5 (\mathbf{V}_{qs} \mathbf{i}_{ds} - \mathbf{V}_{ds} \mathbf{i}_{qs}) \quad \text{Eq.(7.12)}$$

$$\mathbf{S}_s = 3 \mathbf{V}_s \mathbf{I}_s = (\mathbf{P}_s^2 + \mathbf{Q}_s^2)^{1/2} \quad \text{Eq.(7.13)}$$

7.4 MAXIMUM POWER POINT TRACKING TECHNIQUES

Various MPPT techniques are available to maintain the mechanical power to its maximum value for all wind speed conditions. Among these techniques the tip speed ratio TSR technique adjusts the rotor speed to its optimum values at different wind speeds, however this technique is based on measuring the wind and rotor speeds. Also, the reference rotor speed at different wind speeds is calculated as follows:

$$\omega_{\text{ref}} = \lambda_{\text{opt}} R / V_w \quad \text{Eq.(7.14)}$$

Where ω_{ref} is the reference rotor speed, λ_{opt} is the optimum TSR, R is the blade radius and V_w is the wind speed. It is obvious that the TSR control is a simple MPPT strategy but extremely reliant on the accuracy of the wind speed measurement using an anemometer which increases to the system cost.

From Eq. (9) the control of generator speed can be achieved by the control of electromagnetic torque. Moreover, from Eq. (8) the electromagnetic torque is proportional to the q-axis current of PMSG, hence the rotor speed can be controlled by changing the q-axis current of PMSG.

$$i_{\text{qref}} = 2T_m / 3P_p \psi \quad \text{Eq.(7.15)}$$

7.5 CONTROL OF MACHINE SIDE AND GRID SIDE CONVERTERS

Two levels BTB converter acts as a rectifier on the MSC and inverter on GSC. The MSC is used to adjust the rotor speed to its optimal values at different wind speeds. Moreover, the WT operates at maximum power under wind speed variations. The MSC consists of two loops, the outer loop is used to adjust the rotor speed through a PI controller and the inner loop is for the d-axis and q-axis stator currents to its reference values through an MPC. On the other hand, the GSC is used to maintain the dc-link capacitor voltage to its reference value. Also, the GSC is used to control the real and reactive power. The internal control loop is for power control through the MPC. The external loop regulates the dc-link capacitor voltage through a PI controller.

7.6 MODEL PREDICTIVE CONTROL

The MPC contains a wide family of controllers. The controller predicts and estimates the upcoming behavior of variables for a limited horizon of time. Then, the controller selects the optimal actuations by minimising the cost function g . The working principles of MPC are summarized in Fig. 4 and are concluded in three steps as follows:

1. Construct a model for the system to predict the future behavior of variables until a horizon in time.
2. A cost function is applied that represents the desired behavior of the system.
3. The optimal actuation is obtained by minimizing the cost function.

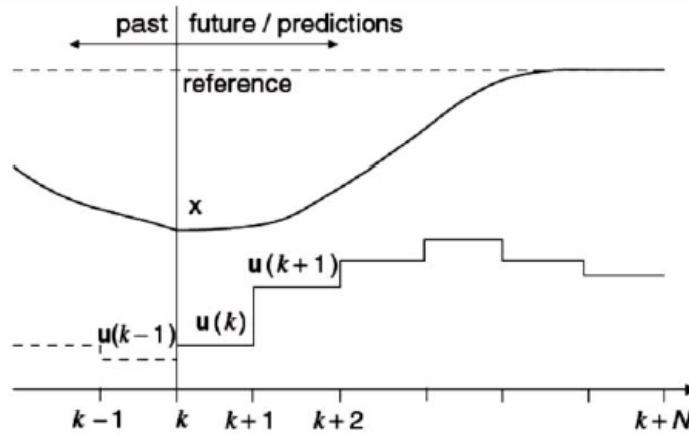


Fig. 7.4 Basic Principles of MPC

In this study, the MPC is used in the MSC as an electromagnetic torque controller to extract maximum power at different wind speeds and to control the reactive power in the GSC uses an MPC.

7.7 MODEL PREDICTIVE CONTROL OF CONVERTORS (GSC/ MSC)

The mathematical model of the GSC connected to the grid through an L filter in the dq synchronous reference frame is characterised by the following relations.

$$d\mathbf{i}_{gd}/ dt = 1/ L_g (\mathbf{V}_{gd} - \mathbf{R}_g \mathbf{i}_{gd} + \omega_g L_g \mathbf{i}_{gq} - \mathbf{V}_{convd}) \quad \text{Eq.(7.16)}$$

$$d\mathbf{i}_{gq}/ dt = 1/ L_g (\mathbf{V}_{gq} - \mathbf{R}_g \mathbf{i}_{gq} - \omega_g L_g \mathbf{i}_{gd} - \mathbf{V}_{convq}) \quad \text{Eq.(7.17)}$$

$$\mathbf{P} = \mathbf{V}_{gd} \mathbf{i}_{gd} + \mathbf{V}_{gq} \mathbf{i}_{gq} \quad \text{Eq.(7.18)}$$

$$\mathbf{Q} = \mathbf{V}_{gq} \mathbf{i}_{gd} - \mathbf{V}_{gd} \mathbf{i}_{gq} \quad \text{Eq.(7.19)}$$

Where \mathbf{i}_{gd} and \mathbf{i}_{gq} (respectively \mathbf{V}_{gd} and \mathbf{V}_{gq}) are the d and q components of the grid current vector (respectively the grid voltage vector) and ω_g is the angular frequency of the grid voltage. \mathbf{V}_{convd} and \mathbf{V}_{convq} are the d and q components of the converter output voltage vector. \mathbf{L}_g and \mathbf{R}_g are respectively the resistor and inductor of the used L-filters. \mathbf{di}_{gd}/dt and \mathbf{di}_{gq}/dt are the the instantaneous grid current time derivatives.

The stator current equation can be discreteised with a sampling time T_s . The discrete-time model can be obtained by a simple Euler approximation of the derivative. The stator current derivative di/dt is replaced by a forward Euler approximation.

The derivative is approximated as follows:

$$\mathbf{di}/dt = \mathbf{i}[k+1] - \mathbf{i}[k] / T_s \quad \text{Eq.(7.20)}$$

Hence, mathematically PMSG can be written as:

$$\mathbf{i}_d[k+1] = (1 - T_s R_s / L_d) * \mathbf{i}_d[k] + (T_s L_q / L_d) * \omega_e * \mathbf{i}_q[k] + T_s V_d[k] / L_d \quad \text{Eq.(7.21)}$$

$$\mathbf{i}_q[k+1] = (1 - T_s R_s / L_q) * \mathbf{i}_q[k] - (T_s L_d / L_q) * \omega_e * \mathbf{i}_d[k] + T_s V_q[k] / L_q - T_s \psi \omega_e / L_q \quad \text{Eq.(7.22)}$$

The cost function, g , is assumed as follows:

$$g = |[\mathbf{i}_{dref}[k+1] - \mathbf{i}_d[k+1]]| + |[\mathbf{i}_{qref}[k+1] - \mathbf{i}_q[k+1]]| \quad \text{Eq.(7.23)}$$

Where $\mathbf{i}_{dref}[k+1]$ and $\mathbf{i}_{qref}[k+1]$ are the reference values of d-axis and q-axis stator currents. The cost function is calculated for each state. The minimum value of cost function is applied at the next sampling instant.

7.8 MPC Based Control OF MSC/ SGSC

The MPC-based control for the MSC/ SGSC is presented in Fig. 5. It is based on the computation of the required converter voltage vector, to be applied during the next sampling period in order to minimise the error between the stator current and its reference in the dq synchronous reference frame. The d axis stator current reference \mathbf{i}_{sd}^* is set to zero in order to obtain the maximum torque at the minimum current, whereas the q axis stator current reference \mathbf{i}_{sq}^* is computed via the external PI-based speed controller. For the development of the digital predictive current controller algorithm, expressions (16) and (17) can be written as follows:

$$d\mathbf{i}_{sd}/dt = 1/L_{sd}(\mathbf{V}_{sd} - \mathbf{R}_s \mathbf{i}_{sd} + \omega_{dq} L_{sq} \mathbf{i}_{sq}) \quad \text{Eq.(7.24)}$$

$$d\mathbf{i}_{sq}/dt = 1/L_{sd}(\mathbf{V}_{sq} - \mathbf{R}_s \mathbf{i}_{sq} + \omega_{dq} L_{sq} \mathbf{i}_{sd} + \omega_{dq} \phi_{rd}) \quad \text{Eq.(7.25)}$$

From Eqs. (7.16) and (7.17), and using the forward Euler discretisation method, the following digital prediction equations are obtained.

$$\mathbf{i}_{sd}[k+1] = \mathbf{a}_0(\mathbf{V}_{sd}[k] - \mathbf{e}_{sd}[k]) + \mathbf{a}_1 \mathbf{i}_{sd}[k] \quad \text{Eq.(7.26)}$$

$$\mathbf{i}_{sq}[k+1] = \mathbf{a}_3(\mathbf{V}_{sq}[k] - \mathbf{e}_{sq}[k]) + \mathbf{a}_2 \mathbf{i}_{sq}[k] \quad \text{Eq.(7.27)}$$

$$\mathbf{e}_{sd}[k] = -L_{sq} \omega_{dq}[k] \mathbf{i}_{sq}[k] \quad \text{Eq.(7.28)}$$

$$\mathbf{e}_{sq}[k] = L_{sd} \omega_{dq}[k] \mathbf{i}_{sd}[k] + \omega_{dq}[k] \phi_{rd}[k] \quad \text{Eq.(7.29)}$$

Where

$$\mathbf{a}_0 = T_s / L_{sd}$$

$$\mathbf{a}_1 = (1 - \mathbf{R}_s T_s / L_{sd})$$

Eq.(30)

$$\mathbf{a}_2 = T_s / L_{sq}$$

$$\mathbf{a}_3 = -(1 - \mathbf{R}_s T_s / L_{sq}) \quad \text{Eq.(7.30)}$$

T_s is the sampling period. $\mathbf{i}_{sd}[k+1]$ and $\mathbf{i}_{sq}[k+1]$ (respectively $\mathbf{i}_{sd}[k]$ and $\mathbf{i}_{sq}[k]$) are the predicted d and q stator current components at the $(k+1)^{\text{th}}$ sampling period (respectively measured d and q stator current components during k^{th} sampling period). The \mathbf{e}_{sd} and \mathbf{e}_{sq} refer respectively to the d and q induced EMF terms. During each sampling period, the evolution of the d and q stator current components depends on the applied stator voltage components $\mathbf{V}_{sd}^j[k]$ and $\mathbf{V}_{sq}^j[k]$ at the k^{th} sampling period. These stator voltage components expressed in the dq synchronous reference frame and can be determined through the application of a rotation operation by an angle equal to θ_{dq} to the $\alpha\beta$ components of the stator voltage vectors as shown in matrix form:-

$$[\mathbf{V}_{sd}^j[k], \mathbf{V}_{sq}^j[k]] = [\cos(\theta_{dq}[k]), \sin(\theta_{dq}[k]), -\sin(\theta_{dq}[k]), \cos(\theta_{dq}[k])] * [\mathbf{V}_{sa}^j[k], \mathbf{V}_{s\beta}^j[k]] \quad \text{Eq.(7.31)}$$

S _{sa}	S _{sb}	S _{sc}	V ^j _{sa}	V ^j _{sβ}	Vector V ^j	Vector V ^j _{sdq}
0	0	0	0	0	V ₀	V ⁰ _{sdq}
1	0	0	2V _{dc} /3	0	V ₁	V ¹ _{sdq}
1	1	0	V _{dc} /3	V _{dc} /√3	V ₂	V ² _{sdq}
0	1	0	-V _{dc} /3	V _{dc} /√3	V ₃	V ³ _{sdq}
0	1	1	-2V _{dc} /3	0	V ₄	V ⁴ _{sdq}
0	0	1	-V _{dc} /3	-V _{dc} /√3	V ₅	V ⁵ _{sdq}
1	0	1	V _{dc} /3	-V _{dc} /√3	V ₆	V ⁶ _{sdq}
1	1	1	0	0	V ₇	V ⁷ _{sdq}

Table.7.1 SGSC/ MSC switching states and corresponding output voltage vector V^j_{sdq}(j=0to7)

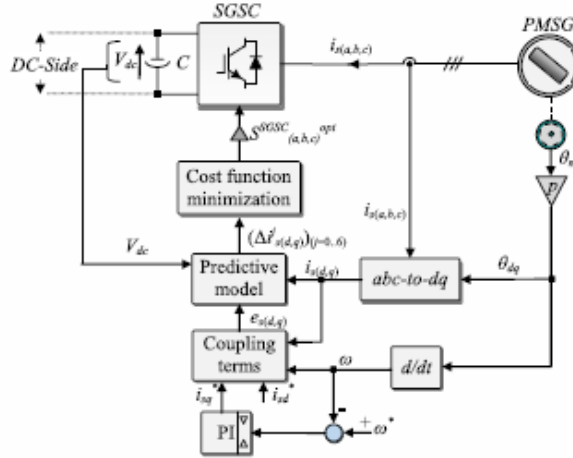


Fig. 7.5 MPC based control for the MSC/ SGSC

Considering the eight switching states combinations of the SGSC with two combinations that lead to null stator voltage vector, Eqs. (7.26) and (7.27) can be expressed for the different possibilities of the d and q stator voltage components V^j_{sd} [k] and V^j_{sq} [k] of the voltage vectors V^j_{sdq} as follows:

$$\{\mathbf{i}_{sd}[k+1] = \mathbf{a}_0(\mathbf{V}_{sd}^j[k] - \mathbf{e}_{sd}[k]) + \mathbf{a}_1\mathbf{i}_{sd}[k]\} \quad \{\text{for } j = 0 \text{ to } 7\} \quad \text{Eq.}(7.32)$$

$$\{\mathbf{i}_{sq}[k+1] = \mathbf{a}_3(\mathbf{V}_{sq}^j[k] - \mathbf{e}_{sq}[k]) + \mathbf{a}_4\mathbf{i}_{sq}[k]\} \quad \{\text{for } j = 0 \text{ to } 7\} \quad \text{Eq.}(7.33)$$

where $\mathbf{i}_{sd}[k+1]$ (j=0to7) and $\mathbf{i}_{sq}[k+1]$ (j=0to7) are the predicted d and q stator current components at the(k+1)th sampling period when the (V^j_{sa}[k]) (j=0to7) and (V^j_{sa}[k]) (j=0to7) voltage vector components are applied during the kth sampling period.

It is possible to predict the dq stator vector components ($\Delta \mathbf{i}_{sd}^j[\mathbf{k}+1]$)^(j=0to7) and ($\Delta \mathbf{i}_{sq}^j[\mathbf{k}+1]$)^(j=0to7). This current errors are defined as the difference between the reference stator current vector at the kth sampling period and the predicted one at the (k+1)th sampling period when the stator voltage vector $\mathbf{V}_{sdq}^j[\mathbf{k}]$ ^(j=0to7) is applied.

Therefore,

$$\Delta \mathbf{i}_{sd}^j[\mathbf{k}+1]_{(j=0to7)} = \mathbf{i}_{sd}^*[\mathbf{k}] - \mathbf{i}_{sd}^j[\mathbf{k}+1]_{(j=0to7)} \quad \text{Eq.(7.34)}$$

$$\Delta \mathbf{i}_{sq}^j[\mathbf{k}+1]_{(j=0to7)} = \mathbf{i}_{sq}^*[\mathbf{k}] - \mathbf{i}_{sq}^j[\mathbf{k}+1]_{(j=0to7)} \quad \text{Eq.(7.35)}$$

Based on relations (7.24)–(7.33), a cost function g_s is applied to the obtained stator current error components. This cost function is defined in Eq. (36).

$$\{g_s^j = |(\Delta \mathbf{i}_{sd}^j[\mathbf{k}+1])| + |(\Delta \mathbf{i}_{sq}^j[\mathbf{k}+1])|\}_{(j=0to7)} \quad \text{Eq.(7.36)}$$

Finally, an optimization procedure is applied. This procedure consists of selecting the optimal switching states combination $S_{\text{opt}(a,b,c)}^{\text{SGSC opt}}$ that leads to the minimal cost function $\text{Min } g_s^j_{(j=0to7)}$.

7.9 MPC BASED CONTROL OF GSC

The MPC-based control for the GSC is presented in Fig. 6. The main objective of the MPC algorithm for the GSC is to control the active and reactive power through the control of the d and q grid current components. The d axis grid current reference \mathbf{i}_{gd}^* is computed by the PI controller of the outer dc-link voltage control loop, whereas the q axis grid current reference \mathbf{i}_{gd}^* is set to zero in order to impose a unit power factor operation.

From Eqs. (7.16), (7.17), (7.26) and (7.27), and using the forward Euler discretisation method, the digital prediction equations are deduced as in (7.37) and (7.38)

$$\mathbf{I}_{gd}[\mathbf{k}+1] = \mathbf{b}_0(\mathbf{V}_{gd}[\mathbf{k}] - \mathbf{V}_{\text{convd}}[\mathbf{k}]) + \mathbf{b}_2\mathbf{i}_{gq}[\mathbf{k}] \quad \text{Eq.(7.37)}$$

$$\mathbf{I}_{gq}[\mathbf{k}+1] = \mathbf{b}_0(\mathbf{V}_{gq}[\mathbf{k}] - \mathbf{V}_{\text{convd}}[\mathbf{k}]) + \mathbf{b}_1\mathbf{i}_{gq}[\mathbf{k}] - \mathbf{b}_2\mathbf{i}_{gd}[\mathbf{k}] \quad \text{Eq.(7.38)}$$

Where T_s is the sampling period and

$$\begin{aligned} \mathbf{b}_0 &= T_s/L_g, \\ \mathbf{b}_1 &= (\mathbf{1} - \mathbf{R}_g T_s/L_g) \\ \mathbf{b}_2 &= \omega_g T_s \mathbf{i}_{gd}[\mathbf{k}+1] \end{aligned} \quad \text{Eq.(7.39)}$$

Where $\mathbf{i}_{gq}[\mathbf{k}+1]$ (respectively $\mathbf{i}_{gd}[\mathbf{k}]$ and $\mathbf{i}_{gq}[\mathbf{k}]$) are the predicted d and q grid current components at the $(\mathbf{k}+1)^{\text{th}}$ sampling period (respectively measured d and q grid current components during \mathbf{k}^{th} sampling period). During each sampling period, the evolution of the d and q grid current components depends on the applied converter voltage components $\mathbf{V}_{\text{convd}}[\mathbf{k}]$ and $\mathbf{V}_{\text{convq}}[\mathbf{k}]$ at the \mathbf{k}^{th} sampling period. These voltage components can be determined through the application of a rotation operation (with an angle equal to the grid voltage vector position θ_{dq} calculated through a PLL) to the $\alpha\beta$ components of the converter voltage vectors. It should be mentioned that the voltage vectors $\mathbf{V}_{\text{convd}}^j[\mathbf{k}]$ and $\mathbf{V}_{\text{convq}}^j[\mathbf{k}]$ depend also on the dc-link voltage V_{dc} level as shown in Eqs. (37) and (38). For simplification reasons the dc-link voltage is supposed equal to its reference V_{dc}^* . Therefore,

$$[\mathbf{V}_{\text{convd}}^j[\mathbf{k}], \mathbf{V}_{\text{convq}}^j[\mathbf{k}]] = [\cos(\theta_{dq}[\mathbf{k}]), \sin(\theta_{dq}[\mathbf{k}]), -\sin(\theta_{dq}[\mathbf{k}]), \cos(\theta_{dq}[\mathbf{k}])] [\mathbf{V}_{\text{conv}\alpha}^j[\mathbf{k}], \mathbf{V}_{\text{conv}\beta}^j[\mathbf{k}]] \quad \text{Eq.(7.40)}$$

$$[\mathbf{V}_{\text{conv}\alpha}^j[\mathbf{k}], \mathbf{V}_{\text{conv}\beta}^j[\mathbf{k}]] = 2/3V_{dc}^* [1, -1/2, -1/2, 0, \sqrt{3}/2, -\sqrt{3}/2] * [S_{ia}[\mathbf{k}], S_{ib}[\mathbf{k}], S_{ic}[\mathbf{k}]] \quad \text{Eq.(7.41)}$$

Where $\mathbf{V}_{\text{conv}\alpha}^j[\mathbf{k}]$ and $\mathbf{V}_{\text{conv}\beta}^j[\mathbf{k}]$ are the output converter voltage vectors in the stationary $\alpha\beta$ coordinates, and $S_{(a,b,c)}^{\text{GSC}}[\mathbf{k}]$ are the switching signals of the GSC.

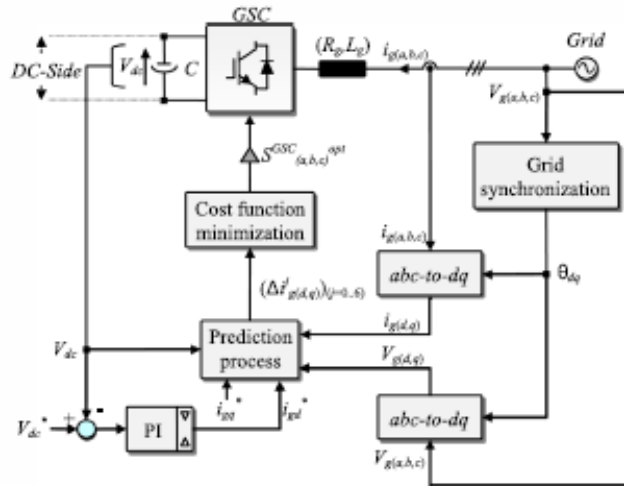


Fig. 7.6 MPC based control for the GSC

Hence, to perform the prediction process, seven cases must be taken into account since the number of switching states combinations is equal to eight with two combinations that lead to null converter voltage vector. Considering these even switching states combinations, Eqs. (26) and (27) can be expressed for the different possibilities of the d and q converter voltage components $V_{\text{convd}}^j[\mathbf{k}]$ and $V_{\text{convq}}^j[\mathbf{k}]$ of the voltage vectors $\mathbf{V}_{\text{convdq}}^j[\mathbf{k}]$ as follows:

$$\{\mathbf{i}_{gd}^j[\mathbf{k}+1] = \mathbf{a}_0(\mathbf{V}_{gd}[\mathbf{k}] - \mathbf{V}_{convd}^j[\mathbf{k}]) + \mathbf{a}_1\mathbf{i}_{gd}^j[\mathbf{k}] + \mathbf{a}_2\mathbf{i}_{gq}^j[\mathbf{k}]\} \quad \{\text{for } j = 0 \text{ to } 7\} \quad \text{Eq.}(7.42)$$

$$\{\mathbf{i}_{gq}^j[\mathbf{k}+1] = \mathbf{a}_3(\mathbf{V}_{gq}[\mathbf{k}] - \mathbf{V}_{convd}^j[\mathbf{k}]) + \mathbf{a}_1\mathbf{i}_{gq}^j[\mathbf{k}] - \mathbf{a}_2\mathbf{i}_{gd}^j[\mathbf{k}]\} \quad \{\text{for } j = 0 \text{ to } 7\} \quad \text{Eq.}(7.43)$$

S _{ia}	S _{ib}	S _{ic}	V ^j _{convα}	V ^j _{convβ}	Vector V ^j	Vector V ^j _{convdq}
0	0	0	0	0	V ₀	V ⁰ _{sdq}
1	0	0	2V _{dc} /3	0	V ₁	V ¹ _{sdq}
1	1	0	V _{dc} /3	V _{dc} /√3	V ₂	V ² _{sdq}
0	1	0	-V _{dc} /3	V _{dc} /√3	V ₃	V ³ _{sdq}
0	1	1	-2V _{dc} /3	0	V ₄	V ⁴ _{sdq}
0	0	1	-V _{dc} /3	-V _{dc} /√3	V ₅	V ⁵ _{sdq}
1	0	1	V _{dc} /3	-V _{dc} /√3	V ₆	V ⁶ _{sdq}
1	1	1	0	0	V ₇	V ⁷ _{sdq}

Table. 7.2 GSC switching states and corresponding output voltage vector V^j_{convdq(j=0to7)}

Where ($\mathbf{i}_{gd}^j[\mathbf{k}+1]$)^(j=0to7) and ($\mathbf{i}_{gq}^j[\mathbf{k}+1]$)^(j=0to7) are the predicted d and q grid current components at the (k+1)th sampling period when the ($\mathbf{V}_{convα}^j[\mathbf{k}]$)^(j=0to7) and ($\mathbf{V}_{convβ}^j[\mathbf{k}]$)^(j=0to7) voltage vector components are applied during the kth sampling period. It is possible to firstly predict the dq grid current error vector components vector ($\Delta\mathbf{i}_{gd}^j[\mathbf{k}+1]$)^(j=0to7) and ($\Delta\mathbf{i}_{gq}^j[\mathbf{k}+1]$)^(j=0to7). These errors are defined as the difference between the reference grid current vector at the kth sampling period and the predicted one at the next sampling period (k+1)th when the converter voltage vector ($\mathbf{V}_{convdq}^j[\mathbf{k}]$)^(j=0to7) is applied. The grid current error vector components are expressed as in (44) and (45).

$$(\Delta\mathbf{i}_{gd}^j[\mathbf{k}+1] = \mathbf{i}_{gd}^*[\mathbf{k}] - \mathbf{i}_{gd}^j[\mathbf{k}+1])^{\text{(j=0to7)}} \quad \text{Eq.}(7.44)$$

$$(\Delta\mathbf{i}_{gq}^j[\mathbf{k}+1] = \mathbf{i}_{gq}^*[\mathbf{k}] - \mathbf{i}_{gq}^j[\mathbf{k}+1])^{\text{(j=0to7)}} \quad \text{Eq.}(7.45)$$

Based on relations (42), (43), (44) and (45), a cost function g_i is applied to the obtained grid current error components. This cost function is defined in Eq. (46).

$$\{\mathbf{g}_i = |\Delta\mathbf{i}_{gd}^j[\mathbf{k}+1]| + |\Delta\mathbf{i}_{gq}^j[\mathbf{k}+1]|\}^{\text{(j=0to7)}} \quad \text{Eq.}(7.46)$$

The core of the predictive algorithm is the cost function minimization [24, 25]. This procedure consists of selecting the optimal switching signals S^{GSC}_(a,b,c)^{opt} that lead to the minimal cost function Min(g_i)^(j=0to7). Note that for the case of null voltage vector, the selected S^{GSC}_(a,b,c)^{opt} switching signals depend on the applied switching signals during the previous sampling period so that the switching frequency is reduced.

7.10. SIMULATION RESULTS AND DISCUSSION

To show the validity and effectiveness of the system, simulation results have been carried out by Matlab/Simulink software. The parameters of the system under study are given in the Appendix. The M file, Simulation algorithm and optimization programme are given below:-

7.10.1 Algorithm

The algorithm flow chart is as under:-

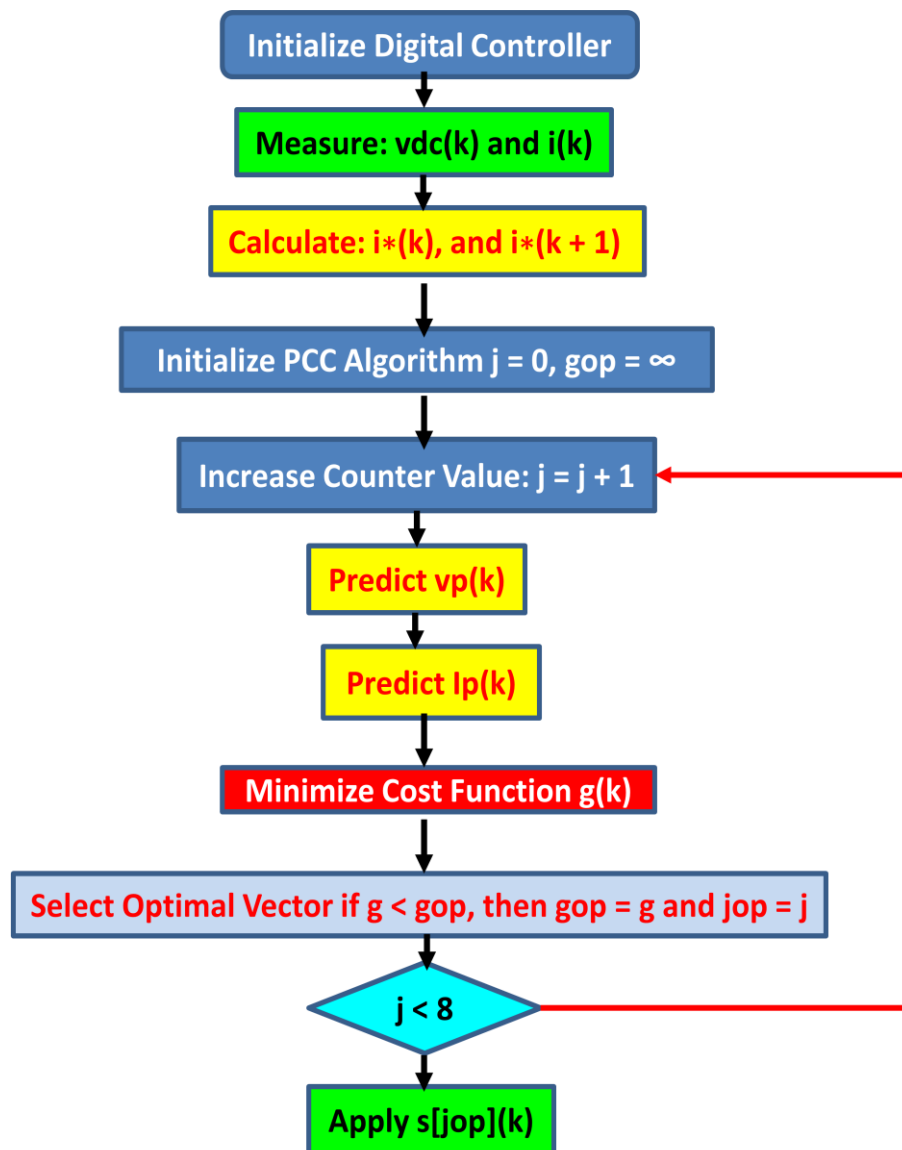


Fig. 7.7 Algorithm MPC

7.10.2 Optimization Program

The Optimization program is as under:-

```
    j_op=1000;  
  
g_op=1000000000;  
for(j=0;j<8;j++)  
{  
    V_abc[0]=Vdc[0]*Vsc[j].Sn_abc[0];  
    V_abc[1]=Vdc[0]*Vsc[j].Sn_abc[1];  
    V_abc[2]=Vdc[0]*Vsc[j].Sn_abc[2];  
    I_abc_k1[0]=Phi*I_abc[0]+Gamma*V_abc[0];  
    I_abc_k1[1]=Phi*I_abc[1]+Gamma*V_abc[1];  
    I_abc_k1[2]=Phi*I_abc[2]+Gamma*V_abc[2];  
    g_a=fabs(I_ref_k1[0]-I_abc_k1[0]);  
    g_b=fabs(I_ref_k1[1]-I_abc_k1[1]);  
    g_c=fabs(I_ref_k1[2]-I_abc_k1[2]);  
    g_k=g_a+g_b+g_c;  
    if(g_k<G-op)  
        {  
            j_op=j;  
            g_op=g_k;  
        }  
    }  
  
    s_a[0]=Vsc[j_op].s_abc[0];  
    s_a[1]=Vsc[j_op].s_abc[1];  
    s_a[2]=Vsc[j_op].s_abc[2];
```

7.10.3 M-file

The M file for simulation is as under:-

```
clc;close all;
clear all;
clc;
HB=1;
% DFIG Parameter
f=50;
Ps=2e6;
Ns=1500;           % Synchronous Speed in RPM
Vs=690;           % rated RMS stator Voltage,V
Is=1760;          % rated RMS stator Current,A
P=2;              % no of pole pair
ws=2*50*pi;      % synchronous speed in rad/sec(electrical)
Tem=12732;       % electromagnetic rated torque,N-m
u=1/3;           % stator /rotor turn ratio
Vr=2070;         % Rated Rotor Voltage (non achieved)V
smax=1/3;        % maximum slip
Vr_stator=(Vr*smax)*u; % rated rotor voltage refered to stator
Rs=2.6e-3;       % stator resistance
Lls=0.087e-3;    % Stator leakage inductance
Rr=2.9e-3;       % Rotor resistance
Llr=0.087e-3;    % Rotor leakage inductance
Lm=2.5e-3;       % magnetizing inductance
Ls=Lm+Lls;
Lr=Lm+Llr;

Vbus=1200;       %DC bus Voltage
sigma=1-(Lm^2/(Ls*Lr));
Fs=Vs*sqrt(2/3)/(100*pi); %stator flux approx.
J=127;          % machine inertia
D=1e-3;
fsw=4e3;        % switching frequency
Ts=1/fsw/50;    % sampling time
Kt=-1.5*P*Lm*Fs/Ls;

%% Turbine gear ratio
N=100;          % gearbox ratio
```



```

subplot(1,2,1)
grid;
plot(tab_lambda,Ct,'linewidth',1.5)
xlabel('lambda','fontsize',14)
ylabel('Ct','fontsize',14)
subplot(1,2,2)
grid;
plot(V,Pt,'linewidth',1.5)
xlabel('Wind Speed (m/s)','fontsize',14)
ylabel('Power (W)','fontsize',14)

%% Regulators values
%%%%%%%%%%%%%%%%%%%%%%%%%%%%%%%%%%%%%%%%%%%%%%%%%%%%%%%%%%%%%%%%%%%%%%%%
%%%%%%%%%%%%%%%%%%%%%%%%%%%%%%%%%%%%%%%%%%%%%%%%%%%%%%%%%%%%%%%%%%%%%%%%
%%RSC controllers
tau_i=(sigma*Lr)/Rr;
tau_n=0.05/4;
wni=100*(1/tau_i);
wnn=1/tau_n;
kp_id=(2*wni*sigma*Lr)-Rr;
kp_iq=kp_id;
ki_id=(wni^2)*Lr*sigma;
ki_iq=ki_id;
kp_n=(2*wnn*J)/P;
ki_n=((wnn^2)*J)/P;
%%
%%%%%%%%%%%%%%%%%%%%%%%%%%%%%%%%%%%%%%%%%%%%%%%%%%%%%%%%%%%%%%%%%%%%%%%%
%%%%%%%%%%%%%%%%%%%%%%%%%%%%%%%%%%%%%%%%%%%%%%%%%%%%%%%%%%%%%%%%%%%%%%%%
%% Grid Side converter %%%
%%%%%%%%%%%%%%%%%%%%%%%%%%%%%%%%%%%%%%%%%%%%%%%%%%%%%%%%%%%%%%%%%%%%%%%%
Cdc=80e-3;
Rg=20e-6; %%%make double both Rg and Lg(initial 10e-6, 200e-6)
Lg= 0.3e-3; %8.5e-5; %400e-6
Kpg=1/(1.5*Vs*sqrt(2/3));
Kqg=-Kpg;
%% GSC PI REgulators
tau_ig=Lg/Rg;
wnig=60*2*pi;
Kp_idg=(2*wnig*Lg)- Rg;
Kp_iqg=Kp_idg;
Ki_idg=(wnig^2)*Lg;
Ki_iqg=Ki_idg;

```

```

Kp_v=-1000;
Ki_v=-300000;
%% Parameter for LLCL double trap filter
L1=.19e-3;
L2=.055e-3;
Cf1=90.5e-6;
Cf2=Cf1;
Lf1=17.5e-6;
Lf2=4.39e-6;
Rf1=.1;
Rf2=.1;
Pp=1;
Bm=0.9;           % Viscosity of air resistive force
Jm=1398.0;        % Moment of inertia in Kg/ m2
Shi_r=8.53;       % Rotor Magnatic flux linkage in Wb(Peak value)
Lqs=0.97e-3;      % Reactance of PMSG mH
Lds=0.679e-3;     % Reactance of PMSG mH
Ltot=0.127e-3;    % Total Reactance of Filter and transformer in mH
fsw=4e3;
p=1;              % pole pair
we=314.285;       % w=2*pi*50
Rd=0.113;
Ri=0.113;
Li=0.0485e-6;
Rg=0.113;
Lg=0.0397e-6;
Cf=125e-6;
Vcf=100;          % Requires clarification
Psmax=1.5e6;
sim('untitled.slx')

```

To study the characteristics of the TSR algorithm in tracking the MPP under different variation in the wind speed. It is assumed that the wind speed profile varies up and down as a step function with mean wind speed of 10 m/sec. Fig. 5 represents the actual wind speed, the measured and reference generator speed, the actual and maximum mechanical power, the turbine's power coefficient, the turbine tip speed ratio and the torque of the PMSG. It is obvious that the controller gives a good tracking of the actual and reference values of the rotor speed. The difference in power between the determined electrical and mechanical powers is very small. On the other hand, it can be observed that the system operates at the optimal power coefficient value (0.48). Moreover, the tip speed ratio reaches maximum value (8.1). Also, the turbine torque T_m and generator torque T_e are coincide well.

The grid-side converter controller is examined under step changing wind speed profile. Fig. 6 shows the dc-link voltage, the grid voltage and current, the grid power and the power factor. The controller regulates the actual value of dc link voltage to the reference level. On the other hand, to achieve unity power factor, the grid voltage and current are kept in-phase. The injected active power has a step change according to the change in the wind speed, whereas the reactive power is zero to achieve unity power factor.

Parameter	Value	Parameter	Value
DC Link Capacitor C	9000 μ F/ 1100V	Pole Pair	1
DC Link Reference Voltage V_{dc}^*	900V	Ts	2 μ S
Initial DC Link Voltage	690V	Flux Linkage ψ	0.433Wb
I_{sd}^* Reference(Stator)	0 for Max Torque	Speed reference PMSG ω^*	22.5Rad/ sec
I_{gd}^* Reference(Grid)	0 for Unit PF	Grid Frequency	50Hz
Ld	0.0097H	Moment of Inertia (J)	0.01197 kgm ²
Lq	0.0097H	Blade Radius	1.8m
Lg(Grid Inductance)	50mH/ 20A	Air Density	1.225Kg/m ³
Filter Inductance Lg	0.002H	Optimal Tip Speed Ratio	8.1
Rg(Grid Resistance)	0.0002 Ω	Max Power Coefficient	0.48
Filter Resistance Rg	3 Ω	No Switching States	08
Stator resistance Rs	0.006 Ω		

Table. 7.3 Simulation Parameters

7.11 CONCLUSIONS

This paper presents the control of grid-tie WECS based on the MPC control strategy. Furthermore, the main idea of the MPPT controller has been discussed in terms of the adjustment of the PMSG rotor speed according to instantaneous wind speed. The torque control is realized through MPC where the q-axis current is used to control the rotational speed of the generator according to the variation of wind speed. Also, the MPC has been proven as a good power controller in grid side. Computer simulations have been carried out in order to evaluate the effectiveness of the MPC. The results proved that the MPC has accurate tracking performance at different wind speed.

Simulation Results

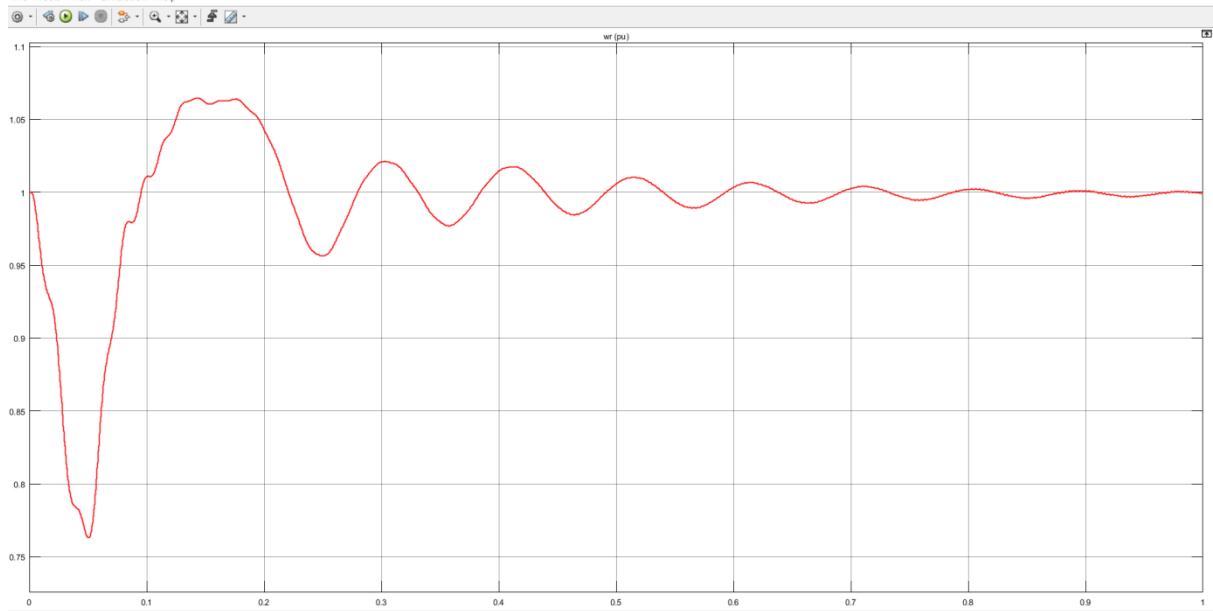


Fig. 7.8 PMSG Rotational Speed (W_r)

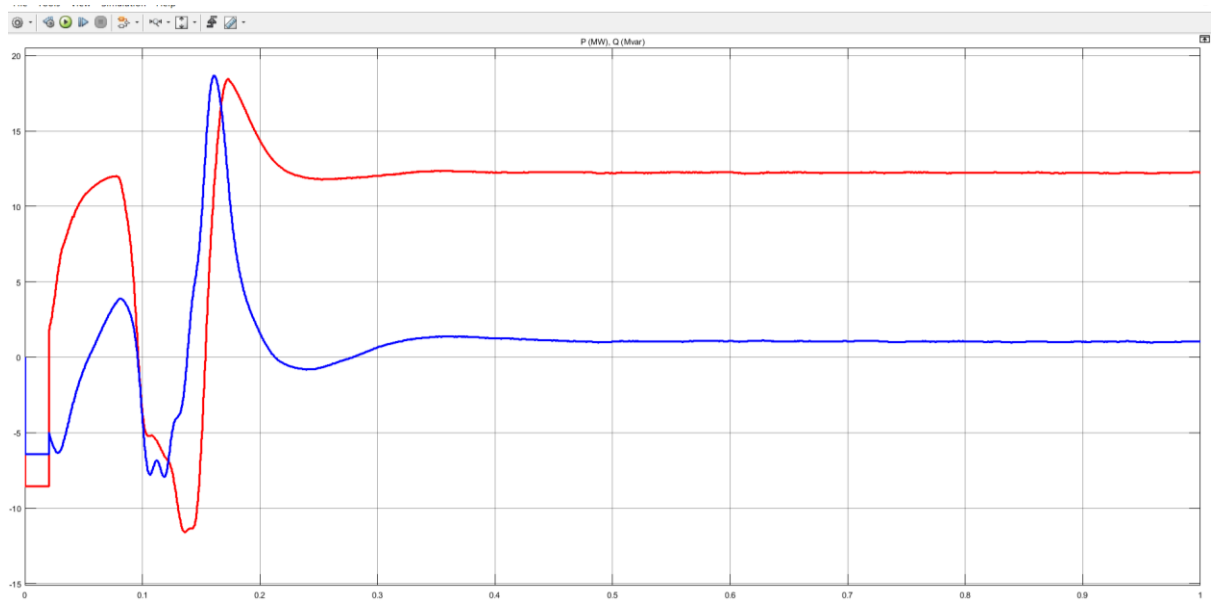


Fig. 7.9 PMSG Power Generation 'P' & 'Q'

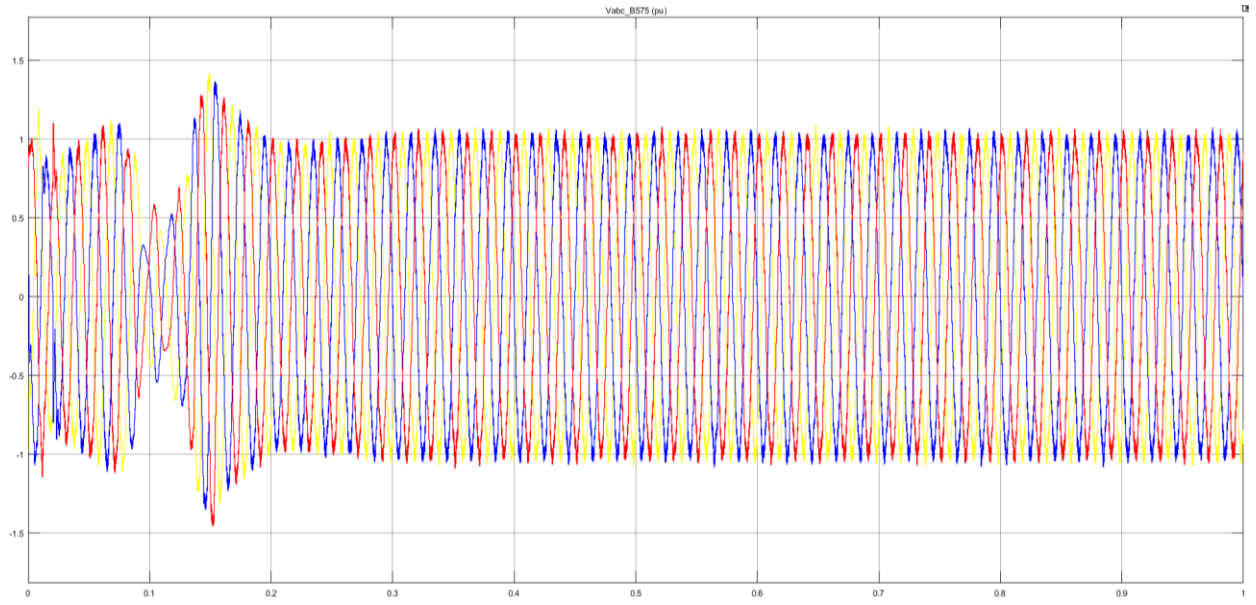


Fig. 7.10 PMSG Convertors Voltage

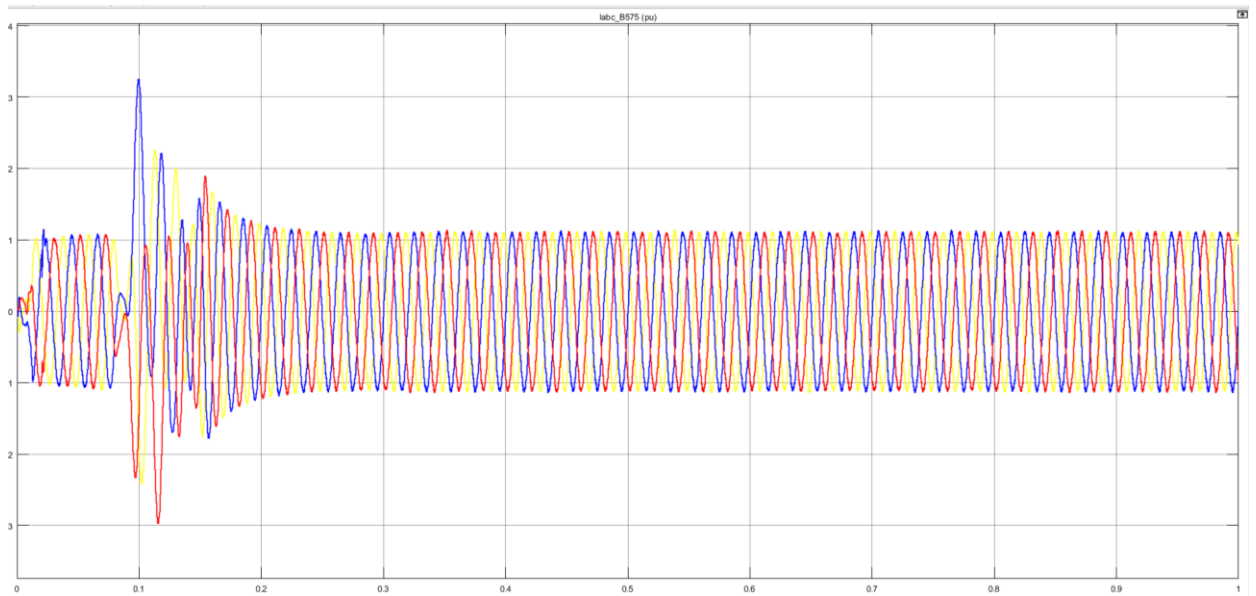


Fig. 7.11 PMSG Convertors Current

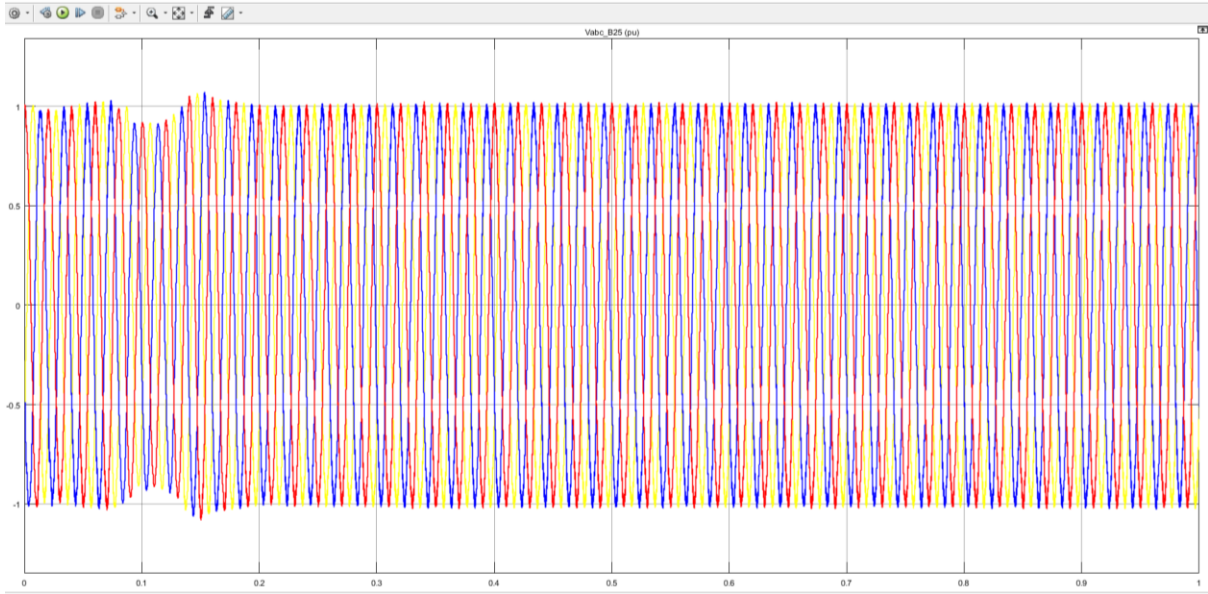


Fig. 7.12 PMSG Grid Voltage

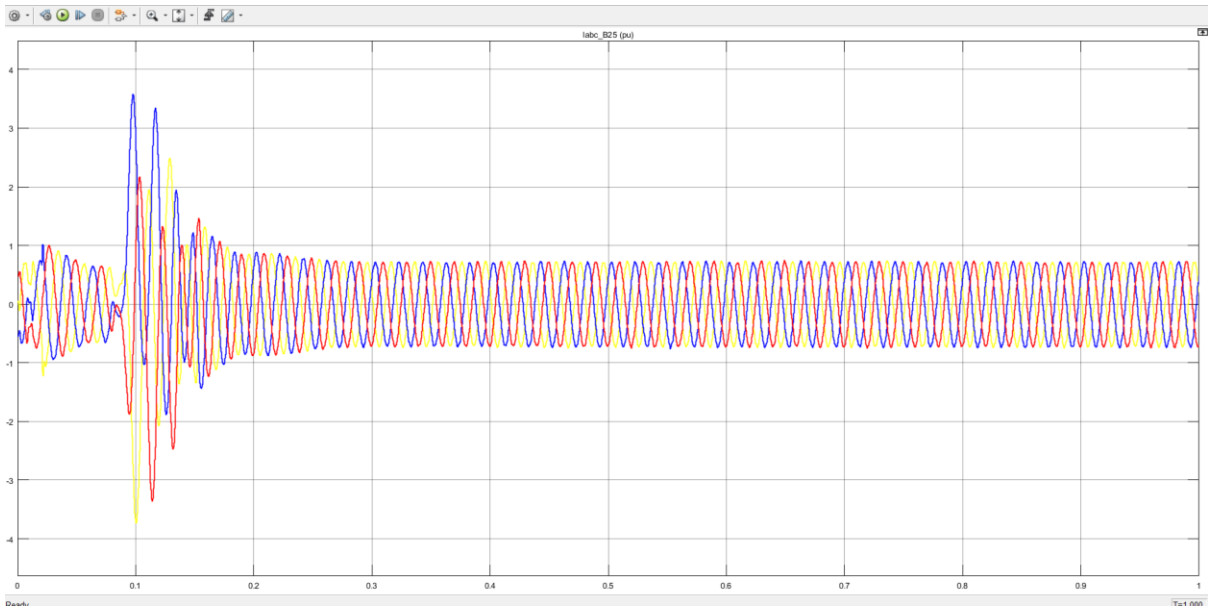


Fig. 7.13 PMSG Grid Current

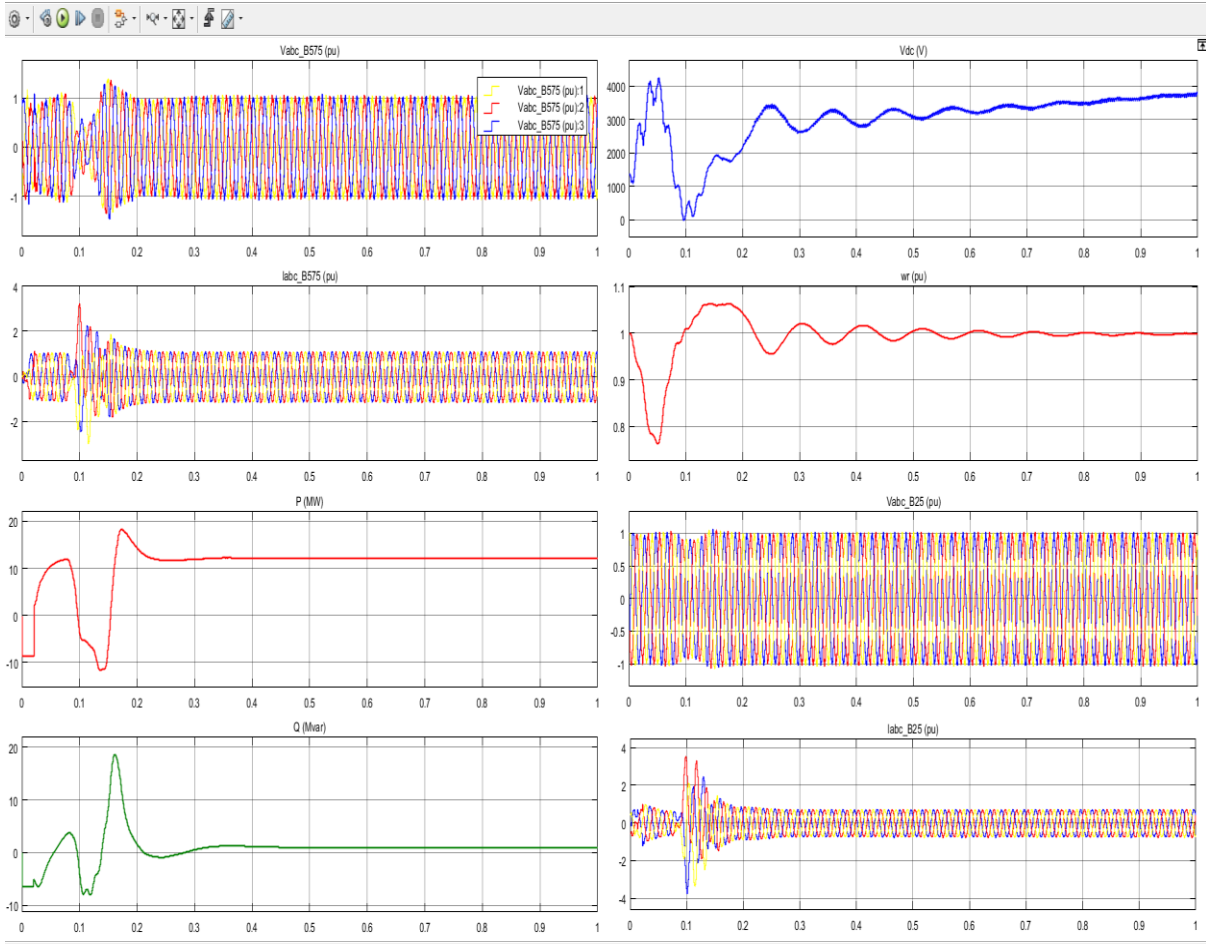


Fig. 7.14 Comparative Simulation Results

7.12 SCOPE OF FUTURE WORK

In this thesis, a simulation study was carried out to validate the proposed control algorithms for a 2 MW wind turbine PMSG system. In order to further test the performance of the control algorithms, an experimental test needs to be done in the future research work. For mitigating the harmonics, effective mitigation methods need to be studied to alleviate the unwelcome effects brought by converters and non linear loads. Few future works proposed are under:-

- (a) Development of hybrid wind and solar energy conversion system for maximum utilization of renewable energy sources.
- (b) Implementation of SWECS with nonlinear and dynamic loads.

- (c) Development of more efficient maximum power tracking method based on variable step size and variable pitch angle of wind turbine.
- (d) Connection of stand-alone wind energy conversion system to a micro grid.
- (e) Development of more efficient voltage frequency controller in order to reduce harmonics and produce low switching losses.
- (f) Hardware implementation of WECS with VF controller connected to three phase four wire loads.

References

- [1] S. Abolhosseini, A. Heshmati, and J. Altmann, “A review of renewable energy supply and energy efficiency technologies”, Discussion paper No. 8145, April- 2014, Institute for the study of labor (IZA).
- [2] G. M. J. Herbert, S. Iniyar, and D. Amutha, “ A review of technical issues on the development of wind farms”, *Renew., Sustain., Energy Rev.*, vol.32, pp619-641,2014.
- [3] I. Munteanu, A. I. Bratcu, N. A. Cutululis, and E.Ceang, “Optimal Control of Wind Energy Systems Towards a Global Approach”, Springer-Verlag London Limited,2008.
- [4] T. Ackermann, “Wind Power in Power System”, Wiley, 2005.
- [5] T. Bookman, “Wind energy’s promise, offshore”, *IEEE technol. Soci. Mag.*, vol. 24,no. 2, pp.9-15, jun.2015.
- [6] X. Sun, D. Huang, and G. Wu, “The current state of offshore wind energy technology development,” *Intern. Journal of Energy*, vol. 41, no. 1, pp. 298-312, 2012.
- [7] S. Lundberg, “Evaluation of wind farms layout,” *Euro. Power electron. drives association,j.*,vol.16, no. 1, 2016.
- [8] D. Das, J. Pan, and S. Bala, “HVDC light for offshore wind farm integration”, *Proc.IEEE,symp. Electron.mech.wind appl. (PEMWA)* pp. 1-7, july 2012.
- [9] K. Friedrich, “Modern HVDC Plus application of in modular multilevel converter topology,” *Proc. IEEE, Int. Sym. Ind. Electron. (ISIE)*, pp.3807-3810, jul.2010.
- [10] N. Flourentzou, V. Agelidis, G. Demetriades, “VSC-based HVDC power transmission system: An overview”, *IEEE, trans. Power Electron.* Vol. 24, no. 3, pp. 592-602, Mar. 2009.
- [11] V. Yaramasu, B. Wu, P. C. Sen, S.Kouro, M. Narimani, “High power wind energy conversion systems:State-of-the-Art and emerging technologies”, *Proc. IEEE*, pp. 1-49, 2015.
- [12] L. Wang, S. Chai, D. Yoo, L. Gan, and K. Ng, “PID and predictive control of electrical drives and power converters using Matlab/Simulink”, Wiley-IEEE press, Singapore, March 2015.

- [13] O. A. Lara, N. Jenkins, J. Ekanayake, P. Cartwright, and M. Hughes, “Wind Wind Energy Generation: Modelling and Control”, Wiley, 2009.
- [14] Executive Summary: World Wind Energy Market Update 2017. “Navigant Research” Available on- <https://www.navigantresearch.com/research/energy-technologies/wind-energy-service>.
- [15] Global Wind Statistics 2017, “Global Wind Energy Council (GWEC)”. Available on- <https://www.gwec.net>.
- [16] B. Wu, N. Zargari, S. Kouro, Y. Lang, “Power Conversion and Control of Wind Energy Systems”, Wiley 2011.
- [17] Indian Wind Energy : A brief outlook 2016, “Global Wind Energy Council”. Available on http://www.indianwindpower.com/pdf/GWEO_2016.pdf
- [18] Indian Wind Energy and Economy, “Indian Wind Turbine Manufacturer Association (IWTMA)”, Available on- http://www.indianwindpower.com/news_views.php
- [19] Wind GBI, “Indian renewable energy development agency ltd.(IREDA),” Available on- <http://www.ireda.gov.in/forms/contentpage.aspx?lid=744>. access on –FEB2018.
- [20] Shuhui Li, Rajab Challo, M.J. Nemmers, “Comparative study of DFIG power control using Stator voltage and stator flux oriented frames”, IEEE-2009, Power and energy society general meeting (PES’09), pp. 1-8.
- [21] H.M. Hasaniien, “A Set-Membership Affine Projection Algorithm-Based Adaptive Controlled SMES Units for Wind Farms Output Power Smoothing, ” IEEE Trans. Sustainable Energy, vol. 5, no. 4, pp. 1226-1233, Oct. 2014.
- [22] G. O. Suvire and P. E. Mercado, “Combined control of a distribution static synchronous compensator/ flywheel energy storage system for wind energy applications,” IET Generation, Transmission & Distribution, vol. 6, no. 6, pp. 483-492, June 2012.
- [23] D. Somayajula and M. L. Crow, “ An Ultra Capacitor integrated power conditioner for intermittency smoothing and improving power quality of distribution grid”, IEEE Trans.Sust.Energy,vol.5,no.4,Oct 2014,pp.1145-1155.
- [24] A. Gaillard, P. Poure, and S. Saadate, “Active filtering capability of WECS With DFIG for grid power quality improvement”, Proc. IEEE Int. Symp. Ind. Electron., June.30, 2008, pp. 2365-2370.

- [25] M. Boutoubat, L. Mokrani, and M. Machmoum, "Control of a wind energy conversion system equipped by a DFIG for active power generation and power quality improvement", *IEEE Renew. Energy*, vol. 50, pp. 378-386, Feb 2013.
- [26] E. trambley, S. Atayde, and A.Chandra, "Direct power control of a DFIG based WECS with active filter capabilities", *IEEE-2009, Electric Power and Energy Conference (EPEC-2009)*, pp. 1-6.
- [27] G. Todeschini, A. E. Emanuel , " Wind energy conversion system as active filters: design and comparison of three controls methods" , *IET Renewable Power generation-2010*,Vol. 4. Iss. 4, pp. 341-353.
- [28] P. Zhan, W. Lin, J. Wen, M. Yao, and N. Li, "Design of LCL filter for the back to back converter in a doubly fed induction generator" , *IEEE-2012, Power and Energy Society (PES) ISGT Asia-2012*, pp. 1-6.
- [29] D. Zhou, F. Blaabjerg, T. Franke, M. Tonnes and M. Lau, " Reduced cost of reactive power in doubly fed induction generator wind turbine system with optimized grid filter", *IEEE transactions on power electronics*, 2015, Vol. 30, no. 10, pp. 5581-5590.
- [30] M. Lissere, F. Blaabjerg, S. Hansen, "Design and Control of an LCL Filter based three phase active rectifier", *IEEE transaction on industry application*, sep/oct-2005, vol. 41, no.5, pp. 1281-1291.
- [31] Parikshith B. C, Dr. Vinod John, " High order output filter design for grid connected power converter", *Fifteenth National Power Systems conference (NPSC)*, IIT Bombay, December-2008, pp. 614-619.
- [32] M. Huang, F. Blaabjerg, Y. Yang, W. Wu, "Step by step design of a high order power filter for three-phase three wire grid connected inverter in renewable energy system", *Proced. Of the 4th IEEE International symposium on power electron. for distr. gener. sys. (PEDG)*,2013, pp. 1-8.
- [33] A.Merabet, A. A. Tanvir, K. Beddek, "Speed control of sensorless induction generator by the artificial neural network in wind energy conversion system", *IET Renew. Power Gener.*, 2016.
- [34] Amit Kumar, D.Giribabu, "Performance Improvement of DFIG fed wind energy conversion system using ANFIS controller" , *IEEE, International conference on Adv. Electr., Electron., Inform., Comm., and Bioinfo.,(AEEICB-16)*, 2016.

- [35] Ahmed A. Z. Diab, Salah A.A. Maksoud, Basem E. Elnaghi, Denis A. Kotin, “Performance of doubly fed induction generator based wind turbine using adaptive neuro-fuzzy inference system”, IEEE, IFOST-2016: Mechatronics, Electrical Engineering and Power Electronics, pp.145-149.
- [36] Arun Shankar V. K, Umashankar S, Sanjeevikumar P, Paramasivam S, “Adaptive neuro-fuzzy inference system (ANFIS) based direct torque control of PMSM driven centrifugal Pump” , International journal of renewable energy research,2017, vol. 7, no.3.
- [37] K. Rebecca Angeline, T. Pidikiti, and S.K. Babu Yadlapati, “Modelling and simulation of ANFIS controlled doubly fed induction generator based wind energy system for performance enhancement” , International science press 2017, 10(5), pp.61-73.
- [38] N. K. S. Naidu , B. Singh, “Doubly fed induction generator for wind energy conversion systems with integrated active filter capabilities”, IEEE, Trans. On Industrial Informatics,2015, pp. 1-11.
- [39] A. M. Eltamaly and A.A. khan, “Investigation of DC link capacitor failures in DFIG based Wind Energy conversion system”, STM Journals, Trends in Electrical Engineering, 2011,Vol. 1, iss.1, pp. 12-21.
- [40] A. M. S. Yunus, A. A. Siada, and M. A. S. Masoum, “Impact of DC link fault on the dynamic performance of DFIG”,IEEE 2012, pp.1-6.
- [41] H. A. Sher, K. E. Addoweesh and Y. Khan, “ Effect of short circuited DC link capacitor of an AC-DC-AC inverter on the performance of induction motor” , Journal of King Saud University-Engineering Sciences, 2014,28,pp. 199-206.
- [42] O. A. Lara, N. Jenkins, J. Ekanayake, P. Cartwright, and M. Hughes, “Wind Energy Generation: Modelling and Control”, Wiley-2009.
- [43] R. Sharma, K. Sahay, and S. Singh, “Effects of varying Load on DC-Link voltage in DFIGbased Wind Energy Conversion System”, International Journal of Advance Research in Electr., Electro., and Instr. Engineering,2014, vol 3 Issue 5.
- [44] G. Abad, J.Lopez, M.A.Rodriguez, L.Marroyo, and G.Iwanski, “Doubly Fed Induction Machine: Modeling and control for wind energy generation”,IEEE press ,Wiley-2011.
- [45] B. K. Bose, “Modern Power Electronics and AC Drives” 4th ed. Pearson prentice hall 2007.
- [46] M. Gopal , “ Digital Control and State Variable Method: Conventional and neuro-fuzzy control system”. 2nd edition, 2003,Tata McGraw-Hill. Chapter 11&12.

- [47] Asit Mohanty, Meera Viswavandya, Prakash K. Ray, Sandipan Patra, "Stability analysis and reactive power compensation issue in a microgrid with DFIG based WECS", Elsevier, 2014, *Electrical Power and Energy Systems* 62, pp753-762.
- [48] D.Bystrov, J.Westin, "Practice Neuro-Fuzzy Logic System-Matlab GUI toolbox".
- [49] T. Ackermann, G. Andersson, L. Soöder, "Distributed generation: a definition," Elsevier, *Electric Power Systems Research*, Vol. 57, pp. 195–204, 2001.
- [50] Thomas Ackermann, *Wind power in power system*, UK: John Wiley & Sons, 2005, pp53-65.
- [51] Y. Shankir, "Review of wind turbines' drive systems and why Gearless direct drive," RCREEE Wind Energy Building Capacity Program – Stage 2 Rabat, Tangier 29 March – 2nd Apr. 2010.
- [52] P. Vas, *Electrical machines and Drive S – A space vector theory approach*, New York: Oxford Univ. Press 1992.
- [53] W. A. Hill and S. C. Kapoor, "Effect of two-level PWMsources on plant power system harmonics," in *Conf. Rec. IEEE-IAS Annu. Meeting*, pp. 1300--1306, 1998.
- [54] M. Liserre, Frede Blaabjerg, Steffan Hansen, "Design and Control of an LCL-filter based Three-phase Active Rectifier," *IEEE Trans, Industry Applications Conference*, Vol. 41 , No. 5, pp. 1281 – 1291, Sept/Oct. 2005.
- [55] V. Blasko and V. Kaura, "A novel control to actively damp resonance in input lc filter of a three-phase voltage source converter," *IEEE Trans.Ind. Appl.*, vol. 33, no. 2, pp. 542--550, Mar./Apr. 1997.
- [56] B. Farid O. Amar, "A Study of New Techniques of Controlled PWM Inverters," *European Journal of Scientific Research*, Vol.32 No.1. pp. 77-87, 2009.
- [57] Siegfried Heier, *Grid integration of wind energy conversion systems*, John Wiley & Sons Ltd 1998, pp. 34-36.
- [58] S.M.Muyeen, Ahmed Al-Durra, J. Tamura, "Variable Speed Wind Turbine Generator System with Current Controlled Voltage Source Inverter", *Energy Conversion and Management*, Vol. 52, No. 7, pp. 2688-2694, Jul. 2011.

- [59] Shuhui Li, Timothy A. Haskew, and Ling Xu "Conventional and novel control design for direct drivrn PMSG wind turbines," Elsevier, Electric Power System research, Vol. 80, pp. 328-338, 2010.
- [60] L. M. Fernandes, C. A. Garcia, F. Jurado, "Operating Capability as a PQ/PV node of a Direct-Drive Wind Turbine based on a permanent magnet synchronous generator, " Elsevier, Renewable Energy, Vol. 35, pp. 1308-1318, 2010.
- [61] S.M.Muyeen, R. Takahashi, T.Murata, J. Tamura, "A Variable Speed Wind Turbine Control Strategy to Meet Wind Farm Grid Code Requirements, " IEEE Trans, Power Systems, Vol .25, No. 1, pp. 331- 340, Feb. 2010.
- [62] Cvejn, J, "PI/PID Controller Design for FOPDT Plants Based on the Modulus Optimum Criterion," In Proceedings of the 18th International Conference on Process Control, Tatranská Lomnica, Slovakia, June 14 – 17, pp. 301–306, Jun, 2011.
- [63] Bouzid AM, Guerrero JM, Cheriti A, Bouhamida M, Sicard P, Benghanem M.A – Survey on control of electric power distributed generation systems for micro grid applications. Renew Sustain Energy Rev2015;44:751–66. [http://dx. doi.org/ 10.1016/ j.rser. 2015.01.016](http://dx.doi.org/10.1016/j.rser.2015.01.016).
- [64] Blaabjerg F, Ma K. Future on power electronics for wind turbine systems. IEEEJ Emerg Sel Top Power Electron 2013; 1:139–52. [http://dx.doi.org/10.1109/ JESTPE.2013.2275978](http://dx.doi.org/10.1109/JESTPE.2013.2275978).
- [65] Khezri R, Bevrani H. Voltage performance enhancement of DFIG-based wind farms integrated in large-scale power systems: coordinated AV Rand PSS. Int J Electr PowerEnergySyst2015;73:400–10. [http://dx.doi.org/10.1016/j.ijepes. 2015.05.014](http://dx.doi.org/10.1016/j.ijepes.2015.05.014).
- [66] Kutija M, Sumina D, Čolović I. Magnetization of speed sensorless squirrel-cage induction generator for wind power application using a phase-locked loop. Electr Power Syst Res2015;122:119. [http://dx.doi.org/10.1016/j.epsr.2015. 01.009 29](http://dx.doi.org/10.1016/j.epsr.2015.01.009).
- [67] Errami Y, Ouassaid M, Maaroufi M. A performance comparison of a nonlinear and a linear control for grid connected PMSG wind energy conversion system. Int JElectrPowerEnergySyst2015;68:1 80–94. [http:// dx.doi.org/ 10.1016/ j. ijepes. 2014.12.027](http://dx.doi.org/10.1016/j.ijepes.2014.12.027).
- [68] JainB, JainS, Nema RK.Control strategies of grid interfaced wind energy conversion system: an overview. Renew Sustain Energy Rev2015;47:983–96. [http:// dx.doi.org/ 10.1016/ j.rser. 2015.03.063](http://dx.doi.org/10.1016/j.rser.2015.03.063).

- [69] Kim H- W, Kim S-S, KoH-S. Modeling and control of PMSG-based variable- speed windturbine. *Electr Power SystRes*2010;80:46–52. <http://dx.doi.org/10.1016/j.epsr.2009.08.003>.
- [70] Ananth DVN, Nagesh KumarGV, Fault ride-through enhancement using an enhanced field oriented control technique for converters of grid connected DFIG and STATCOM for different types of faults. *ISA Transaction*; n.d. <http://dx.doi.org/10.1016/j.isatra.2015.02.014>.
- [71] Zhang Y, Zhang Q, LiZ, ZhangY .Comparative study of model predictive current control and voltage oriented control for PWM rectifiers. In : *Proceedings of International Conference on Electrical Machines and Systems (ICEMS2013)*; 2013.p.2207–2212. <http://dx.doi.org/10.1109/ICEMS.2013.6713193>.
- [72]Abdelli R, Rekioua D, Rekioua T, Tounzi A. Improved direct torque control of an induction generator used in a wind conversion system connected to the grid. *ISA Trans*2013;52:525–38. <http://dx.doi.org/10.1016/j.isatra.2013.03.001>.
- [73]LiS, Haskew TA, Swatloski RP, Gathings W. Optimal and direct-current vector control of direct-driven PMSG wind turbines. *IEEE Trans Power Electron* 2012;27:2325–37. <http://dx.doi.org/10.1109/TPEL.2011.2174254>.
- [74]YinX, LinY, LiW, GuY, LeiP, LiuH.Sliding mode voltage control strategy for capturing maximum windenergy based on fuzzy logic control. *IntJ Electr Power Energy Syst*2015;70:45–51. <http://dx.doi.org/10.1016/j.ijepes.2015.01.029>.
- [75] Cortes P, Kazmier kowski MP, Kennel RM, Quevedo DE, Rodriguez J. Predictive control in power electronics and drives. *IEEE Trans Ind Electron* 2008;55 (4312):424. <http://dx.doi.org/10.1109/TIE.2008.2007480>.
- [76]XiY-G, LiD-W, LinS. Model predictive control status and challenges. *Acta Autom Sin* 2013;39:222–36. [http://dx.doi.org/10.1016/S1874-1029\(13\)60024-5](http://dx.doi.org/10.1016/S1874-1029(13)60024-5).
- [77]Rivera M, Wilson A, Rojas CA, Rodriguez J, Espinoza JR, Wheeler PW, etal. A comparative assessment of model predictive current control and space vector modulation in a direct matrix converter. *IEEE Trans Ind Electron*2013;60:578– 88. <http://dx.doi.org/10.1109/TIE.2012.2206347>.
- [78]Junping H, Lei Y, Xuesong W, Jian W. Research on dead beat control of a three- level grid-connected inverter based on $\alpha\beta$ transform. *Procedia Eng* 2011;23:397–402. <http://dx.doi.org/10.1016/j.proeng.2011.11.2520>.

- [79] Li N, Ming Y, Dian-Guo X. Predictive current control for Permanent Magnet Synchronous Motor based on deadbeat control. In: Proceedings of the 7th IEEE Conference on Industrial Electronics and Applications (ICIEA 2012); 2012. p. 46-51. <http://dx.doi.org/10.1109/ICIEA.2012.6360695>

APPENDICES

A.1 REFERENCE FRAME TRANSFORMATION

The reference frame transformation can be used to make easy the analysis of the electric component and also it simplifies the simulation and digital implementation of the control scheme for WECS and other system [16]. There are mainly two types of reference frames, (i) stationary reference frame, abc – $\alpha\beta$ and (ii) Synchronous frame abc-dq frame.

A.1.1 abc/ $\alpha\beta$ Reference Frame Transformation

The transformation of three phase variable in to two phase variable in the stationary frame is often referred as abc/ $\alpha\beta$ transformation. The three phase system ideally represented as-

$$\left. \begin{aligned} x_a &= \widehat{X} \cos(wt + \phi) \\ x_b &= \widehat{X} \cos(wt + \phi + \frac{4\pi}{3}) \\ x_c &= \widehat{X} \cos(wt + \phi + \frac{2\pi}{3}) \end{aligned} \right\} \quad (A.1)$$

The three phase vector can be decomposed in real and imaginary axis. So the x_α is the sum of real components of x_a, x_b, x_c while the x_β is the sum of imaginary component of the x_a, x_b, x_c . Since the $\alpha\beta$ reference frame does not rotate in space thus $wt=0$ and then abc to $\alpha\beta$ transformation is given below-

$$\begin{bmatrix} x_\alpha \\ x_\beta \end{bmatrix} = \frac{2}{3} \begin{bmatrix} 1 & -1/2 & -1/2 \\ 0 & \sqrt{3}/2 & -\sqrt{3}/2 \end{bmatrix} \begin{bmatrix} x_a \\ x_b \\ x_c \end{bmatrix} \quad (A.2)$$

This is also known as Clark's transformation and the $\alpha\beta$ to abc transformation also known as inverse Clark's transformation. The Inverse transformation is shown below-

$$\begin{bmatrix} x_a \\ x_b \\ x_c \end{bmatrix} = \begin{bmatrix} 1 & 0 \\ -1/2 & \sqrt{3}/2 \\ -1/2 & -\sqrt{3}/2 \end{bmatrix} \begin{bmatrix} x_\alpha \\ x_\beta \end{bmatrix} \quad (A.3)$$

A.1.2 abc /dq Reference Frame Transformation

The three phase variable in the abc stationary frame can be transformed into two phase variable In a reference frame defined by the d (direct) and q (quadrature) axes that are perpendicular to each other. The angle θ between the dq axes and the abc axes are formed

because of rotation of dq axes with arbitrary speed in space. The transformation of abc stationary frame vector in to the rotating dq axes by orthogonal projection with trigonometric function. The transformation of abc to dq done with the help of relation which given below. For the vector representation refer the figure (3.1).

$$\begin{bmatrix} x_d \\ x_q \end{bmatrix} = \frac{2}{3} \begin{bmatrix} \cos \theta & \cos(\theta - \frac{2\pi}{3}) & \cos(\theta + \frac{2\pi}{3}) \\ -\sin \theta & -\sin(\theta - \frac{2\pi}{3}) & -\sin(\theta + \frac{2\pi}{3}) \end{bmatrix} \begin{bmatrix} x_a \\ x_b \\ x_c \end{bmatrix} \quad (\text{A.4})$$

It is points to be kept in mind that the coefficient $2/3$ arbitrarily added to the equation. The commonly used value is $2/3$ or $\sqrt{2/3}$. The magnitude of two phase voltage is equal to the three phase voltage after transformation by the application of $2/3$.

The inverse transformation obtained by the matrix operation and is known as the dq to abc transformation.

$$\begin{bmatrix} x_a \\ x_b \\ x_c \end{bmatrix} = \begin{bmatrix} \cos \theta & -\sin \theta \\ \cos(\theta - \frac{2\pi}{3}) & -\sin(\theta - \frac{2\pi}{3}) \\ \cos(\theta + \frac{2\pi}{3}) & -\sin(\theta + \frac{2\pi}{3}) \end{bmatrix} \begin{bmatrix} x_d \\ x_q \end{bmatrix} \quad (\text{A.5})$$

A.2 Sinusoidal Pulse Width Modulation (SPWM)

In wind energy conversion system the extensively used converters are back to back 2 level converters. In this thesis the 2 level back to back voltage source converters are used for the operation of DFIG based system. The each converter is composed of six switches S1-S6 with an anti parallel free-wheeling diode for each switch. The switches can be Insulated gate bipolar transistor (IGBT)/ integrated gate communicated thyristor (IGCT). In this thesis the IGBTs based converter used. When the converter transform the fixed DC voltage to Ac voltage with variable magnitude and frequency for a load is called the inverter and when the converter transform the fixed grid voltage with fixed frequency to a variable DC voltage for a DC load is called as an rectifier or the PWM rectifier. The power flow in the converter circuit is bidirectional; the power can flow from the AC to DC side and vice versa.

In this section the pulse width modulation scheme describe for the two level voltage source converters. There are extensively used three modulation techniques, Carrier based sinusoidal PWM; Carrier based SPWM with third harmonic injection [44] and the Space vector modulation (SVM) technique and many others techniques

Here the work only focuses on the carrier based PWM technique. The sinusoidal reference signal is compared with the triangular carrier signal and generates the pulses as accordingly.

If $V_j^* > V_{tri}$ then the switch $S_j=1$ means (UPPER Switch) ON and $j= a, b, c$.

Where V_a^*, V_b^*, V_c^* a, b, c reference voltages

V_{tri} = triangular carrier wave

The switching pulses generation shows in figure (A.2.1)[16].

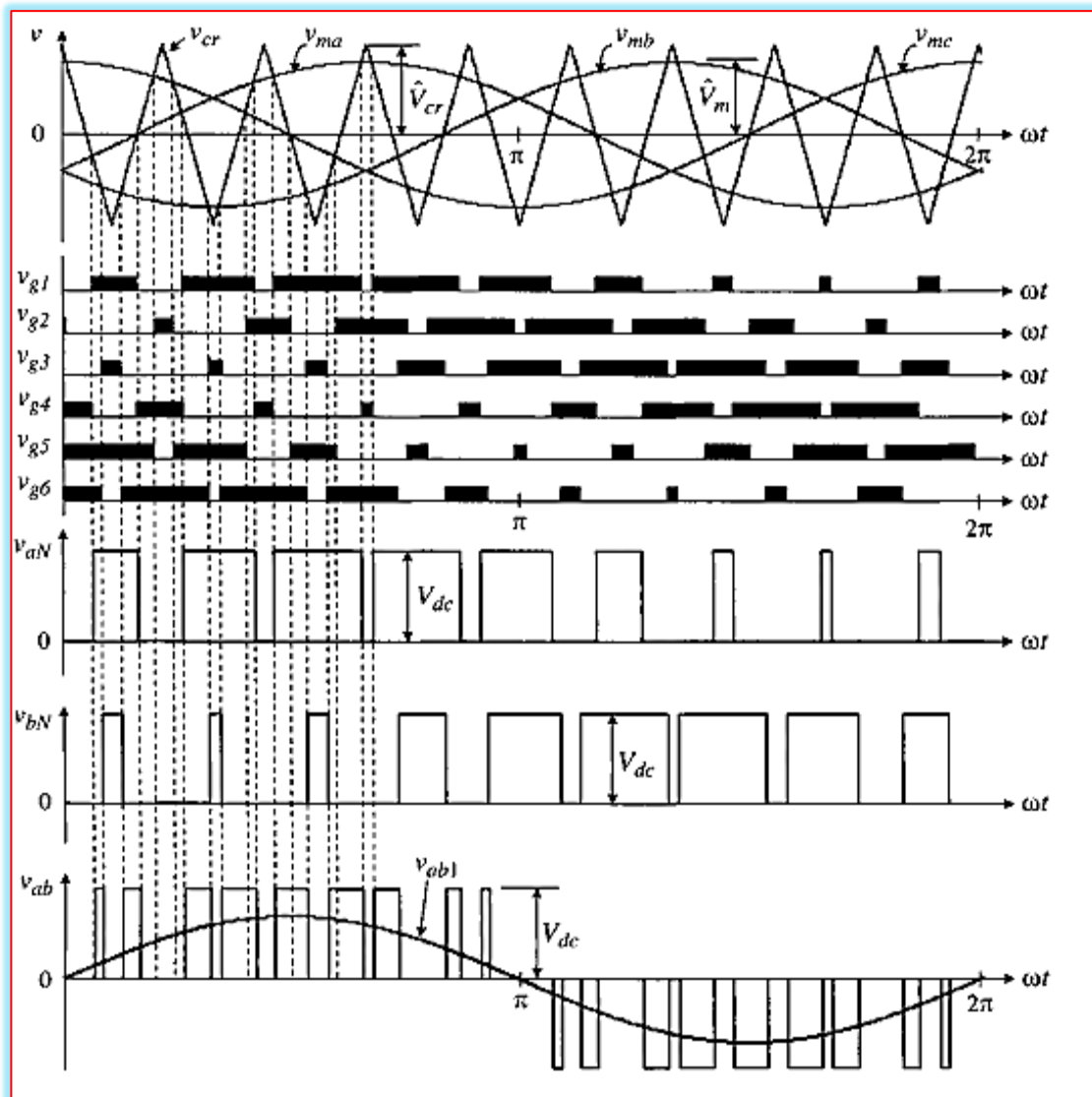


Figure A.2.1 SPWM with carrier and three phase modulating signal and switching states [16]

The fundamental frequency component in the inverter output voltage can be controlled by the amplitude modulation index.

$$m_a = \frac{|V^*|}{|V_{tri}|} \quad (\text{A.2.1})$$

Where m_a is the modulation index. The amplitude modulation index is usually adjusted by varying the reference sinusoidal voltages. The frequency modulation index is defined as-

$$m_f = \frac{f_{cr}}{f_m} \quad (\text{A.2.2})$$

Where f_{cr} , f_m are the frequencies of the carrier and modulating signals respectively.

When the carrier wave is synchronised with the modulating wave the modulation scheme is known as the synchronous PWM while the asynchronous PWM feature a fixed switching frequency and easy implementation with analog circuits. The asynchronous PWM generates the non-characteristics of harmonics whose frequency is not a multiple of fundamental frequency. The synchronous PWM scheme is more suitable for implementation with digital processor.

A.3 Hysteresis Band Based PWM

The hysteresis based current control method is mostly used because of its easy implementation and simplicity. Hysteresis current controller reduces the current error in order to maintain the switching pulses. It is a nonlinear control technique. It is basically the instantaneous feedback current control method where the actual current continually tracks the command current within the hysteresis band [45]. The basic working principle of hysteresis band current control is shown in figure (A.3.1). When the measured current rise up to the upper limit of hysteresis band then the upper switch of converter will be OFF, and when the measured signal crosses the lower hysteresis band limit the lower switch become turned off.

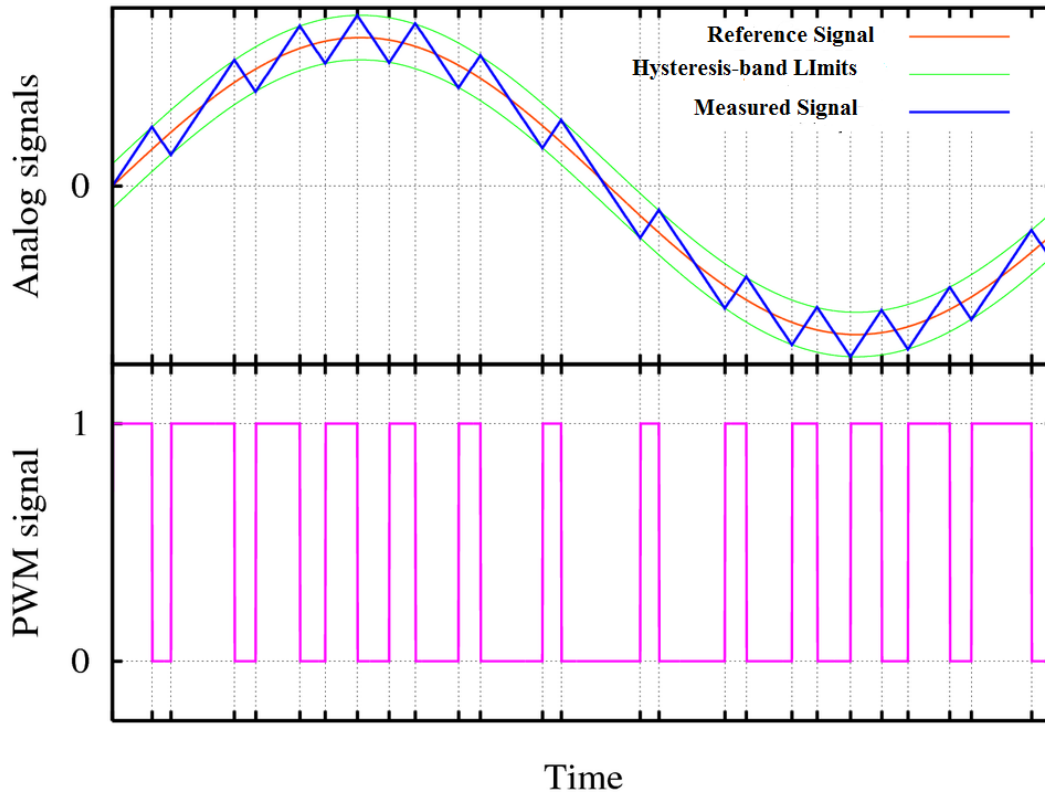


Figure A.3.1 Principle of Hysteresis band current control

The state of the switching devices [45] are defined below as-

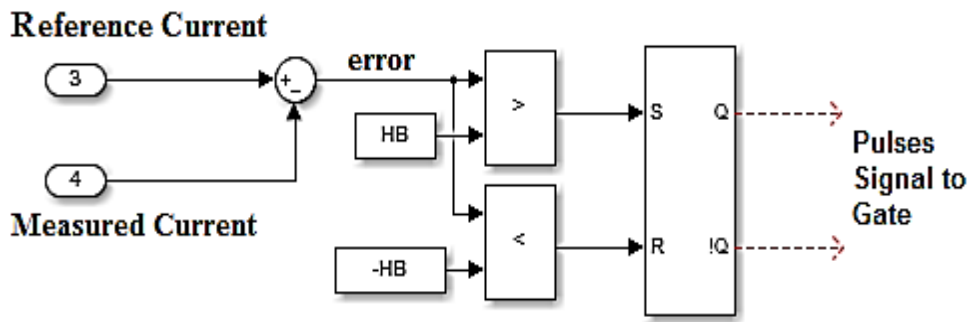
$i^* - i > +1$; Upper switch ON

$i^* - i < -1$; Lower Switch ON

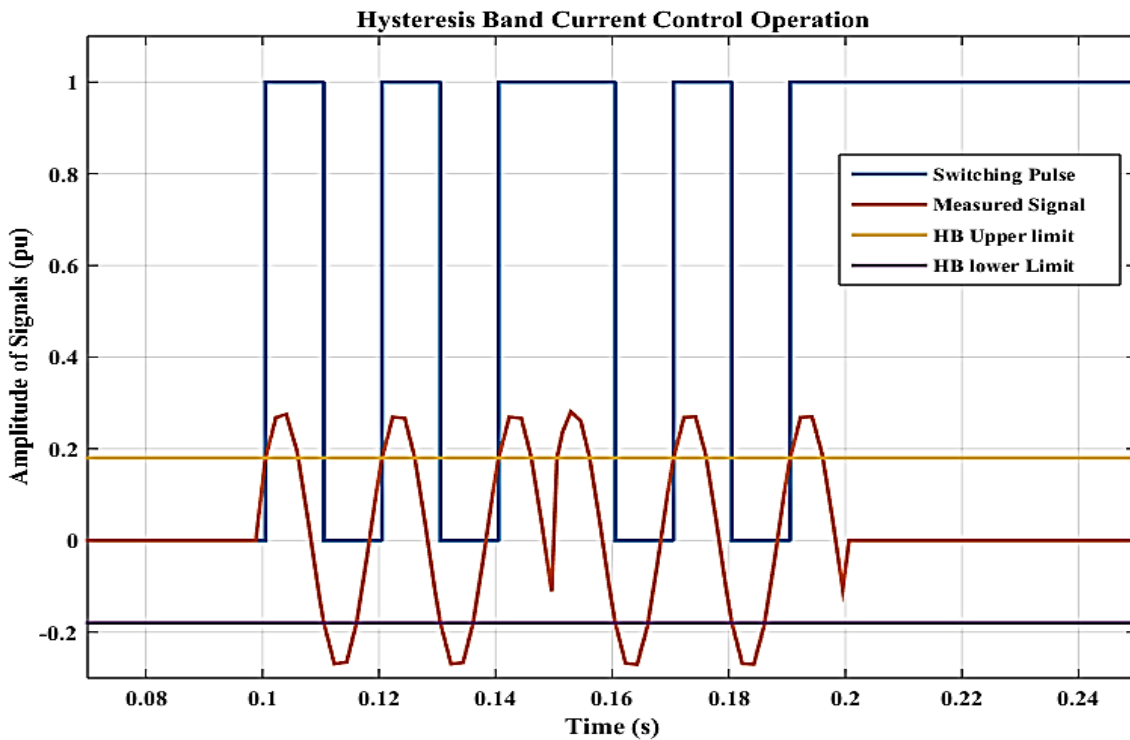
The peak to peak current ripple and switching frequency are related to the width of the hysteresis band. Smaller band will increase the switching frequency and lower ripple.

A.3.1 Designing and Matlab Model of Hysteresis Based Current Controller

The hysteresis based current controller design is easy and simple to implement. The SR flip flop used here to design the hysteresis based current controller. The hysteresis based controller is displayed in figure (A.3.2) (a & b).



(a)



(b)

Figure A.3.2 (a) Matlab model of HB controller, (b) Matlab response of HB controller

The HB current controller has fast transient response, direct limiting of device peak current and practical insensitive to dc voltage ripple. There are few drawbacks of this HB current controller that PWM frequency is not constant, non-optimal harmonic generated in machine. Fundamental current suffers the phase lag that increase at higher frequency.

Parameters

Parameters : Windmill

<u>Parameter</u>	<u>Values</u>
Rated Power	2 MW
Cut in wind speed	4 m/ sec
Rated wind speed	13 m/ sec
Cut out wind speed	25 m/ sec
No of rotor blades	03
Rotor Area	4587 m ²
Rotor Diameter	76.42 m
Air Density	1.225 kg/ m ²
Optimal Power Coefficient Cp	0.4
Moment of inertia in Kg/ m2 (J)	1398 kg/ m ²
Viscosity of air resistive force (B _m)	0.9
Wind Turbine Inertia Constant	4.32

$c_1 = 0.5176, c_2 = 116, c_3 = 0.4, c_4 = 5, c_5 = 21$ and $c_6 = 0.0068$

c_p ($c_{pmax} = 0.48$) at $\beta = 00$ and for $\lambda = 8.1$.

Parameters : PMSG

<u>Parameter</u>	<u>Values</u>
Generator Type	PMSG
Rated Mechanical Power (P in MW)	2 MW
Rated Apparent Power (S in MVA)	2.24 MVA
Rated L-L Voltage (in Volt)	690
Rated Power Factor (pf)	0.85
Rated Rotor Speed ω_m (rpm)	22.5
Pole Pairs (Pp, Np or P)	01
Rated Mechanical Torque	848.83 kNM
Flux Linkage (Ψ_f)	4.971 Wb
Stator winding Resistance	0.006 Ω
Stator d-axis Inductance (L_{ds})	0.97e-06
Stator q-axis Inductance (L_{qs})	0.97e-06
DC link Capacitance	9000e-06 μF
DC Link Voltage	1100 V
Direct Axis Voltage (Vds)	548.5 V
Quadrature Axis Voltage (Vqs)	357.3 V
Direct Axis Current (Ids)	1465.32 A
Quadrature Axis Current (Iqs)	1225.21 A
Line Voltage	575 V
Outer Diameter of Stator	3890 mm
Outer Diameter of Rotor	3470 mm
Effective Length	730 mm
Air Gap	6 mm

Babu Banarasi Das University, Lucknow

Plagiarism report

Student Name	-	Pravin Garg
Roll No	-	1170450003
Enrollment No	-	11704500643
Thesis Title	-	Model Predictive Control for Wind Energy Conversion System based Permanent Magnet Synchronous Generator.
Guides	-	Prof. V K Maurya, HOD, Electrical Engineering Deptt, BBD, University, Lucknow. Prof. Rakesh Sharma, Electrical Engineering Deptt, BBD, University, Lucknow.
Plagiarism Report Details (Checked at https://www.turnitin.com/solutions/plagiarism-prevention)	-	89% - Unique Content 11% - Plagiarism

Babu Banarasi Das University, Lucknow

List of Research Paper Publication

- 1. ‘Review of Controller Design for PMSG based Wind Generator with LCL Filter for Wind Energy Conversion System based on Permanent Magnet Synchronous Generator’ in UGC Approved Journal “International Journal of advance engineering and Research Development (IJAERD)’, ISSN Print: 2348-6404 and online ISSN: 2348-4470 with Impact factor of 5.71 (SJIF-2017).**
- 2. ‘Review of Predictive Control Strategy for Wind Energy Conversion System based on Permanent Magnet Synchronous Generator’ in UGC Approved Journal “International Journal of advance engineering and Research Development (IJAERD)’, ISSN Print: 2348-6404 and online ISSN: 2348-4470 with Impact factor of 5.71 (SJIF-2017).**

(Signature of Candidate)

(Pravin Garg)

Dated : May 2019

Babu Banarasi Das University, Lucknow

CERTIFICATE OF FINAL THESIS SUBMISSION

- | | | | |
|-----|---|---|---|
| 1. | Student Name | - | Pravin Garg |
| 2. | Roll No | - | 1170450003 |
| 3. | Enrollment No | - | 11704500643 |
| 4. | Thesis Title | - | Model Predictive Control for Wind Energy Conversion System based Permanent Magnet Synchronous Generator |
| 5. | Degree for which thesis is submitted | - | Master of Technology (Power System & Control) |
| 6. | School (of the university to which the Thesis is submitted) | - | School of Engineering |
| 7. | Thesis Preparation Guide was referred to for preparing the thesis | - | YES/ NO |
| 8. | The Content of the thesis have been organized based on the Guidelines | - | YES/ NO |
| 9. | The thesis has been prepared Without resorting to plagiarism | - | YES/ NO |
| 10. | All sources used have been cited appropriately | - | YES/ NO |
| 11. | The thesis has not been submitted elsewhere for a degree | - | YES/ NO |
| 12. | All the corrections have been Incorporated | - | YES/ NO |
| 13. | Submitted four hard bound Copies alongwith one CD | - | YES/ NO |

(Signature of Guide)
(Prof. V K Maurya)
Head of Deptt.(Elect Engg.)
BBD University, Lucknow.

(Signature of Guide)
(Prof. Rakesh Sharma)
BBD University, Lucknow.

(Signature of Candidate)
(Pravin Garg)
Dated : May 2019

CURRICULUM VITAE

Name : Pravin Garg

Mobile Phone No : 09230008830

Email ID: pravingarg72@gmail.com

Address : H. No. M G - 84, Sector- 'C', Aliganj, Lucknow.

Academic Qualification

- **M. Tech.** in Power System and Controls from **BBD, University, Lucknow.**
- **M. Sc.** In Information and Technology from **KSOU, Karnataka.**
- **Diploma** in Defence Management from **Devi Ahilya University, Indore.**
- **B. Tech** in Electrical engineering in 1994 from Kamla Nehru Institute of Technology, Sultanpur (Awadh University/ UPTU/ AKTU).
- **Intermediate** from Mahanagar Boys Inter College, Lucknow affiliated to U.P. Board, in 1989.
- **High School** from Mahanagar Boys Inter College, Lucknow affiliated to U.P. Board, in 1987.

Work Experience

Since **12 June 1994** to till date working as **Group -1 Officer** in **Min of Defence.**

Technical Skills

- **Hardware Description Language:** Matlab2019a, P-spice, Microprocessor (8085/ 8086 software), Windows Project Manager Software.
- **Languages:** C, C++ and MS- DOS.
- **Operating System:** Windows 10.

Extra Co-Curricular Activities

- Play all troop games in Armed Forces.
- Certified 'Project Manager' in IA.
- Certified in 'Power Management'.
- Experience of **Six Years** as **Works Officer** at Baramulla (J&K) and Lonavla, Pune (Maharastra) and handled projects worth 1200 Crores.
- Post completion of M. Tech. posted back as Works Officer in IA.

Personal Profile

Father's Name : Late Shri Laxmi Narayan Garg
Nationality : Indian
Date of Birth : 22 May 1972